POLITECNICO DI MILANO

School of Industrial and Information Engineering

M.Sc. in Aeronautical Engineering

STUDY OF A NOVEL LARGE BANDWIDTH ACTUATION SYSTEM FOR A MORPHING CONTROL SURFACE

Supervisor: Prof. Alessandro De Gaspari

Co-Supervisor: Dott. Vittorio Cavalieri

Author:

Corti Matteo 970204

Academic Year 2023-2024

Acknowledgments

I want to thank Prof. Alessandro De Gaspari and Dott. Vittorio Cavalieri for allowing me to carry out this small part in a much larger project and for helping me in every step of the development of this study. You both accommodated my a bit unorthodox situation gracefully and lent me the trust I could have delivered a result aligned with the department's standards. I hope I repaid that trust.

Also, I'm thankful for the encouragement of emeritus professor Luigi Quartapelle, himself an institution in the department. I first asked him about an opinion on the feasibility of this second academic arc of mine, back in 2020. His hopeful words back then helped me greatly.

Finally, I would like to thank my wife for the energy and grace, so typical of her, with which she accompanied me in this revival of my academic career. You were always there ready to help me through the most demanding times: ready to cheer me in the victories and console me in the setbacks. You gave a different taste to this last chapter at Politecnico. With you, I'm sure this was the right choice for our family.

Abstract

This study is an exploration of a novel actuation system for controlling a morphing aileron of a high aspect ratio wing, with an induction electric motor capable of high bandwidth actuation. Due to special constrains, the actuation is based upon a mechanism that allows the motor to be mounded spanwise in the wingbox. After a first 3D model, necessary for understanding the dimensional constraints of the assembly, a digital twin has been developed with Simscape. Several simulations and experiments that would have required a functioning prototype, such as frequency response analyses, gust reaction and the implementation of a controller, have been run on it. Its validation has been carried out with data from an Abaqus simulation and with data from the known analytical solution.

Sommario

Studio di un sistema di attuazione di un flap morphing con un motore elettrico ad induzione, capace di pilotare la superficie di controllo con un'ampia banda passante. A causa delle limitazioni in termini di spazio, è stato necessario sviluppare un meccanismo che permetta al motore di essere installato parallelo all'ala. Lo sviluppo di un modello 3D è stato necessario al fine di configurare un meccanismo che possa soddisfare gli ingombri e fornire lo spostamento voluto. Un Digital Twin è stato poi sviluppato in Simscape e diverse simulazioni ed esperimenti, che avrebbero richiesto un primo prototipo, sono stati eseguiti su di esso: risposta in frequenza, reazione alla raffica ed implementazione di un controller, sono stati trattati in questo documento. Il modello è stato validato con dati proveniente da simulazioni Abaqus e con i dati ricavati dalla soluzione statica analitica.

Table of Contents

List of tables

List of figures

List of Acronyms

MBD	Model-Based Design
CF	Carbon Fibre
SA	Spring Assist
DOF	Degree Of Freedom
HIL	Hardware In the Loop
HUMS	Health and Usage Monitoring System
HERWINGT	Hybrid Electric Regional Wing Integration Novel Green Technologies
CST	Class/Shape function Transformation

Chapter 1 Introduction

1.1 Problem description

The scope of this study is to describe the introduction of a novel technology, in the contest of the actuation of a control surface, historically hydraulically controlled, and to describe how such technology could be proficiently studied with the implementation of model-based design, with the development of a digital twin, built in the Matlab derived environment Simscape.

In a first part we will explore the development of the mechanism needed to obtain the desired aileron deflection, under a series of dimensional requirements due to the location of the ailerons. Once the geometry of the actuation mechanism is clear we will build the digital twin and proceed with its validation.

Only once we are sure the model we have developed, well describes the reality, we will perform tests and experiments that would have otherwise required a working physical prototype, while still in a quite early development phase of the project.

The need to explore a new approach, radically different than the industry standard, is due to the continuously increasing attention directed towards the environmental impact of the aviation industry. Several projects, in accordance with EU vision for the future of aviation [8], have been issued, targeting different sources of inefficiencies. One of the most interesting and promising initiative is the EU-funded Hybrid Electric Regional Wing Integration Novel Green Technologies (HERWINGT) project. This project aims to build a hybrid solution for short range flights, up to 1000km, accommodating about 100 passengers.

There are several ways this project aims to improve efficiency. In the interview of 28/6/2023, Antonio Hernandez Martin de Arriva, Clean Aviation chief engineer at Airbus Defence & Space, foresees a possible fuel burn reduction of 50%, at an aircraft level. This will be accomplished by working on three major aspects.

1. new wing design
2. a better integration of many subsystems and introduction of new materials such as thermoset, thermoplastic, and resin-infused composite that would enable highly integrated structures and limit the number of joints and bondings
3. introduction of sustainable aviation fuel

Regarding the first point, the aerodynamic drag will be reduced thanks to the introduction of a high aspect ratio wing. The wing prosed is quite extreme, with a semi-wing span of 18m and a root chord of 2m. Interest in high aspect wing ratio wing has been growing in the past years. The more widespread use of both composite material and advanced aerodynamic models, allow to take advantage of the higher efficiently of such designs. We can see in Figure 1 the result of a study carried out in the contest of HERWINGT project itself in which a traditional wing is compared to an equivalent, in terms of aerodynamic load, high aspect ratio one. The increase in efficiency is quite notable, the result of the paper testifies for a significant increase in efficiency and a lowering of the wing's weight.

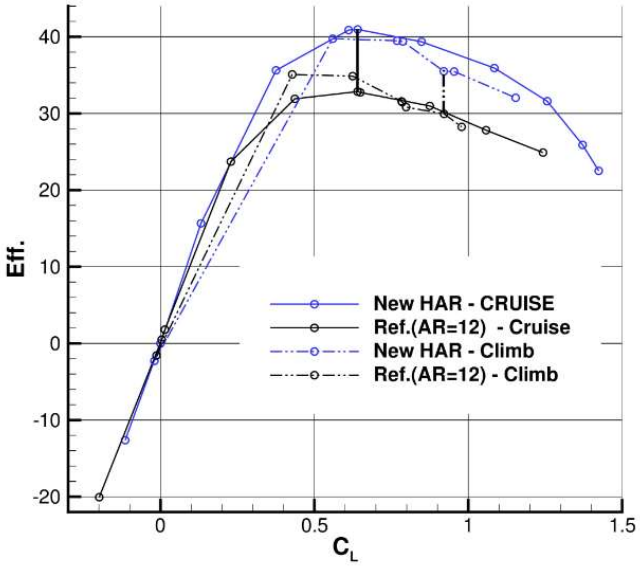

Figure 1. Efficiency of the designed high aspect-ratio wing in cruise and climb condition [1]

The peculiarity of this wing lies not only in the extreme aspect ratio, but also in the control surface: instead of conventional ailerons, spanning the last 5m of the wing a morphing structure will be implemented.

Instead of a conventional aileron, which introduce a discontinuity in the airfoil, implementing a smooth and continuous skin provides a reduced drag an also can decrease the actuation force needed [10]. The fact that a lower force is required to deflect the surface is key since it would allow us to install a smaller actuation system, with the motor located right in the wingbox. This would bring a significant reduction in weight of the system since the bulk of it is indeed due to the actuation assembly.

In the following figures we can see the differences between the 2 designs, developed in the contest of ICAS 2024 [7]. The increase in efficiency of the control surface, allows us to deflect the morphing structure less, causing a decrease in the needed force.

We can see in Figure 2**Error! Reference source not found.** the maximum and minimum rotation of the conventional aileron needed in order to generate the desired aerodynamic load.

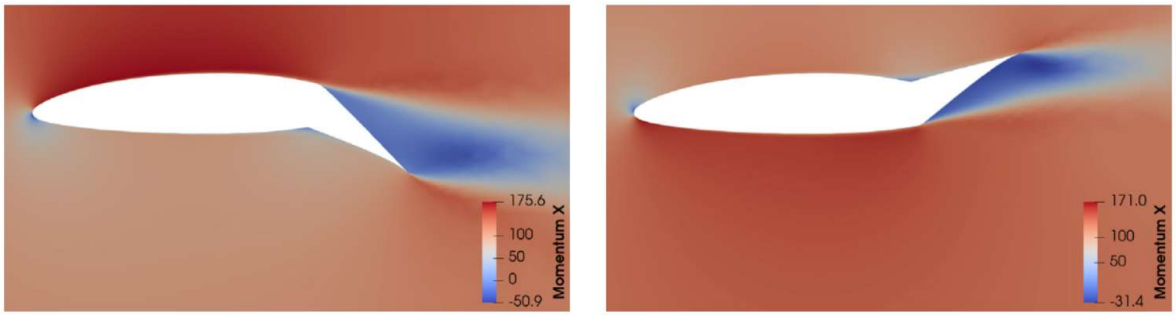

Figure 2. Conventional aileron maximum and minimum rotation [7]

In Figure 3 we can appreciate how, in order to generate the very same aerodynamic load, the morphing deflection needed is much smaller while greatly lowering the flow separation and therefore the drag.

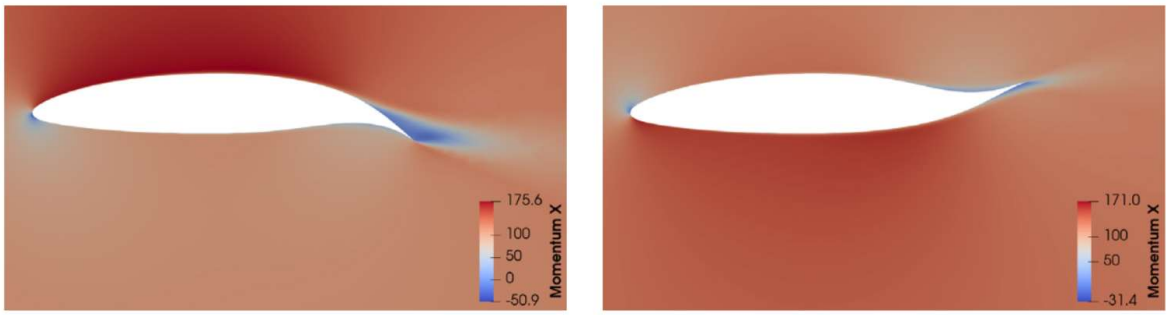

Figure 3. Morphing aileron maximum and minimum deflection [7]

The morphing shape is obtained from an optimization that considers aerodynamic and structural aspect. Both aspects are taken into account in a nested optimization loop, where the inner loop checks that the morphing shape satisfy the structural requirement while the outer one evaluates the aerodynamics characteristics [9]. This scheme is coupled with a parametrization method CST technique and can provide the optimal deflections, as reported in Figure 4. The CST method applied with the aerodynamic model allows also for an evaluation of the deformation energy required for the actuation.

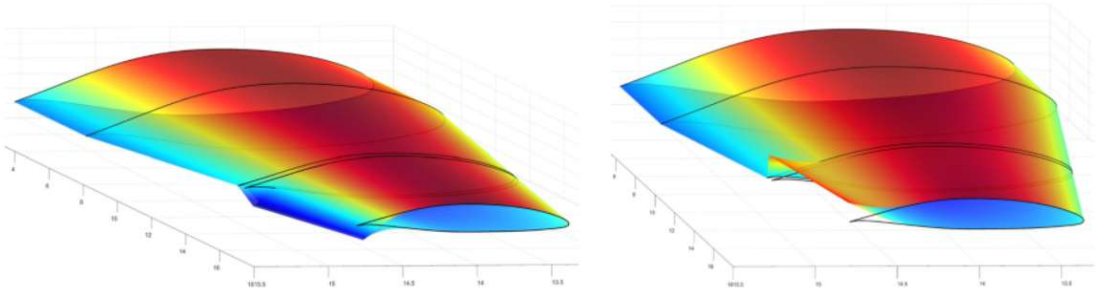

Figure 4. 3D CST models of the optimal downward and upward deflections of the morphing aileron

Once the morphing shape have been computed, the underlying structural design, that will display the computed shape, must be taken in consideration. Using a multi objective genetic algorithm and a non-linear FEM analysis we can optimize for both achieving optimal downward deflection and optimal upwards deflection.

In Figure 5 we can see the results. We can see in grey the structure at rest and superimposed both the maximum upwards deflection and downwards deflection.

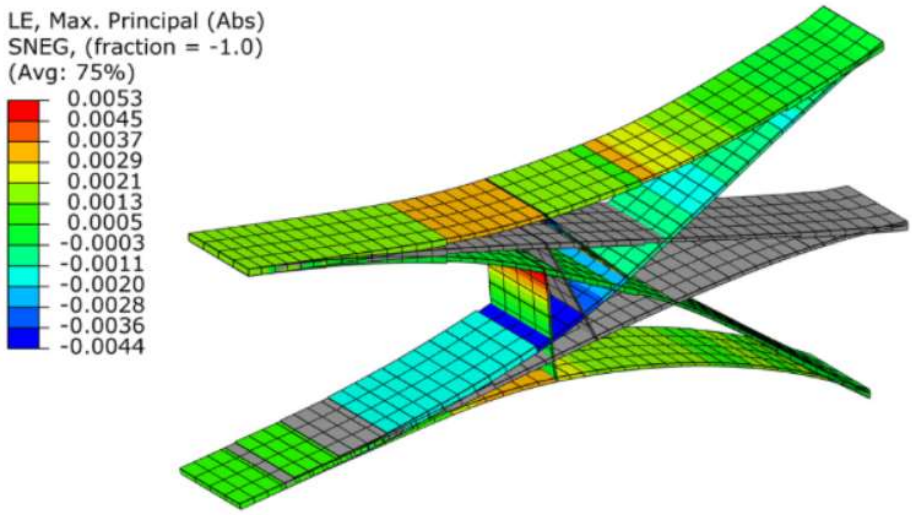

Figure 5. Finite element model of the optimum structural solution of morphing aileron from topology optimization

The requirement to actuate such a control surface are indeed more favourable, as compared with a traditional aileron. We can appreciate in Figure 6 that the force required is much smaller. It is also worth noting that we are able to achieve the desired lift variation with about half the deflection of the control surface.

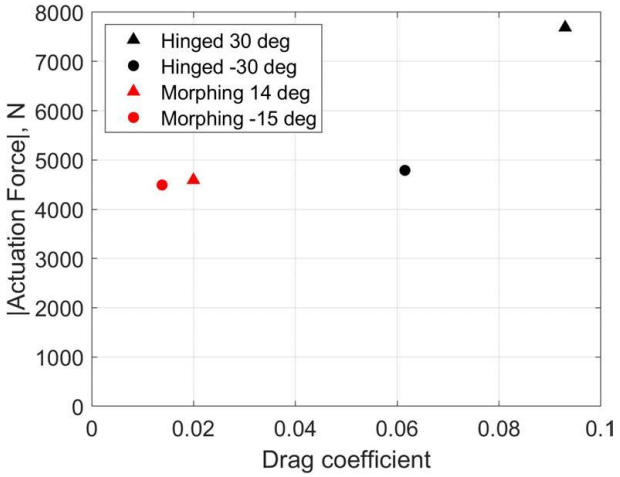

Figure 6. Comparison of aerodynamic and actuation performances between hinged and morphing

The force itself is applied to the lower skin, tangentially to the airfoil. The actuation system will provide the linear displacement required for the deformation: it will "push" the lower, reinforced, section of Figure 5 in order to obtain an upwards deflection, and it will "pull" the lower section to obtain a downwards deflection. The force itself will be applied in several discrete dedicated points. More details regarding the interaction between morphing structure and actuation assembly are discussed in Chapter 3 and Chapter 4.

This significant decrease in the actuation force needed, allows us to explore different technologies, that were previously non-satisfactory of the requirements. The general aim of the electrification of the plane and the requirement of a fast responding actuation has therefore tilted the choice for the actuation towards an electric motor, instead of the industry standard hydraulic ones.

Electric actuators have many advantages over the hydraulic solution. They are generally lighter and require a simpler system, they are easier to drive and without complex components such as distributors which are always focus of careful maintenance, due to their key role in governing the airplane.

1.2 Current solution

The industry standard for operating flaps and control surface at large, is without a doubt hydraulic power. The need for assisted control surface is old almost as the aviation industry itself. It was introduced for the first time, in the contest of civil aviation, in 1938 with the “flying boat” Boeing 314. The size of the airplane, which could carry 75 passengers, rendered direct mechanical actuation of control surfaces impossible, therefore a hydraulic system was developed to provide the needed forces, unloading the pilot from a very demanding task.

As per other systems in an airplane, we could think of the hydraulic system as composed of 4 stages: generation, control, transfer and use. Each one can be developed following different design logic, that can require specific knowledge often time empirical based. For instance, hydraulic power is often produced with displacement pumps, such as piston pumps. These solutions produce a discontinuous flow. This behaviour must be mitigated with the introduction of multiple cylinder. The number of cylinders which is appropriate to use can depend upon the specific installation and therefore can require a deep knowledge of such pumps, often experience based.

This solution became the paradigm in the aviation industry due to the many advantages it provides.

1- Scalable. Although the upper limit for the force the pilot can continuously provide is normed by FAA and EASA in FAR Part 25 (for transport category airplanes) and EASA CS-25, the introduction of servo assisted actuation allows the pilot to operate an indefinably big airplane, since the power for control the surfaces comes from the engine themselves, via hydraulic power.
2- Safe. Although only a recent development, the fluid nowadays used, such as MIL-H-87257, Skydrol™, Hyjet™ are flame resistant.
3- Well developed. The technology is well established and well-studied since it is deployed in a variety of other industries when we must actuate significant load. From heavy machinery to automotive there are several decades in research and development which brought by a plethora of solution that can be employed on aircraft as well. It is true that aeronautical components must satisfy peculiar and unique requisites, but the underlying theory is very well understood.
4- Fast and proportional. Due to the low compressibility of the hydraulic fluid, the frequency response is good, at least when considering human time scales. The servo assistance circuits allow usually to preserve a sense of proportionality between the control input and the action of the controlled surfaces.
5- High power to weight ratio. Due to the pressures that we can develop in the pumps, typically 21 MPa, a small area in the actuators can generate a great amount of force

It is also true that there are also downsides to this technology

1- Complexity. From generating to distributing, to regulating hydraulic power, the complexity of the system is notable and require a careful study of the interdependence between the different layer of redundancy to eliminate single point of failure. This task is not always possible. Notable is the example of the Boeing 747 which has 4 independent subsystems, powered by 4 engine driven pumps, one per each engine. Also, the APU is able to power part of the system. An historical example is presented in the form of the hydraulic control system of the Boeing 727, which first took flight on February 1964. In Figure 7 we can appreciate the need for redundancy up to the lines that brings fluid to the actuators and the actuators themselves.

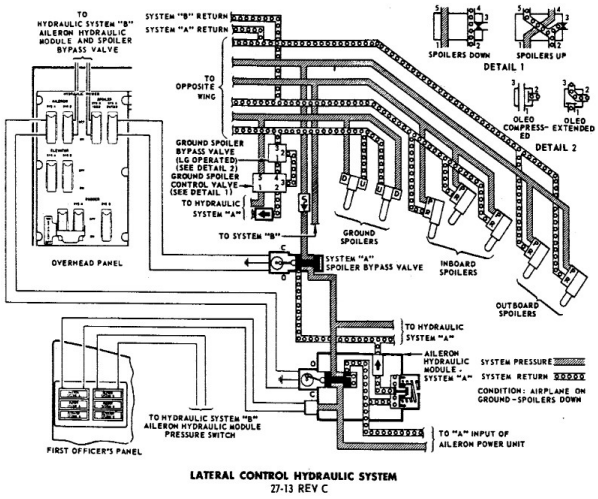

Figure 7. Boeing 727-51/251 maintenance training manual lateral control hydraulic system [3]

The system must me thought from the designing stage with manageability in mind. Given the need of pumps and reservoirs, in Figure 8, we can see how a simple fluid service must consider the presence of a variety of components in the system.

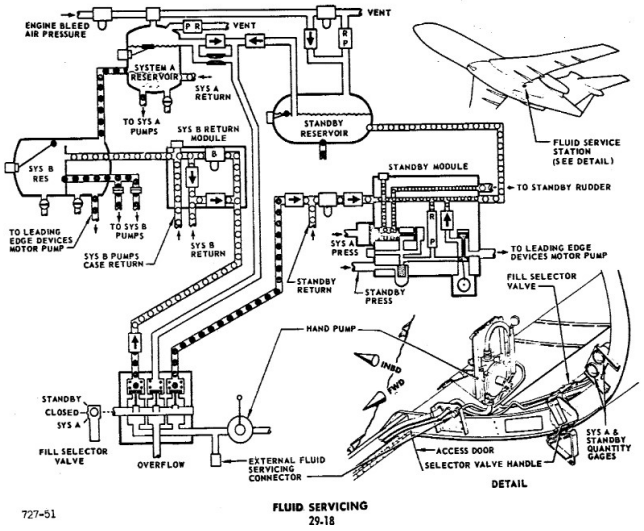

Figure 8. Boeing 727-51/251 maintenance training manual hydraulic power system [3]

It is notable the great number of different components required for this system: from accumulator to pressure reducing valve, to relief valve, to pumps the number of completely different components, each with its own maintenance interval and requirement, its own installation and testing procedure, renders the system quite hard to manage and requires a great deal of very detailed expertise to be properly understood.

2- Digital compatibility. It is not always obvious how to link the pilot input, coming typically as a voltage setpoint, to an actual motion of the control surface. Usually the stage of control, in a hydraulic system, is managed with a constant pressure approach. This provides a few benefits: it's easier to size the components, in consequence of a known external load, and renders possible to increase the number of actuators, without lowering the performance of the one already presents in the system. On the other way, it is now always immediate how to transmit an appropriate feedback, back into the hands of the pilot.

3- Environmental concerns. The use of first mineral oil and afterwards dedicated fluids, that require periodic flushing, raises environmental concerns and introduce complex and costly procedures for the handling and disposal of such materials.

4- Frequency response. If it's true that hydraulic distributors and actuators can reach easily human speed scale response, this can still be too poor a performance for solving complex aeroelasticity problems

1.3 Novel approach

The downsides described in the previous chapter, the general electrification of the aviation industry and the introduction of hybrid solutions, such the ones described in HERWINGT project, lead to a growing interest towards alternative actuation solution.

An electric motor is an excellent candidate that allows us to bypass several issues intrinsic in the legacy solution.

1. Natively digital. The actuation is an electric one, there's no need to convert an input, coming in as a voltage setpoint, into a pressure and a flow in distribution valves. We can reference the input to the measurement of the motor encoder.
2. Easy control. Most motors come with integrated encoders which allows us to determine the configuration of the kinematic chain.
3. Simplicity. There are simply fewer components and, more significantly, fewer types of components. We don't need to spill power for the motor, nor we need pumps for generating pressure, rigid lines to carry around the airplane fluid and all the other essential components needed in a hydraulic system. We use electric power which is already generated on the airplane, flexible wires that routers said power to the single actuator's control unit and thicker wires still up to the actuator itself. We find the difference in complexity that we can also find between an internal combustion engine vehicle and an EV.
4. Speed. We can now input much faster signals into the control surfaces improving the airplane response speed.
5. Weight reduction. It is true that the actuator itself is heavier than a hydraulic one, since it has integrated the motor, but we don't need pumps nor heavy lines nor distribution circuit, leading to an overall reduction in weight.
6. Safety. Except for power generation, that would need to be redundant (this is itself a requisite of the utmost importance in the fly by wire modern airplane), there are no single points of failure. Since each actuator needs its own control unit, the loss of one assembly actuator/ control unit would not compromise the performance of the remaining ones. The overall authority of the control surface would decrease but in a proportional manner, not unlike the loss of a single engine in a multiengine aircraft.
7. Synergy with a morphing structure. Since this actuation is been developed for the actuation of a morphing structure we can take advantage of the fact that we can use a greater number of motors, each actuating a portion of the 5m long morphing aileron. This would allow for complex form of automations, since we are not limited to move rigidly the whole aileron. A source of drag is given from change in the airfoil profile. Every time the airfoil's section changes, a vortex detaches, lowering sharply the circulation and generating drag. In Figure 9 an example of the consequence of exaggerate shape change, is depicted. On the other hand, if we manage to change progressively the shape of the airfoil, we can lower the drag caused by the detaching vortexes. This would be possible by deploying different motors assigned to

different section of the aileron and actuate them in a progressive manner, imposing a smaller deflection towards the wing root, and a bigger one towards the wingtip.

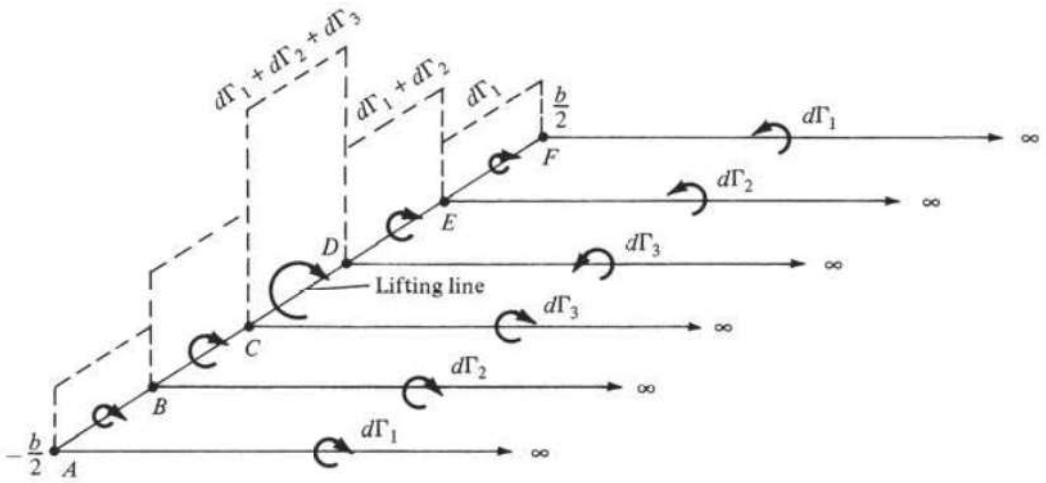

Figure 9. Superposition of a finite number of horseshoe vortices along the lifting line. [6]

In lieu of these advantages, an electric motor has been selected. Since we aim to actuate the control surface with a 10Hz signal, we could not rely to classic lead/screw electric actuators, which due to its internal mechanics can reach speeds up 1m/s. In Figure 10 we can see an example of such classic actuators. The motor is situated inline to the stem, although a parallel configuration is possible.

Figure 10. Example of lead/screw Parker ETH actuator

In Table 1 we can see an overview of the solutions proposed by the most commonly used brands:

Table 1. Comparison of lead/screw actuators

n	manufacturer	model	F [KN]	l[mm]	v [m/s]	f [Hz]
1	parker	ETH032	3.7	308.5	0.667	3.3
2	parker	ETH032	2.4	308.5	1.067	5.3
3	parker	ETH050	7	331	0.667	3.3
4	parker	ETH050	4.4	331	1.333	6.7
5	tolomatic	IMA22	1.4	250	0.711	3.6
6	tolomatic	IMA33	1.23		1.219	6.1
7	firgelliauto	F-SD-H-45(	2	217	0	0.0
8	Linak	LA25	2.5	218	0.025	0.1
9	Linak	la23	2.5	210	0.025	0.1
10	Actuonix	P16-P	0.3	147	0	0.0

As we can see, the possible frequency is far lower than the desired 10Hz. Currently there are no lead/screw electric solution which can surpass the limit of 1m/s actuation speed.

We had to expand our research into other technologies. The most promising one are the induction based linear actuator. These types of motors don't have any moving parts except for the shaft, and therefore can achieve much higher speeds. They actuate the stem via powerful electromagnetic fields, which can be manipulated to reach our 10Hz goal. In Figure 11 we can see how an induction moto is very different from the lead/screw solution. There's no conventional "motor", since the force is transmitted from the stator via powerful electromagnetic fields.

Figure 11. Example of induction-based actuator

The stem, acting as a shaft, is not in direct contact with the stator. Not even the position system needs physical contact between the shaft and the stem, as we can see in Figure 12, since only the three hall sensors are needed to gauge the phases of the windings. A differential sine and cosine signal are obtained that can be used to measure the position considering a 40mm period.

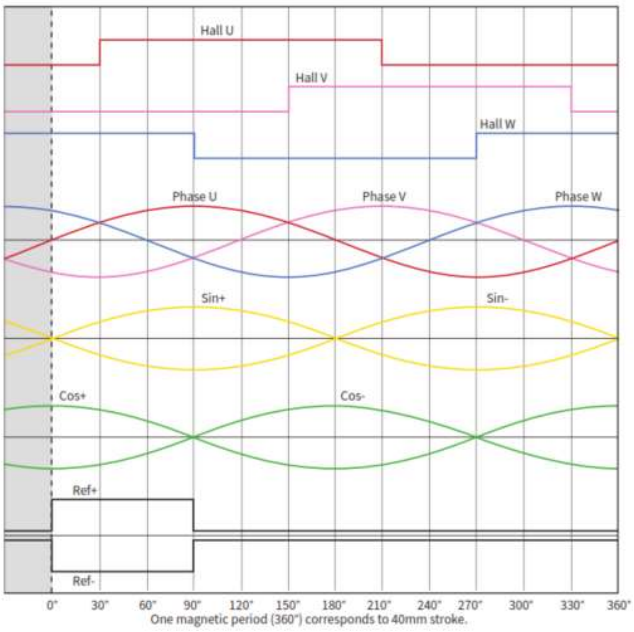

Figure 12. Encoder logic in an induction actuator

The LinMot P10-70X400U provides the speed required, with an adequate force. It is worth remembering that this technology has a few drawbacks.

1. Reversibility. Unlike the lead/screw solution, with an efficiency less than 50%, linear induction motors are reversable. This means that we need to provide constant power to maintain a desired position, leading to wasted energy. In this specific application this may not be relevant since the ailerons are used during manoeuvres. During a standard mission, as described in Figure 13, this is usually a small percentage of the totally fly time.

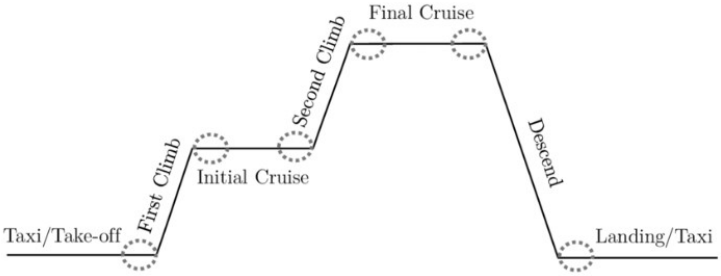

Figure 13. Example of a mission profile

   The lack of reversibility could also be considered positively, safety wise, since a failure in the actuator would lead to a "free" controlled surface. This behaviour could be considered safer, contrasted to the controlled surface stuck in an unwanted position. Alaska Airline flight 261 comes to mind, when the vertical stabilizer of the McDonnell Douglas MD-83 became stuck in a very aggressive position due to a stripped jackscrew assembly, leading to a catastrophic loss of control of the airplane. Since several actuators are needed, in order to actuate the wing 5m aileron, the loss of a single actuator (which would become free) would lower the authority of the control surface but leave the pilot ample margin for safely conduct the airplane.
2. Temperature. The electro-magnetic fields generated produce a lot of heat, which must be monitored and managed for avoiding damage to the motors. A water-cooling system is needed to achieve the actuation forces we need. Flexible cooling lines need to be routed to the motors and a small pump/radiator system must be implemented. Due to the hybridization intent of project HERWINGT, source of heat would become scarcer; it is not unforeseeable that due to the increase efficiency of hybrid propulsion systems, alternative sources of heat could become useful. This trend has become quite clear in the EV architecture:

now that there is basically no more free heat coming from the internal combustion engine, providing adequate heating for the cabin, especially in colder climates, has become an energy demanding task, to be solved with dedicated, and unfortunately inefficient, hardware.

Chapter 2 Kinematics

Due to the space restrictions and the performance required of the motor, it is not feasible to insert the motor parallel to the actuation direction. This would be the most straightforward way to actuate the aileron but with current electric motor technology this would not be feasible. A linkage is therefore required to translate the motion provided by the motor, which will need to be installed parallel to the wing, to the actuation point.

We chose to implement the simplest Scott Russell linkage in lieu of the following considerations:

1. Fewer components needed. This linkage needs, at minimum, only 2 parts. It is important to keep the number of components, and therefore their mass, to a minimum since all components in between the motor and the actuation point, are considered “unsprung mass”, and therefore would decrease the dynamic performance of the assembly
2. Acting on 3 parameters (rod length and starting conditions), it is possible to perform different actuations in different actuation points, using only one motor. In our simulations, we use a single motor for operating 2 actuation points but this concept could be expanded in two ways: increasing the number of actuation points connected to a single motor, thereby limiting the mass and the complexity of the system, or increasing the number of the motors, allowing the designer to morph in a complex manner the aileron, with a penalty of weight.
3. This mechanism can resist unwanted transversal load, that would be absorbed by the main bearings in D. This renders this solution more resilient to unexpected scenarios, protecting the most delicate part of the system: the motor.

2.1 Kinematics analysis

We aim to use the horizontal displacement of point A as the one DOF, since this will be directly linked to the linear actuator. We write the equations that links the horizontal displacement of A with the vertical displacement in C. The resulting Scott Russell mechanism is depicted in Figure 14.

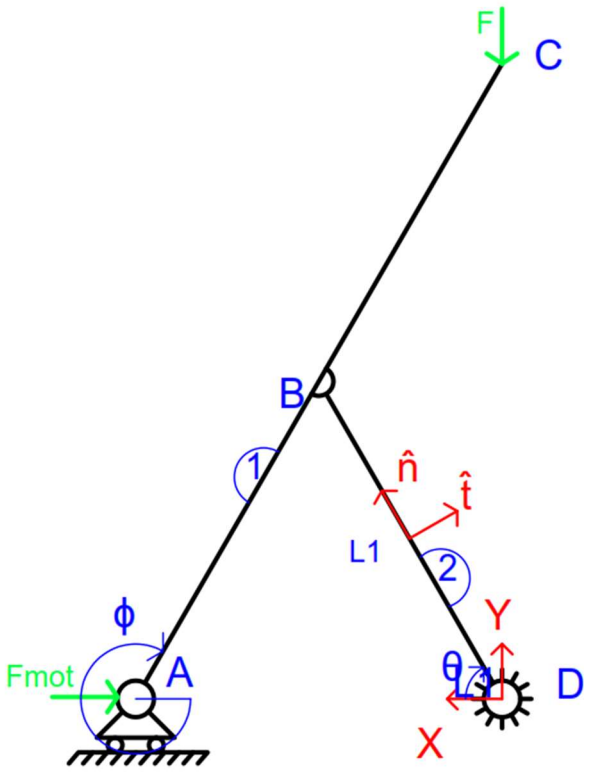

Figure 14. Schematic representation of Scott Russell mechanism

We aim to find the kinematic relation between the actuator displacement, and the movement of point C:

$\overrightarrow{x_a} = x_a\hat{x}$
$\overrightarrow{x_{B2}} = l_1 e^{i\theta} = l_1\cos(\theta)\,\hat{x} + l_1\sin(\theta)\,\hat{y} = l_1\hat{n}$
$\overrightarrow{x_{B1}} = \overrightarrow{x_a} + l_1 e^{i\phi} = (x_A + l_1\cos\phi)\hat{x} + l_1\sin\phi\ \hat{y}$

Due to the hinge in B:

$\overrightarrow{x_{B1}} = \overrightarrow{x_{B2}}$

$$\begin{cases} l_1\cos\theta = x_a + l_1\cos\phi \\ l_1\sin\theta = l_1\sin\phi \end{cases} \quad \begin{cases} \cos\theta = \frac{x_a}{2l_1} \\ \phi = \pi - \theta \end{cases}$$

Finally, I can write the displacement in C:

$\overrightarrow{x_c} = \overrightarrow{x_a} + 2l_1\cos\phi\,\hat{x} + 2l_1\sin\phi\,\hat{y} = \sqrt{4l_1^2 - x_a^2}\ \hat{y} = (x_A - 2l_1\cos\theta)\hat{x} + 2l_1\sin\theta\,\hat{y}$

$y_C = \sqrt{4l_1^2 - x_a^2}$

We can plot the relationship between the horizontal displacement in A and the vertical one in C, in Figure 15.

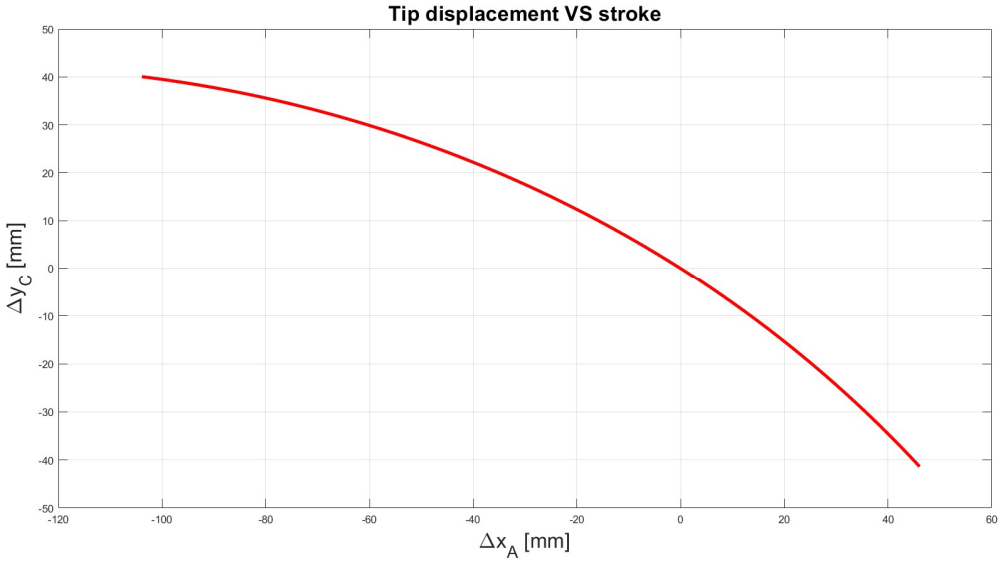

Figure 15. Relationship between movement of actuator and tip movement

We can appreciate the non-linearity of the relationship, in Figure 15 due to the trigonometric nature of the equations. In Figure 16 we can see the relationship between the motor's position and the angle the mechanism forms.

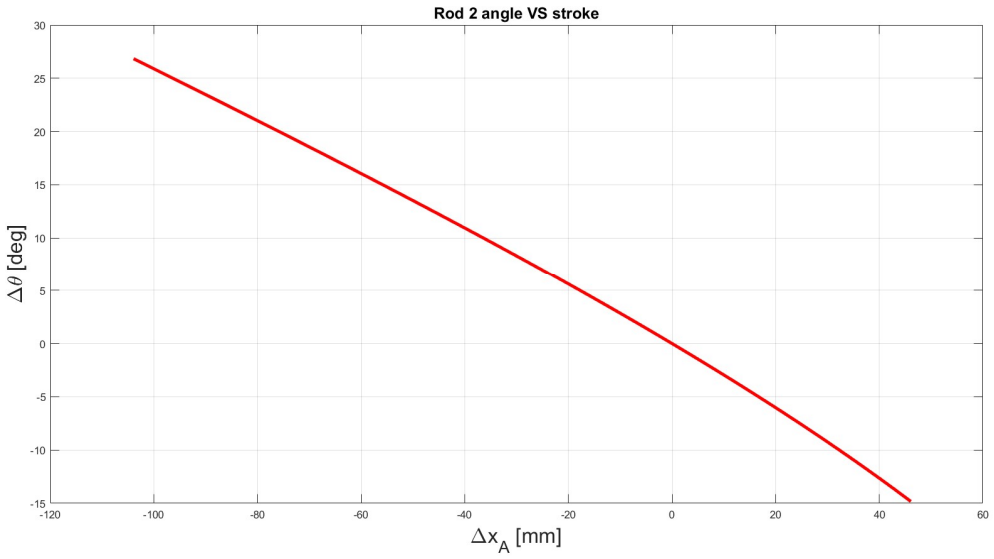

Figure 16. Relationship between movement of actuator and rod angle

Given the space constrains this mechanism will be installed in, we looked for an acceptable configuration, as described in Table 2.

Table 2. Mechanism configuration setting

L1 [mm]	120
Stroke [mm]	150
xa start [mm]	32
yc [mm]	238
yc'[mm]	156

With the so described configuration we can actuate the vertex C from a most extended position to a least extended position as shown in Figure 17.

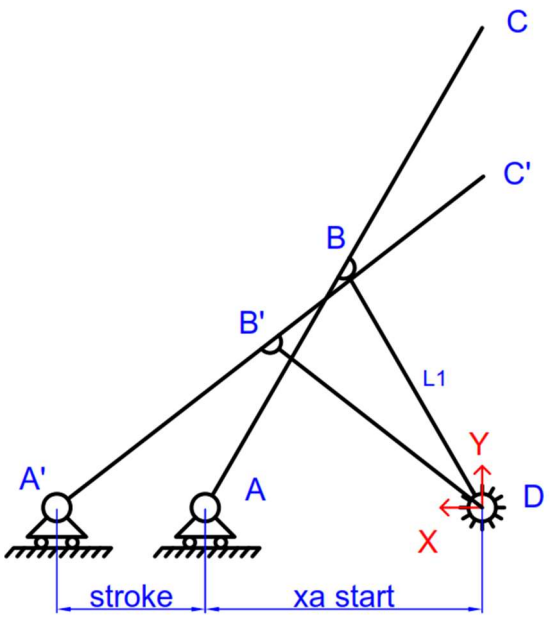

Figure 17. Difference between contract and extended position

2.2 Static analysis

Given a vertical load in C we aim to calculate the static reaction in C needed to maintain equilibrium. We can study the static problem which has only one degree of freedom. We can analytically solve the problem by decomposing the structure as done in Figure 18.

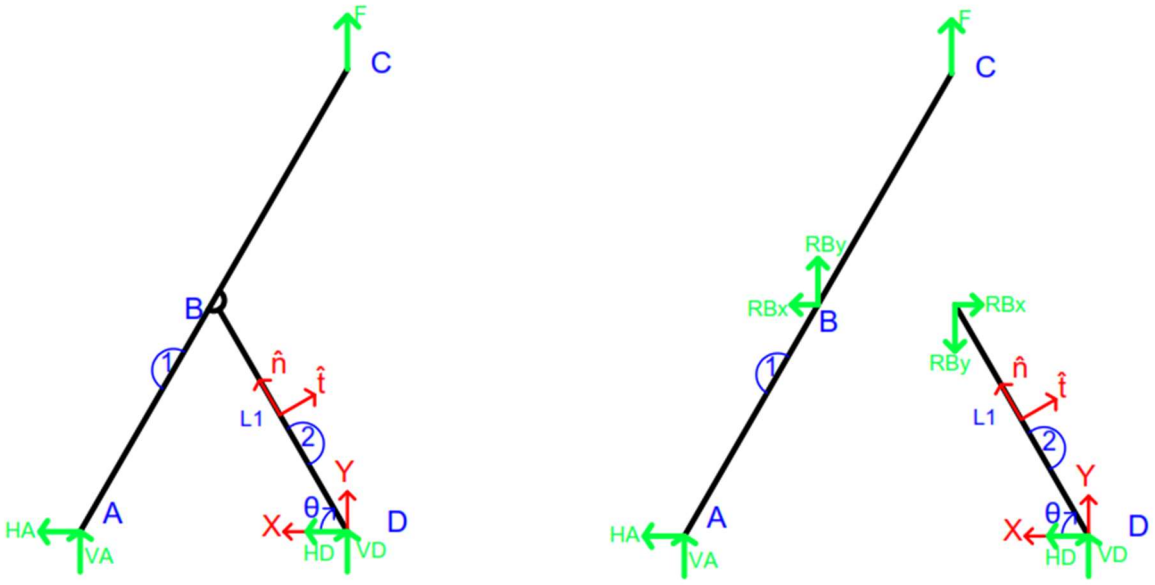

Figure 18. Static analysis

$$\sum M_d = V_A 2l_1 \cos\theta = 0 \quad V_A = 0$$

$$\sum R_y = V_A + V_D + F = 0 \quad V_D = -F$$

$$\sum M_B = -F l_1 \cos\theta + H_A l_1 \sin\theta \quad H_A = \frac{F}{\tan\theta}$$

$$\sum R_X = H_A + H_D = 0 \quad H_D = -H_A = -\frac{F}{\tan\theta}$$

To provide equilibrium, the motor will have to provide a horizontal reaction in A. Its value will change depending upon the configuration. The non-linear relationship described in the previous equations can be also seen in Figure 19.

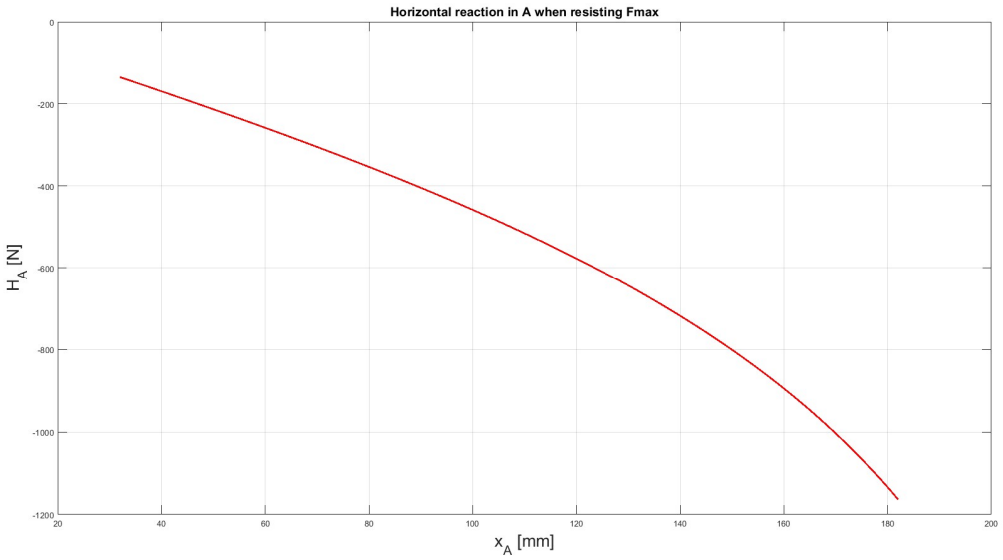

Figure 19. Relationship between actuator position and static force

In this graph we see the resisting force H_a which the motor must exert when in C a constant force is applied. We can see that when the mechanism is in the most extended configuration, the resulting leverage is favourable to the actuator, in fact for resisting a force of 1000N, the motor must produce only 200N. The leverage gets progressively less favourable for the motor, even requiring a bigger force that the one exerted in C.

Chapter 3 Load model

The actual load cannot be described with a constant force due to only aerodynamic forces, we need a more complex model, that we'll describe in this chapter. The purpose of the mechanism will be to drive the extension and retraction of the skin of the morphing structure. Unlike a conventional control surface, the morphing structure has a more complex behaviour: we need to model it with a mass/spring approximation, that provides maximum resistance at the end of the excursion of vertex C, in either direction.

From the CST and FEM simulation we can model the behaviour of the morphing structure. Unlike with a conventional aileron, the force needed for its deflection is due not only to the aerodynamic load but also to the deformation needed. From the simulation we can see, as depicted in Figure 20, that we can with good approximation model the load as a spring.

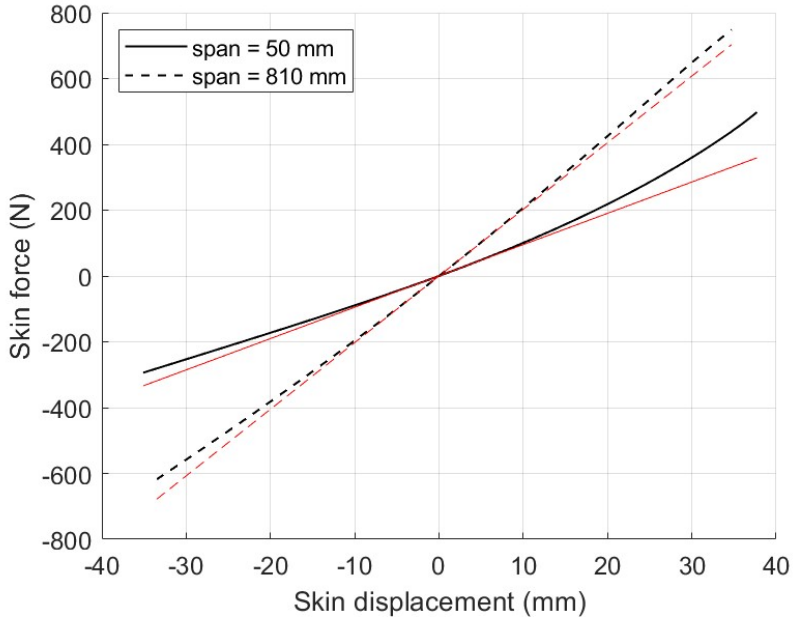

Figure 20. Load from Abaqus simulation

We can therefore proceed with a linearization of the load, modelling it with 2 springs as describes in Table 3.

Table 3. Load springs model values

$k_{root}\ [^{N}/_{mm}]$	9.5
$k_{tip}[^{N}/_{mm}]$	20.3

In the contest of the HERWIGT project a demonstrator will be built. It will be full scale in chord but limited spanwise to 2 meters. Each meter of the demonstrator, as shown in Figure 21, will be independent from the other. The test will be carried out in Polimi's Wind Tunnel, with a maximum Mach number of 0.15.

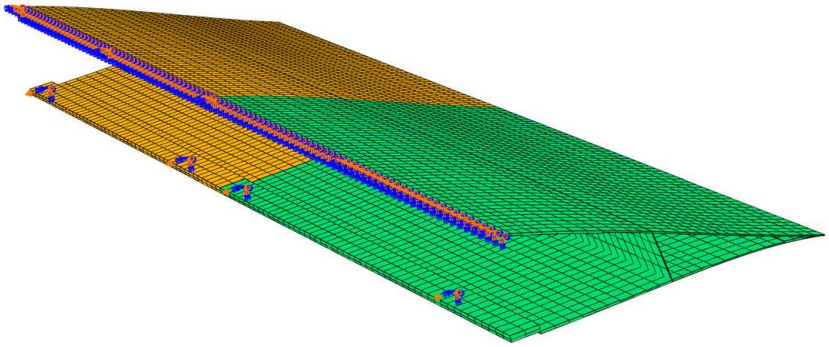

Figure 21. Finite element model of the complete morphing aileron demonstrator.

Each section has 2 actuation points, that will be actuated by one motor, via a double Scott Russell mechanism, as shown in Figure 22. The demonstrator will therefore have 2 motors, which will actuate independently each section.

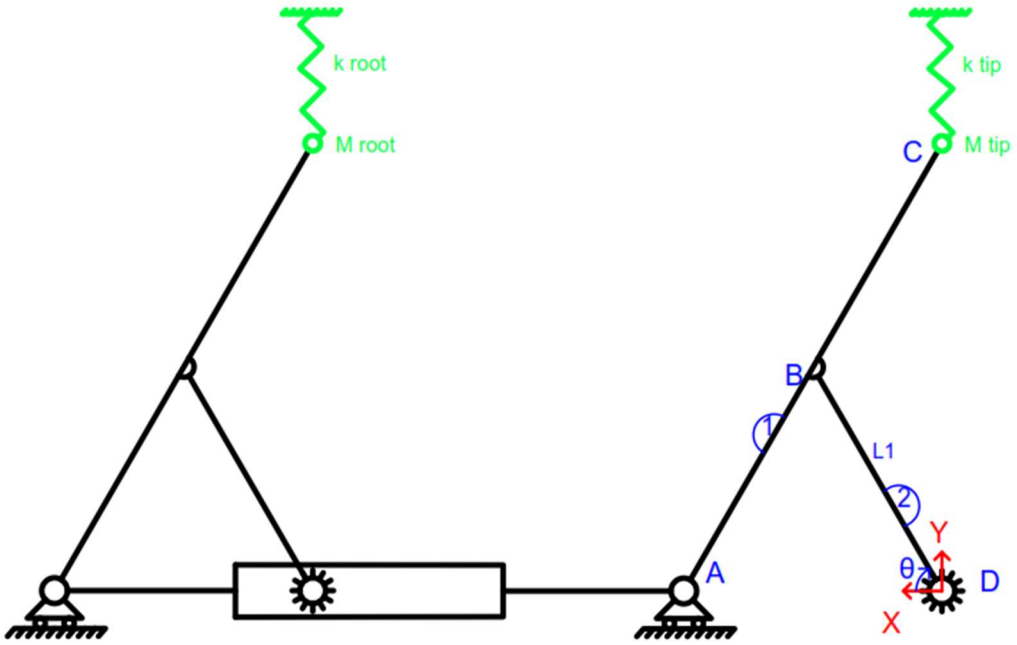

Figure 22. Double Scott Russell mechanism

The result of the linear actuation of the points indicated in Figure 21, is shown in Figure 23. Of note, the reinforcements installed in the actuation zone, where the Scott Russel system transfer the force to the morphing structure.

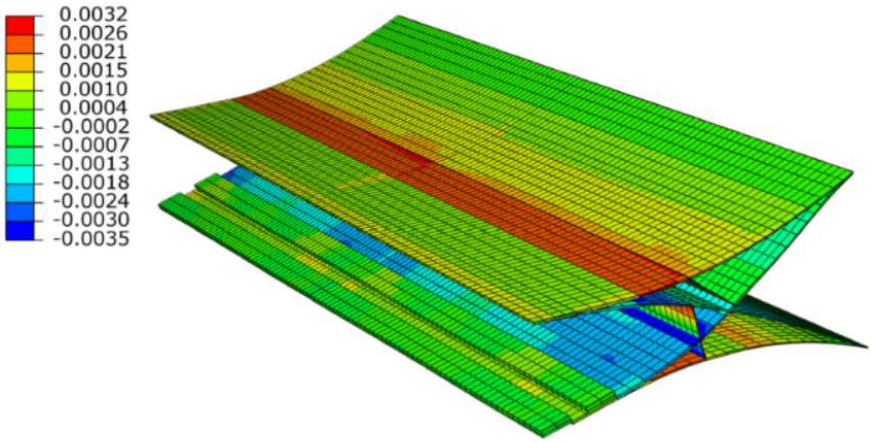

Figure 23. Finite element results in terms of maximum principal strains for the complete morphing aileron demonstrator, for downward and upward maximum deflections.

If we consider the rigid static case, we can equate the scheme of Figure 22 to the simplify system mass/spring of Figure 24 with characteristics of Table 4.

$$K = k_{root} + k_{tip}$$

$$M = M_{root} + M_{tip}$$

Table 4. Load model configuration

K [N/mm]	29.8
M [kg]	11.12

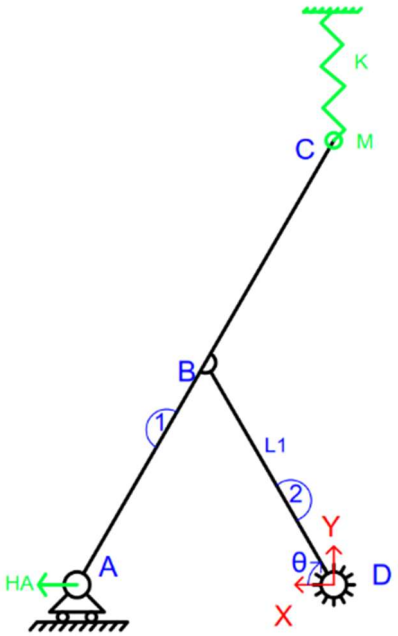

Figure 24. Mechanism with load

The force that the actuator will need to provide to balance the force of the spring and leaving the vertex C in the desired position will be depending on the position itself according to the Figure 25.

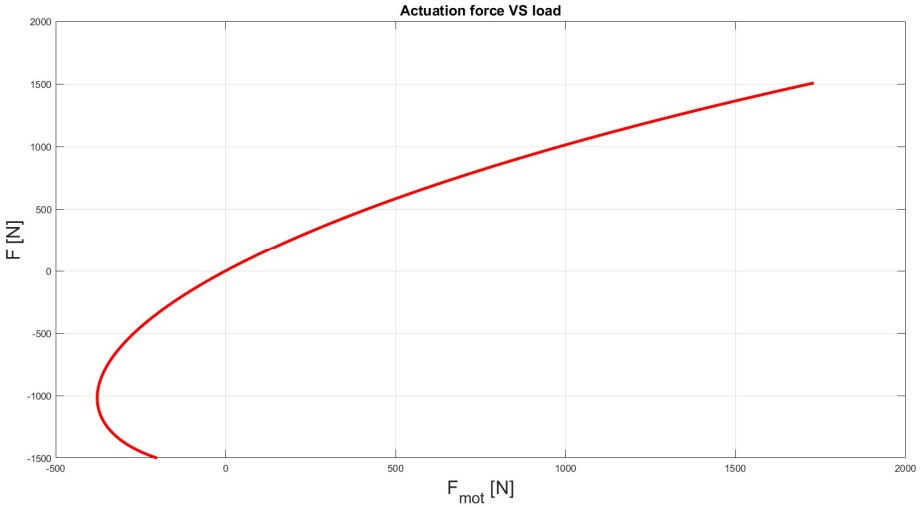

Figure 25. Actuation force with modelled load

We expect to have a free natural frequency provided by the Abaqus simulation of 8.24Hz.

$$\omega = 2\pi f$$

$$M = \frac{K}{\omega^2}$$

Chapter 4 3D model

The development of a 3d model is necessary in order to evaluate the dimensions of the components needed for providing the desired range of motion. At this stage it's also important to have a precise idea of the size of all the linkages and connecting components of the mechanism. This information will be important in the following chapters. The HERWINGT aircraft has been developed using the CAD software. We can appreciate an overview of the high aspect ratio wing, in Figure 26 and a detail of the quite narrow tip, in Figure 27.

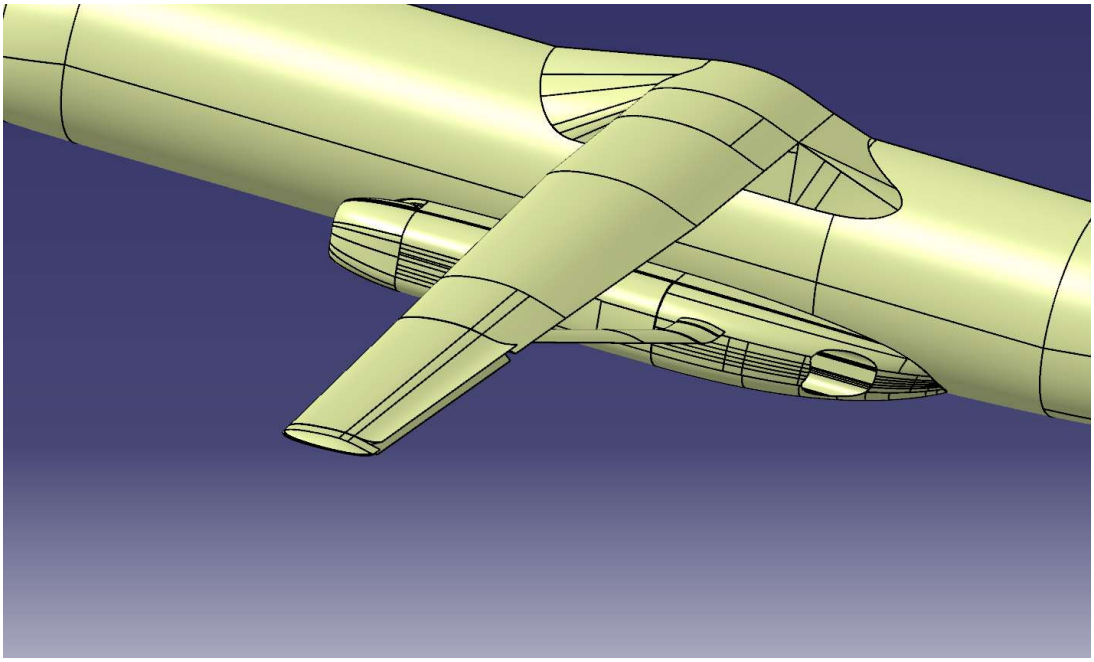

Figure 26. CAD model of the complete aircraft in Catia V5

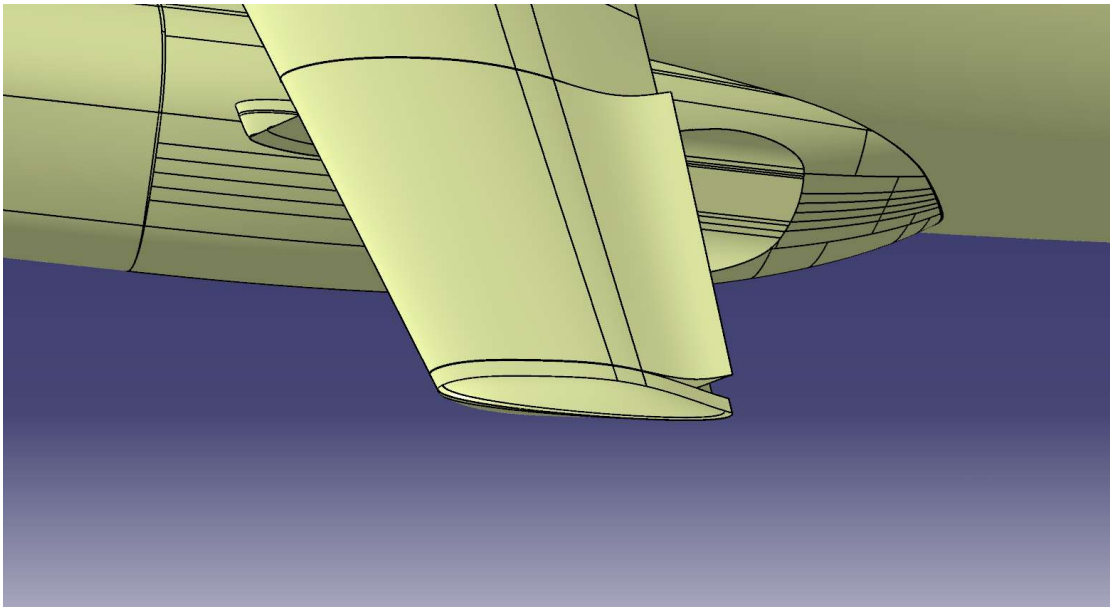

Figure 27. CAD tip detail

To gauge the available space for the motor, we start from the already developed Catia V5 model of the entire aircraft. We can see, in Figure 28, how limited the available space is.

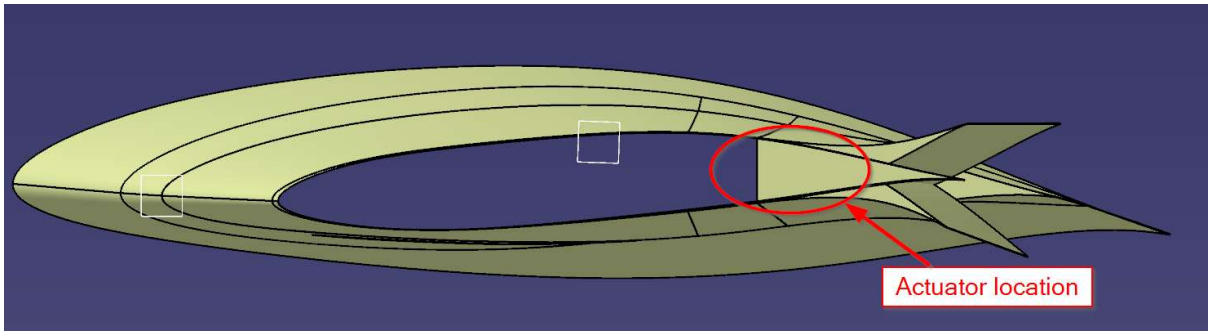

Figure 28. CAD detail of the available space

We will install the actuator on the outside of the wingbox, to facilitate installation and to aid the general maintainability of the system. We aim to design the mechanism in order to fit in the most narrow wing, section, the tip, which has dimensions as described in Figure 29 and Table 5.

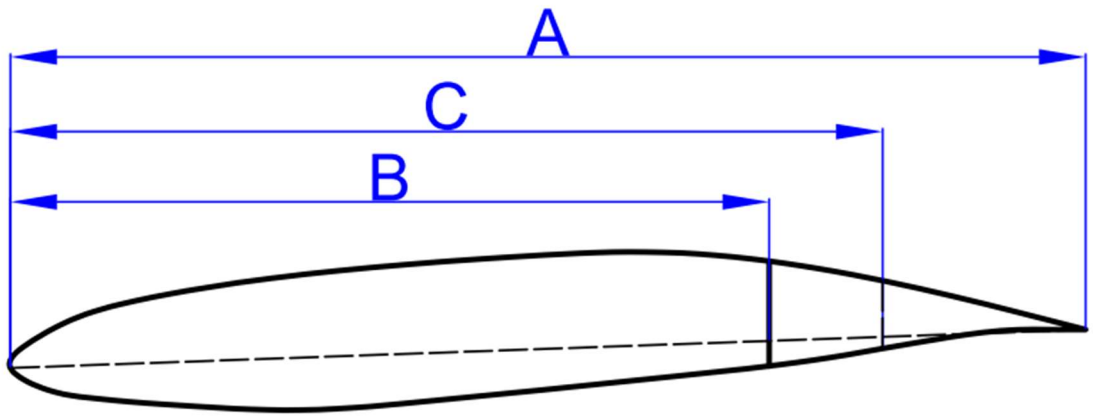

Figure 29. Characteristic dimension of the wing tip

Table 5. Wing dimensions

A[mm]	1420
B[mm]	852
C[mm]	1036

The quote C indicates where the mechanism shall attach itself with the extensible skin. Having considered the tip, where the dimensions are most constrained we have only a small space for placing the mechanism. Since we aim to move the skin by about 80mm, it is not possible to install the motor parallel to the chord. We must indeed implement a mechanism to comply with the stringent space requirement.

The goal is to mount the induction motor directly onto the wing box, in the direction of the wing, as shown in Figure 30. The additional ribs will be mounted orthogonal to the wingbox. Attention will be needed to route the cooling lines of the motor as well as the data cable and the 3 phase power wires.

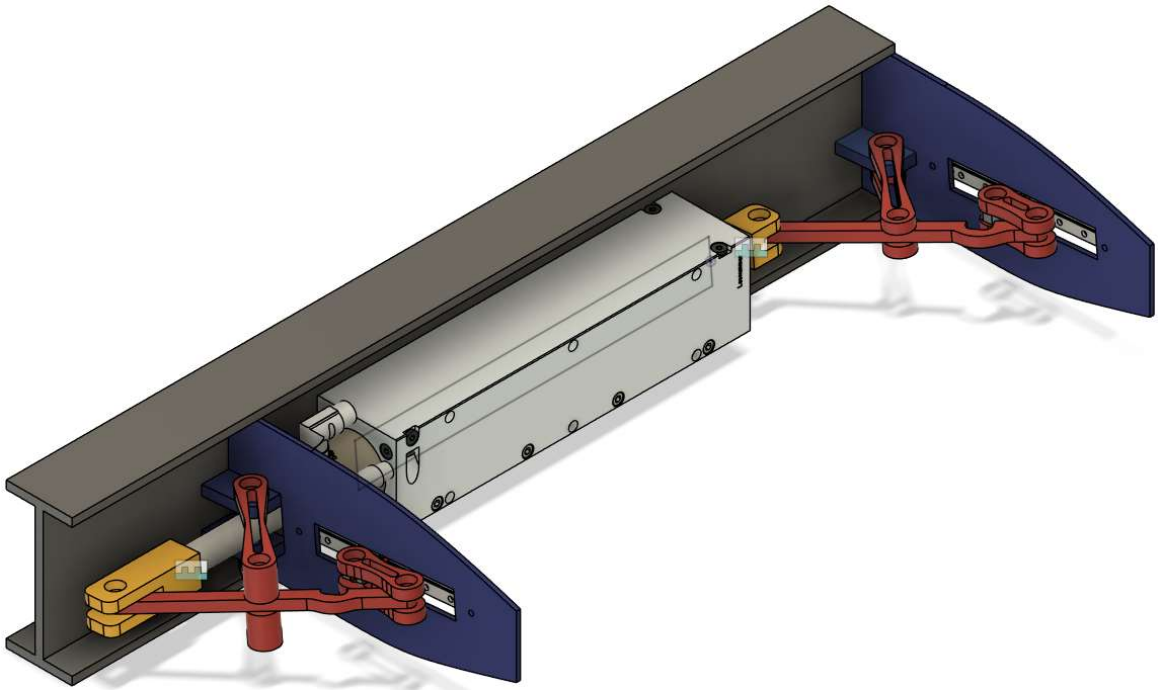

Figure 30. Fusion 360 model.

Rotation between the components will be granted via bearings. Slots for hosting them are provided.

A linear slider, a detail of which can be appreciated in Figure 31 and Figure 32, has been also installed for taking care of potential perpendicular loads. This would be unwanted loads for the motor which can provide only forces aligned with its axis.

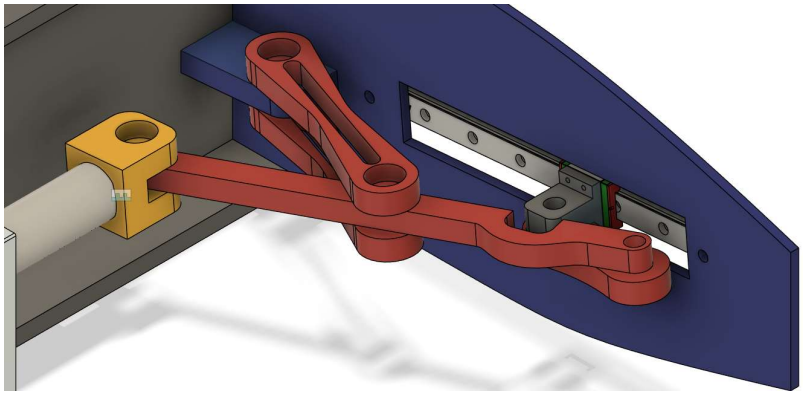

Figure 31. Fusion 360 model, Scott Russell detail

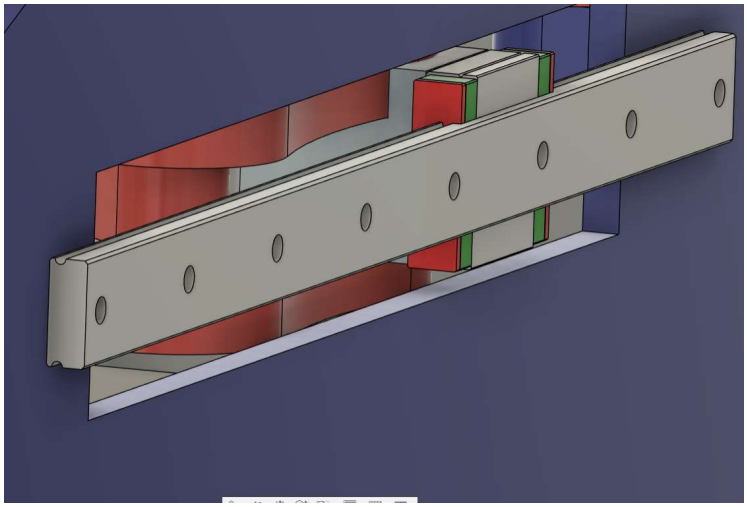

Figure 32. Fusion 360 model, extra support detail

The supporting rib provides an angle in order to actuate the morphing structure as per design. This inclination, evident in Figure 33, does not affect the motor, which can actuate in an axial-symmetrical manner.

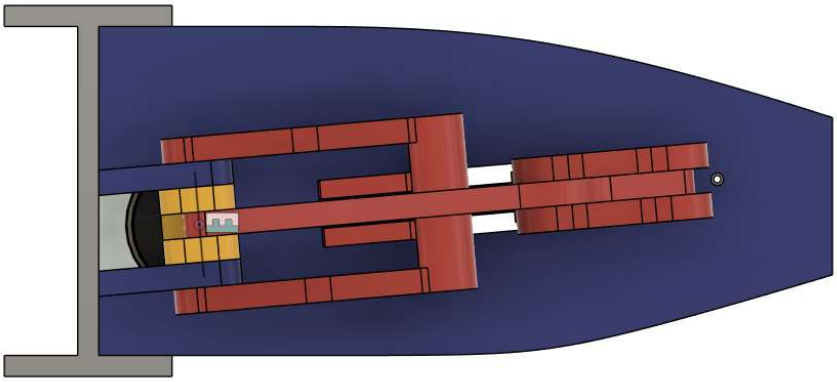

Figure 33. Fusion 360 model. Lateral view.

This mechanism will allow us all the positions between the least retracted configuration of Figure 34, and the most extended configuration of Figure 35.

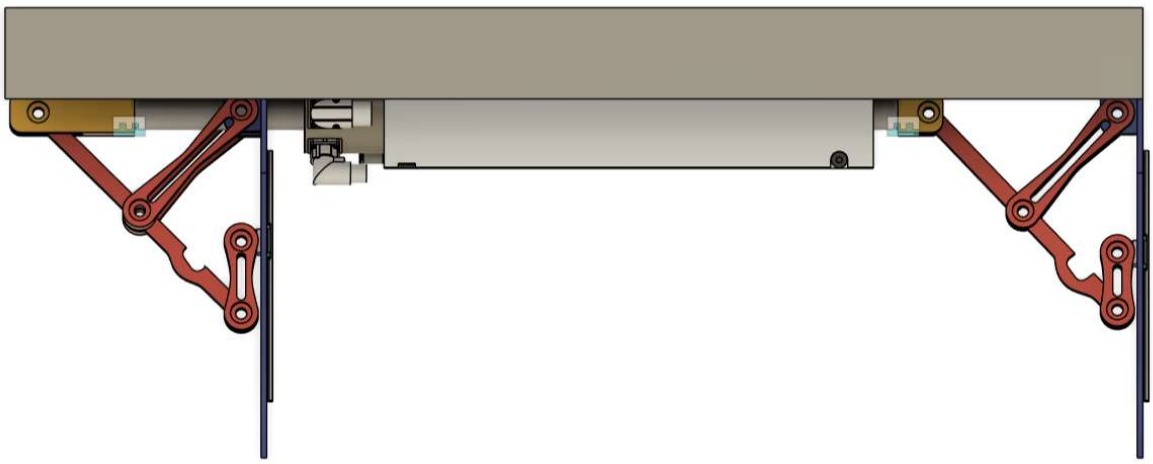

Figure 34. Collapsed configuration

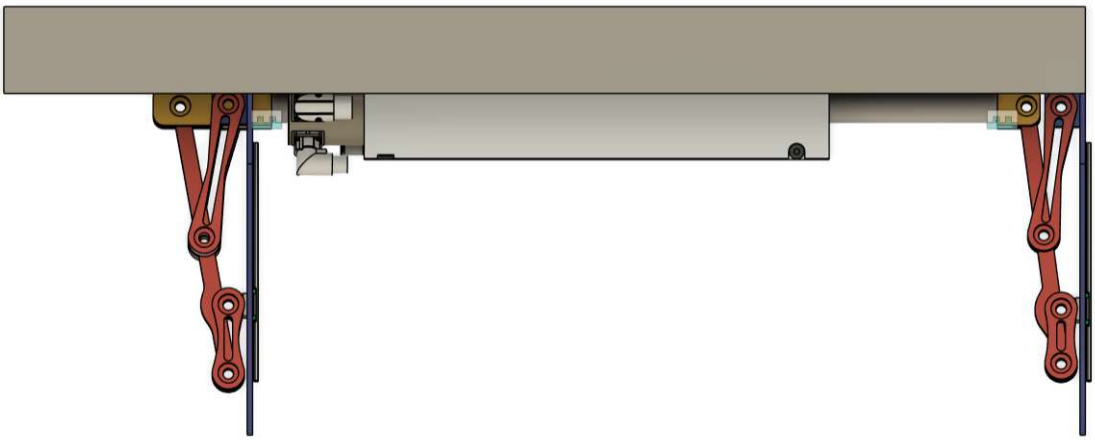

Figure 35. Extended configuration

With a precise positioning system provided by the encoder installed natively inside the motor we can determine the position of the vertex of the mechanism.

We will install two of such assemblies on the demonstrator, as described in Figure 36.

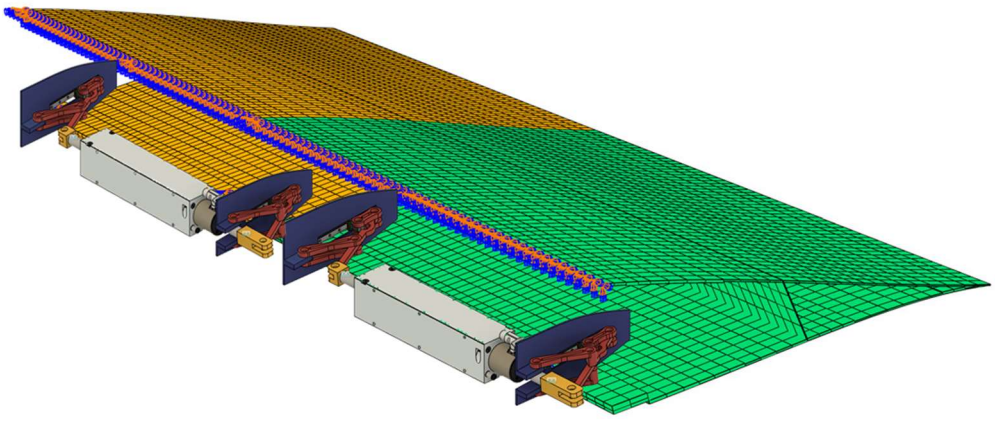

Figure 36. Configuration on the demonstrator mock up

Chapter 5 Dynamic model

An important output of the 3d model is the dimension of all the linkages and components needed. We need the size of the mechanism's components to study the dynamic characteristic of the system. The need of a mechanism, caused by the dimensional limitation due to the size of the wing, introduces another element in the chain between the motor and the load. We must be able to model and evaluate the consequence of the presence of such a mechanism, especially since it introduces a nonlinear relationship between the position of the actuator and the position of the load. A dynamic model will allow us to answer questions about its behaviour, when subjected with certain input or control logic. We need a solid dynamic model to test if our solution can perform according to the requirements.

5.1 Analytical approach

An analytical approach would be possible, by studying Euler–Lagrange equation. It is true that the system has only 1 DOF, but it would be hard to model the mass distribution of the numerous components, given the relative complexity of the moving parts. One approach, when dealing with complex mass distributions, would be to deploy a Lumped-element model. This would be a valid approximation, but we'll lose the actual mass distribution of the components themselves. Since certain linkages are subject to significant gradient acceleration, this would not be advisable.

We would also need to model damping matrix C. Modelling this matrix is always complex, we could, for instance, deploy the Rayleigh Damping model.

This approach involves a certain number of approximations, namely in the modelling of the distribution of mass. It would also be limiting in a parametric study of the problem. Finally, it would be a useful result specifically in the study of a dynamic response. We would love to obtain a solution that we could use in different domains.

5.2 Model based design (MBD)

Model based design is a novel approach that aim to build a digital twin of the system we are studying, capable of running simulations. On this model we can validate the requirements by running scenarios, to make sure that the system can indeed provide the required performance, in terms of safety and general behaviour.

We could also study the response of linear and nonlinear input with much more ease that with the previous approach.

This approach is only in recent years become viable, industry side, since the computational load is significant. Even performing a simulation with a few DOFs, can be demanding since we are solving a complex dynamic system, possibly across different domains.

We aim to build a life like model and this means modelling all system components, with their peculiar behaviour: we need to be able to describe motors, gears, joints, controllers and so on, across different domains.

With computers powerful enough, we could even implement hardware in the loop logic, with a high-level architecture shown in Figure 37 .

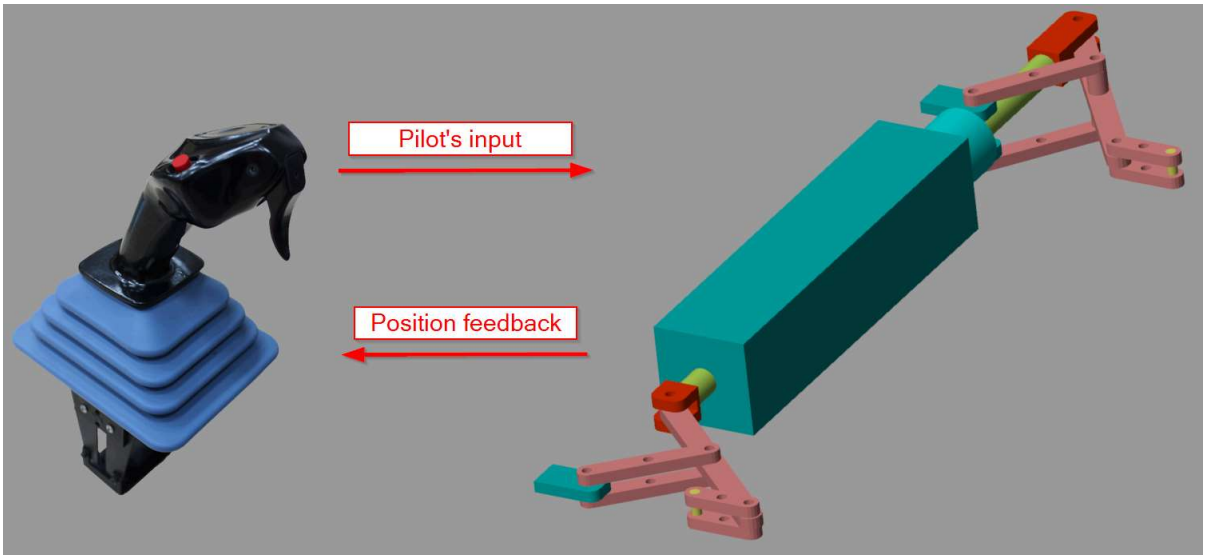

Figure 37. Possible Hardware in the Loop configuration

This would mean connect to the model the physical cloche with which the user could input a roll command. This could be doubly useful. In one way we could see how an actual command input would affect the dynamic of the control logic, and on the other hand we could use a feedback from the model for designing the resistant force on the command. Since the advent of command by wire all pilots feedbacks have always been "artificial". Since the introduction of the Airbus A320, fly by wire has become the norm in civil aeronautics. The command is not physically connected to the physical actuation, it just provides a voltage setpoint that the control logic must manage accordingly. This raised the problem of lack of feedback on the actual command, used by the pilot. It is important to simulate a lifelike "resistance" on the command. HIL could speed up significantly the development of modelling a feedback that has be as communicative as possible.

A MBD allows us the explore several approaches regarding the control logic. We could implement a PID controller or adopt a more complex approach instead. With the control logic in place we could see how the system reacts to disturbances: we could study its robustness and stability, after having injected in the simulation sources of uncertainties.

No matter how accurately we describe our model, we must always validate the result of the simulation with other methods. This could be a simple analytical static model, or a model developed using radically different technologies, such as with Abaqus.

Building a model in Simscape would give us the means to explore the problem in much more detail. Simscape is a powerful Matlab environment which allow us the create physical model of our system, with its exact geometry and dynamic characteristics. It represents a digital prototype which we can use at will, in the advance phases of design. At this stage a physical prototype would be usually needed, since most of the components have been defined. We would need to procure all the components such as motors, controllers and bearing, as well as to manufacture all the needed linkages (possibly in carbon fibre). On this physical prototype we could then perform a series of test such as ground vibration test, frequency response test, control law test and so on.

All of that can be performed in the Simscape environment, given us several advantages:

1. Time. Instead of waiting for the procurement and manufacturing of parts, we could start performing the desired analysis right away after the 3D modelling phase.
2. Cost. Expensive reworks of components can be avoided. By studying the Simscape model we could catch issues soon and avoid time consuming and costly refittings.
3. Optimization loops. In consequence of the analysis performed on the Simscape model we could go back in the 3D model and optimize certain geometry to better suit out need.

In short, we can now far more quickly iterate different solutions and performing prototyping loops much faster and cheaper than with a physical prototype. Ideally, after all the tests have been performed in Simscape, we would then produce a prototype which is in no need of further tweaking: we would only need to test that the experiments performed on the physical prototype are aligned with the one in the digital world.

The strength of this solution is that, once we have developed the highly parametrized model, we can then perform great number of experiments on it, ranging from time-based frequency response to frequency base stability study.

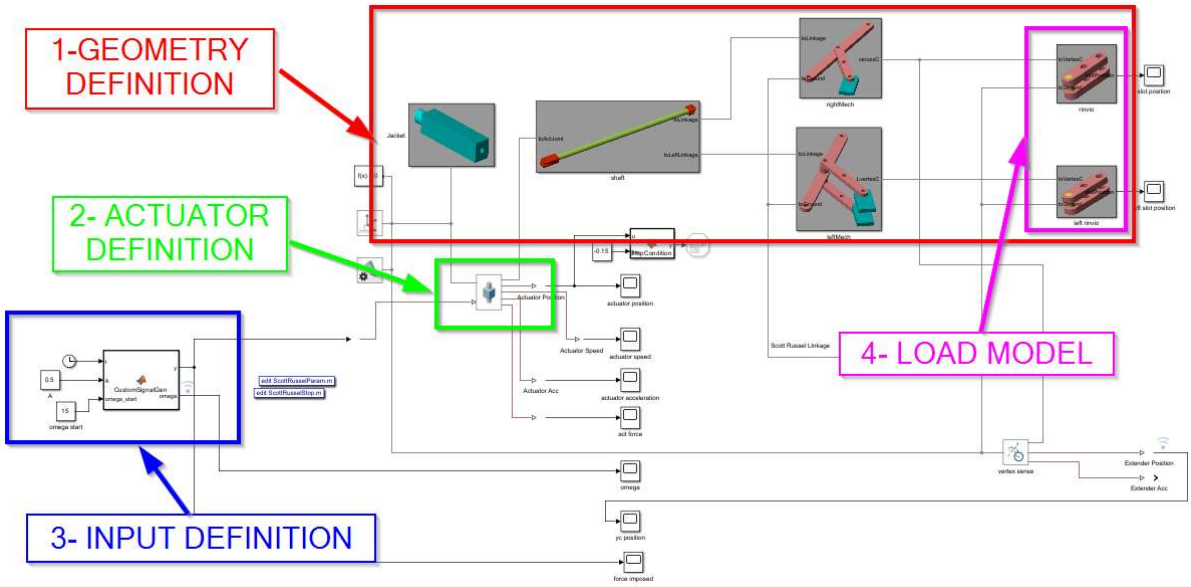

Figure 38. Model architecture

We can broadly speaking divide the model three macro areas as shown in Figure 38:

1. Geometry definition. Here we can import a geometry from our favourite CAD software or design an equivalent component using integrated tools and Matlab functions. Components have inertial qualities that can be defined in detail. Here we define also the relationships between components. We can characterize joints with a stiffness and a dumping coefficient. Most of our joints are ball bearings, such information is usually provided by the manufactures. For SKF deep groove ball bearing we could model the damping coefficient with the formula: $\eta_v = 2\,\pi f c \backslash k$, with a model derived by the dynamic system of Figure 39. η_v is about 1% and represents a loss factor. k is the stiffness of the bearing and f is the frequency we are testing the bearing at. This empirical data is provided by the manufacture who has conducted extensive test on its products

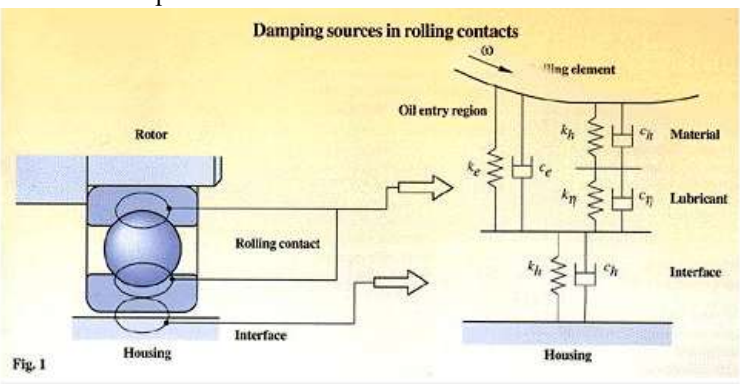

Damping sources in rolling contacts

Figure 39. Manufacture's damping model

Inside Simscape, a joint can be described in detail, as shown in Figure 40. We can integrate our result in the model of the joints.

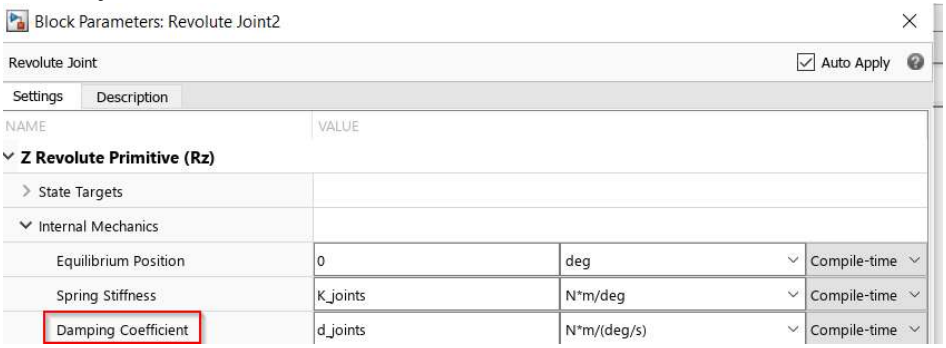

Figure 40. Example of joint configuration in Simscape

2. Actuator definition. Here we can model the actuator with its internal dynamic. We can assign a stiffness and a damping and define how we want to control the action. A possible improve of the present model would be to integrate the electric model of the motor since Simscape allows for cross domain modelling we could model the dynamic equation of the induction motor.
3. Input definition. We can provide here the time-based signal with which we wish to control the actuator. This could be a fixed frequency signal, a sweep, a set-point or any other input we deem of interest.
4. Load model. With the result previously gathered we can input here the model of the load. We have decided to model it as a spring mass element therefore we can tune the internal stiffness of a sliding joint to provide such stiffness. We can model the mass as the yellow component which hold half the mass of the model. The load model was developed after a linearization, we could develop a more sophisticated model, one that considers even the damping caused by the morphing component. We could then easily insert the more complex model here, quickly analysing the result of such a change.

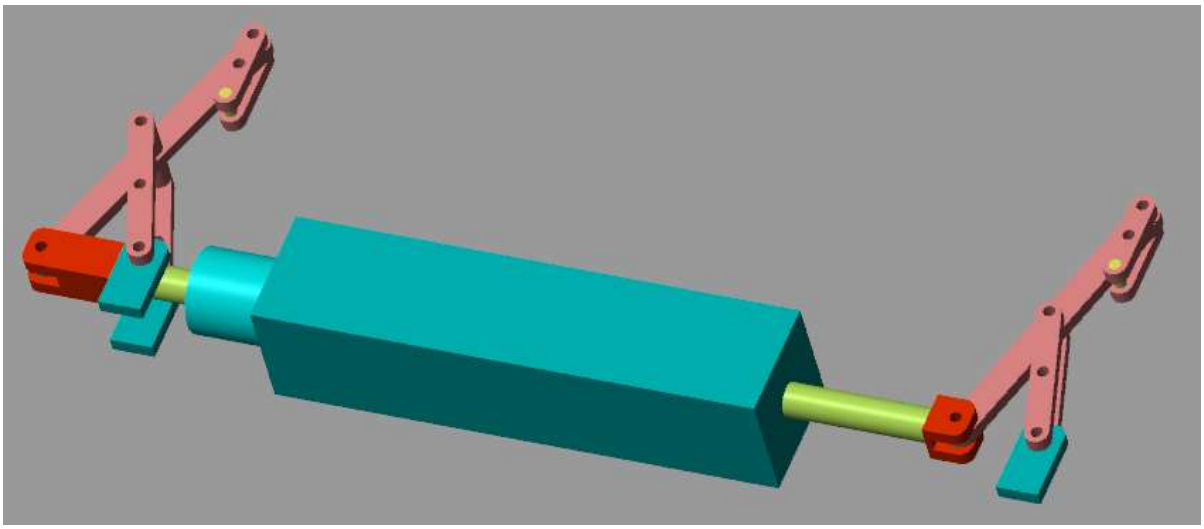

Figure 41. Simscape 3D model

We can see the Simscape model in Figure 41. This model is less geometrically detailed than the one developed in Fusion360. This is not an issue because this model has not the purpose of stress analysis, for doing so we could deploy FEM simulation, carried out in dedicated software, where the rigidity of the components can be properly considered.

Chapter 6 Validation

It is very important to validate the model developed with Simscape. Since several test and experiments will be run on said model, it is paramount to validate its accuracy, to indeed treat it as a digital twin. We can carry on this task in two ways: first we validate it against the static analytical case, which we discussed in the previous chapter, then we validate it against another model developed using a radically different technology.

6.1 Static model

Since we solved analytically the kinematic model, we can perform a verification of the digital twin by applying an actuation force, and monitoring the position of the vertex C. Given the load described in chapter "Load model", the relationship between force applied and actuator position, is known and described in Figure 42.

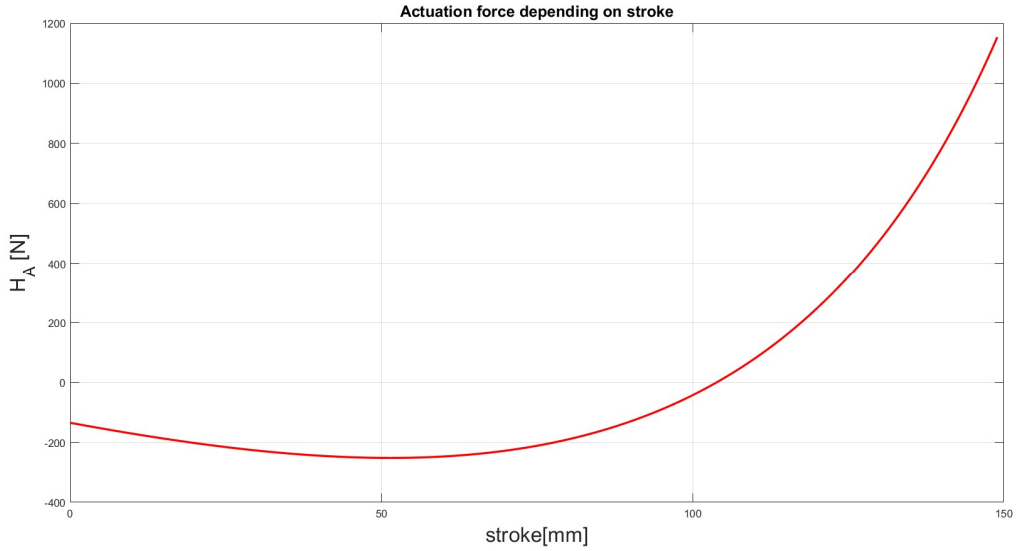

Figure 42. Stroke vs actuation force

The first validation test we can perform is just to ask the motor to provide a desired force and check the position of the actuator. We must note that the relationship is not monotone: in the first part of the stroke, the obtained position will depend upon the starting condition. The validation regarding these configurations will be described in the chapter 8.5, after the introduction of the PID controller.

In Figure 43, Figure 44, Figure 45, Figure 46 we apply a force to the model, and we test where the actuator finds its equilibrium. We compare this result with the expected position, from the analytical solution.

In the following figures useful specification needed for reproducing the simulation are noted, such as the dimensional dumping coefficient d.

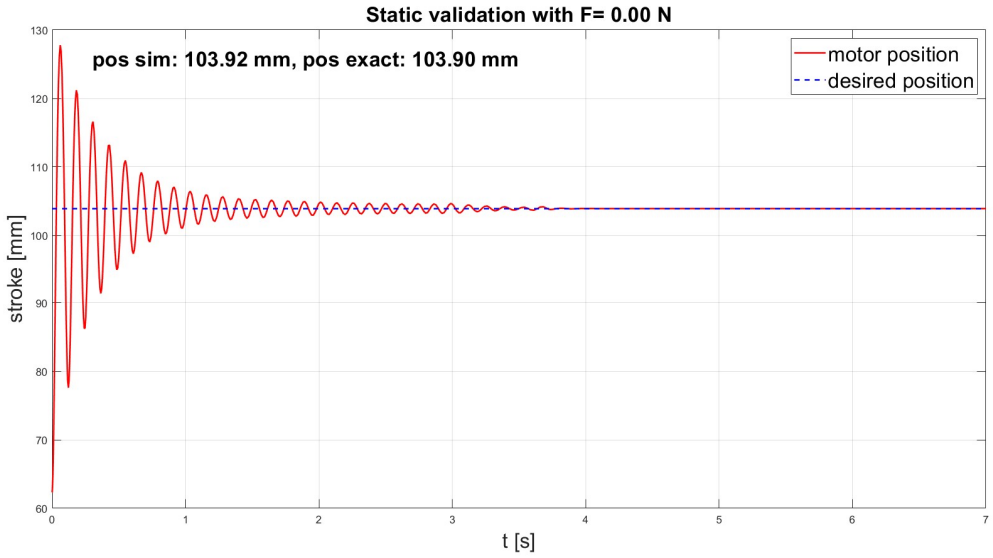

Figure 43. Static validation. F = 0N, lever_V12, d=30, stroke start = 80mm, mood4_20240905_1708.dat

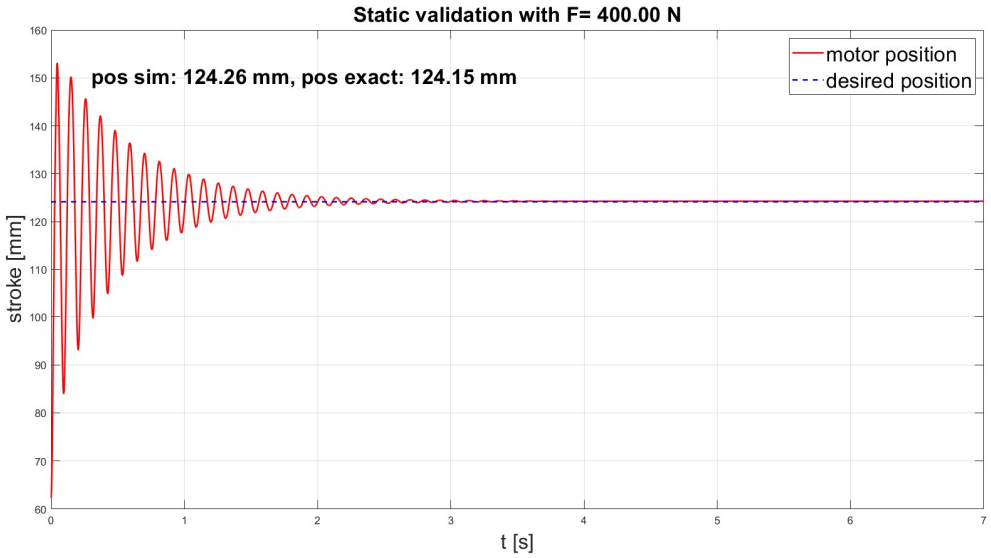

Figure 44. Static validation. F = 400N, lever_V12, d=20, stroke start = 80mm, mood4_20240905_1714.dat

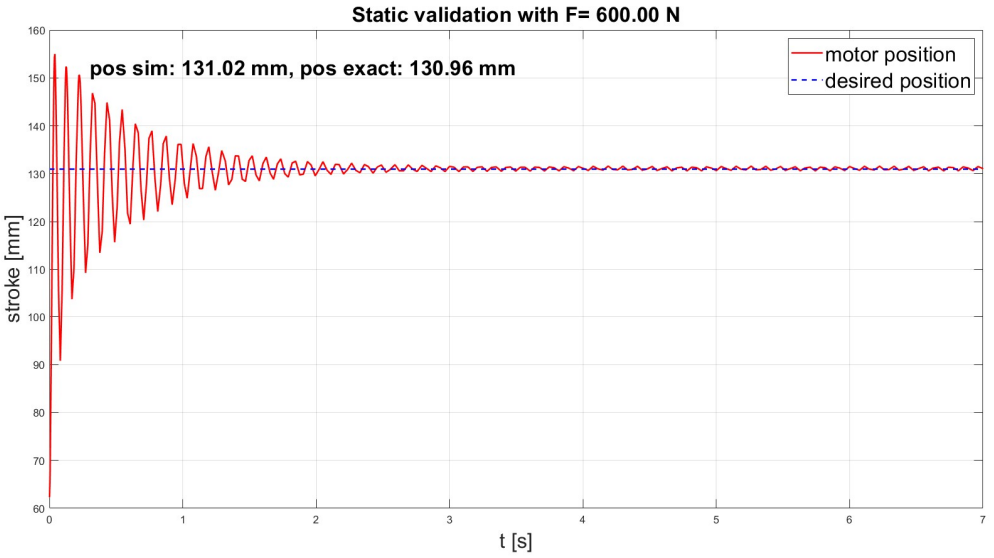

Figure 45. Static validation. F = 600N, lever_V12, d=30, stroke start = 80mm, mood4_20240905_1716.dat

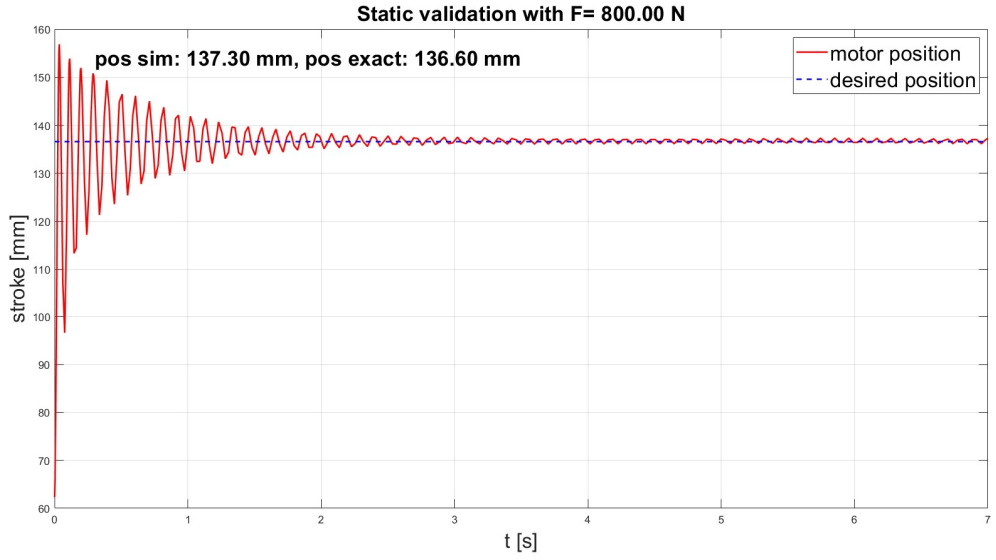

Figure 46. Static validation. F = 800N, lever_V12, d=30, stroke start = 80mm, mood4_20240905_1723.dat

Finally, we can compare the result of these tests, in Table 6. The Simscape model provides results aligned with the static analytical solution.

Table 6. Static validation results

F[N]	Simulated position [mm]	Analytic position [mm]	err [%]
0	103.92	103.84	-0.08
400	124.26	124.15	-0.09
600	131.02	130.96	-0.05
800	137.30	136.6	-0.51

6.2 Abaqus simulation

Another relevant way to validate our model, is to compare it with another obtained in a radically different environment. In this case we will compare with the results of an Abaqus simulation.

Abaqus is a powerful environment that allow for performing finite element analysis. One of the most interesting simulation, was the analysis of the response of a signal with a sweep excitation. The signal used has a variable frequency, from 0 to 15Hz as depicted in Figure 47. The signal's frequency keeps increasing, with time, thereby exciting the system on a large spectrum. In the response the natural frequency will be quite visible.

We can feed the very same excitation signal to the Simscape model and compare its response to the one provided by Abaqus.

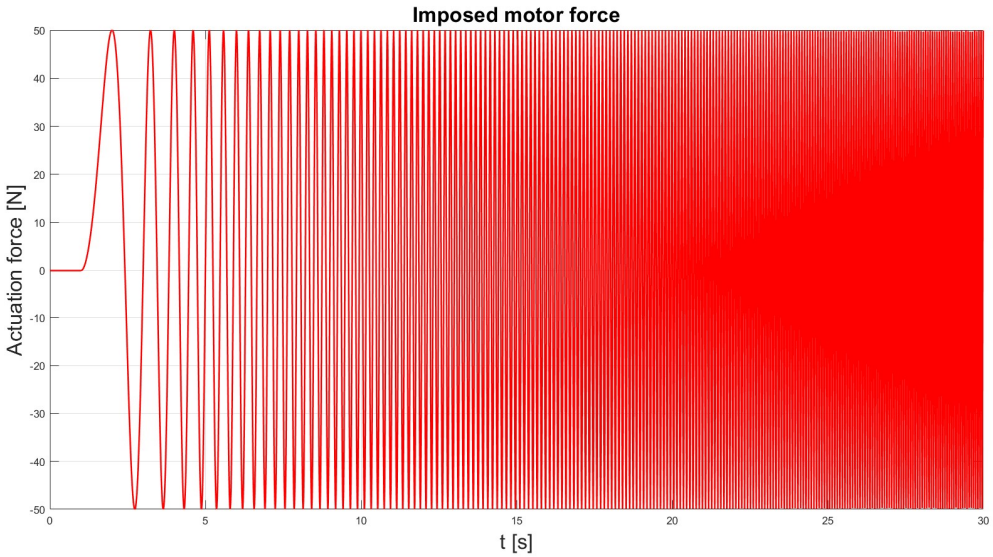

Figure 47. Imposed force. Sweep from 0 to 15Hz.

When ask the actuator to impose such a force, we obtain a movement of the mechanism. In Figure 48 we can appreciate how the two very different in nature models, predict analogues movement.

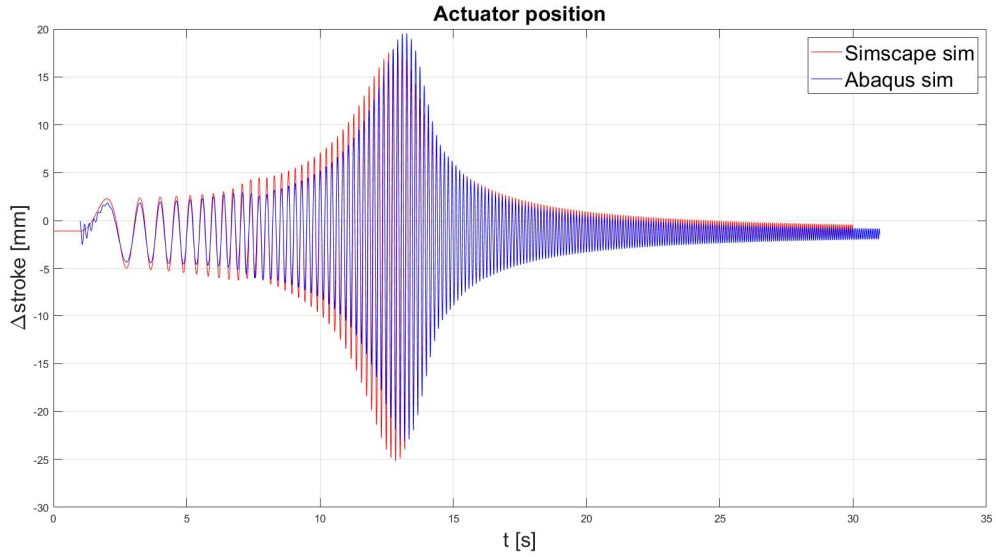

Figure 48. Comparison, regarding the motion obtained after a signal is imposed via actuation force in two different simulations. mood2_20240827_0735, lever_V12, d=62

Another interesting behaviour highlighted by the Abaqus simulation in a phase inversion, which occurs after we cross the natural frequency, of the obtained movement in respect to the applied force. This interesting characteristic emerges in our model as well and we can observe by overlapping the two signals, one (the force) imposed and one (the shaft's position) obtained, as we do in Figure 49.

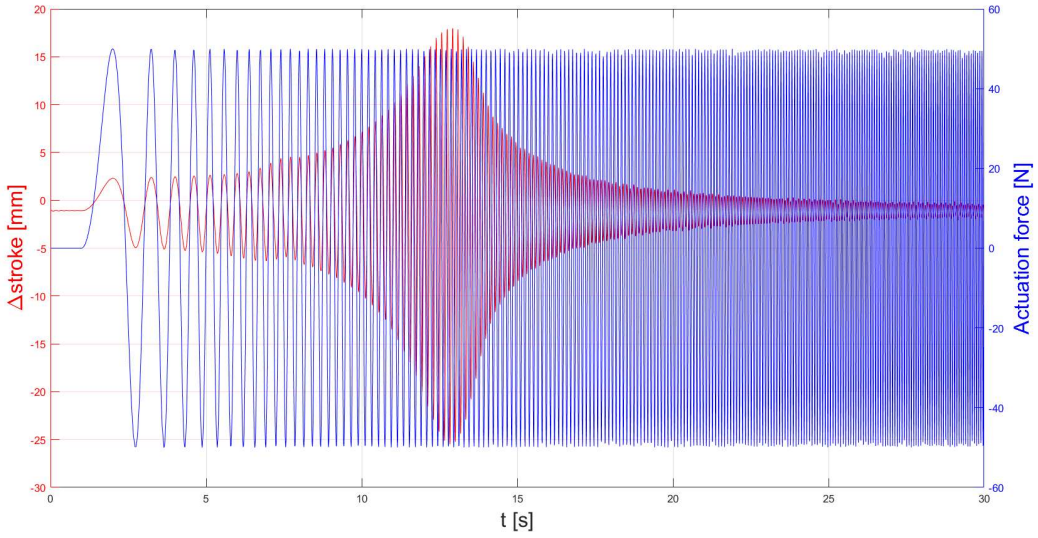

Figure 49. Analysis of the movement obtained when a force signal is imposed. mood2_20240827_0951, d=62

We note, in Figure 50, that if we impose a force with a frequency smaller than the natural frequency, the movement obtained is in phase.

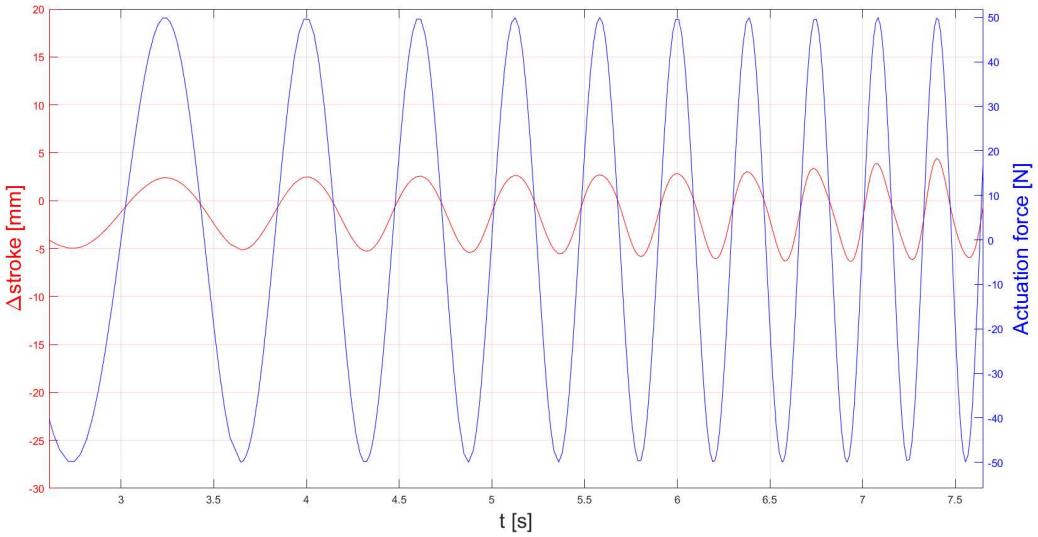

Figure 50. Movement obtained when a force is imposed with a frequency less than the natural frequency.

On the other hand, we can see that is Figure 51, that if we force the motor with a frequency greater than the natural frequency, the movement is out of phase.

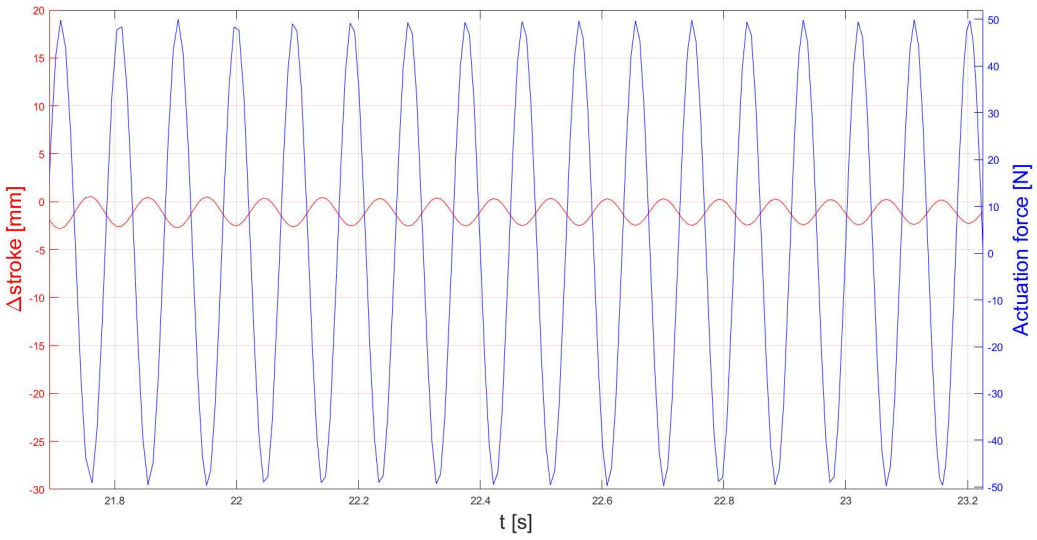

Figure 51. Movement obtained when a force is imposed with a frequency greater than the natural frequency.

We must also verify that the frequency response is also well captured by our model.

Knowing the nature of the model, 1 degree of freedom, mass spring damper system, we can approximate the transfer function as having 2 poles and no zeros, in the form:

$$H(s) = \frac{X(s)}{F(s)} = \frac{1/m}{s^2 + c/m\, s + k/m}$$

We can therefore deploy the Matlab function "tfest" which estimates the transfer function using time domain data coming from the two different simulations. We can appreciate that the models are well aligned, especially in the evaluation of the natural frequency, as evident in Figure 52.

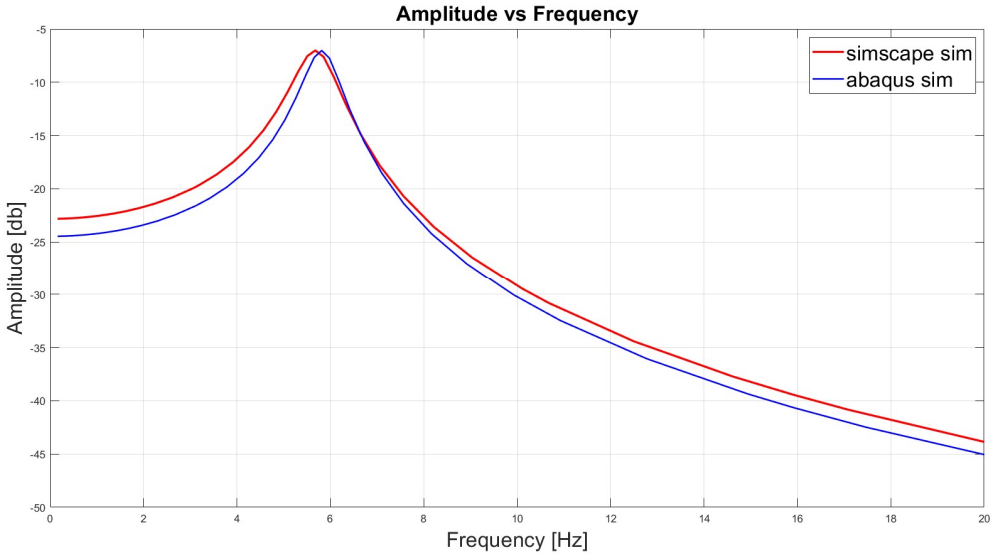

Figure 52. Frequency response of the2 models. mood2_20240828_0743, lever v12, d=62

We can also evaluate in Figure 53 the bode diagram of the results coming from the two different models.

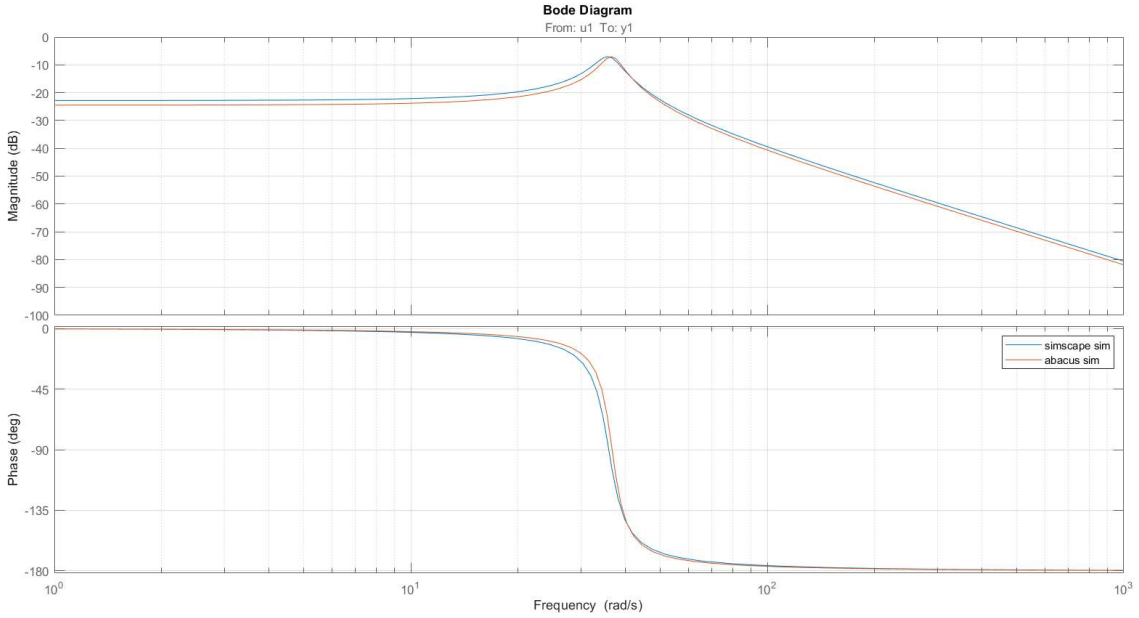

Figure 53. Bode diagram of the two simulations

The phase inversion becomes evident in the bode diagram.

To validate the approximation, we made about the nature of the system, we can perform an FFT straight from the data provided by the Abaqus simulation. We can see the comparison in terms of amplitude in Figure 54 and in terms of phase in Figure 56.

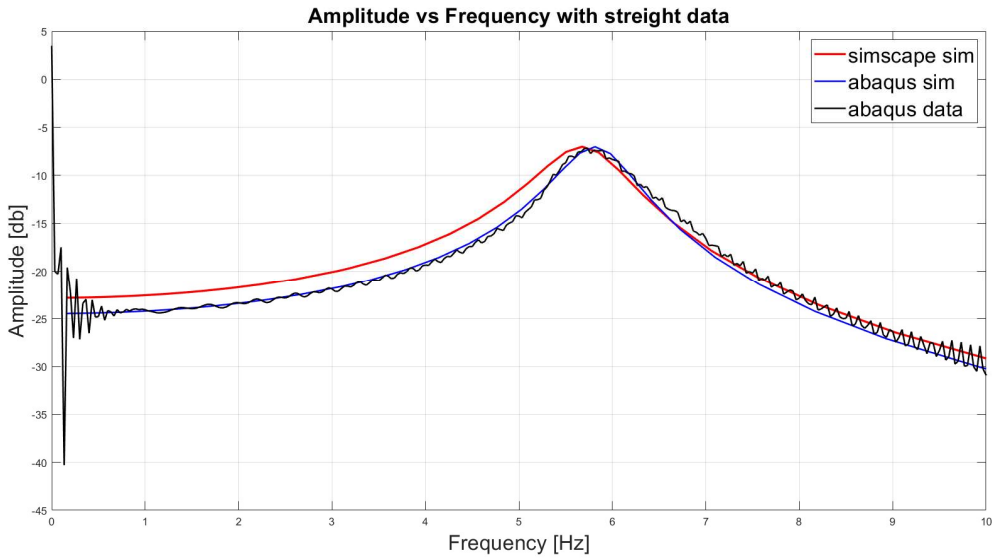

Figure 54. Frequency response with straight data. mood2_20240828_0743, lever v12, d=62

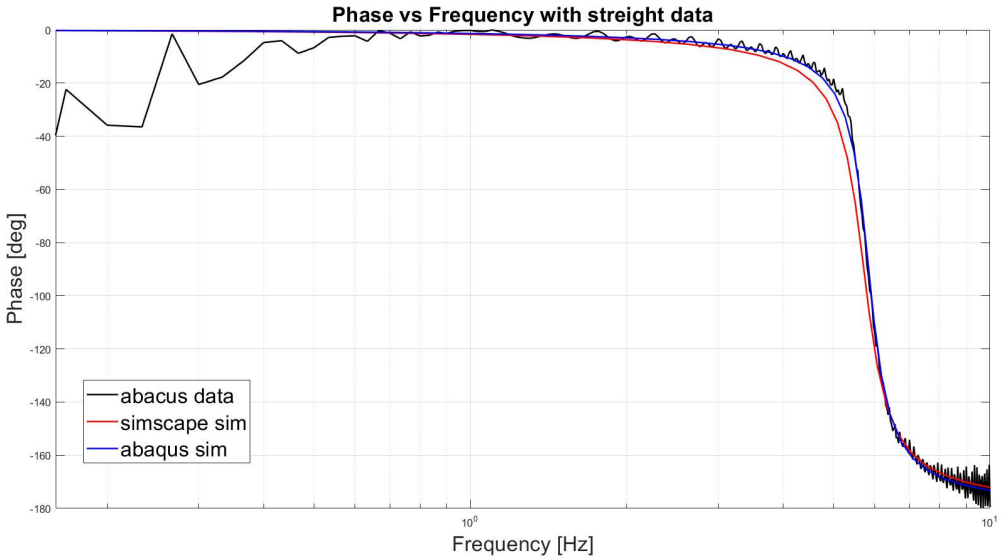

Figure 55. Phase shift with straight data. mood2_20240828_0743, lever v12, d=62

We can appreciate the good representation the Simscape model is able to provide, as well as the excellent approximation with a dynamic system with two poles and no zeros.

Another peculiar aspect that emerges from the Abaqus simulation is the fact that if the position of the motor is imposed, the force required decreases with the frequency, and only after we have surpassed the natural frequency it grows, but even here, only progressively. We can see in Figure 56 that we impose a movement with a sweeping frequency, the same used in the prior experiment, from 0 to 15Hz. We can indeed appreciate the fact that the force needed decreases while the frequency increases, up we reach the natural frequency.

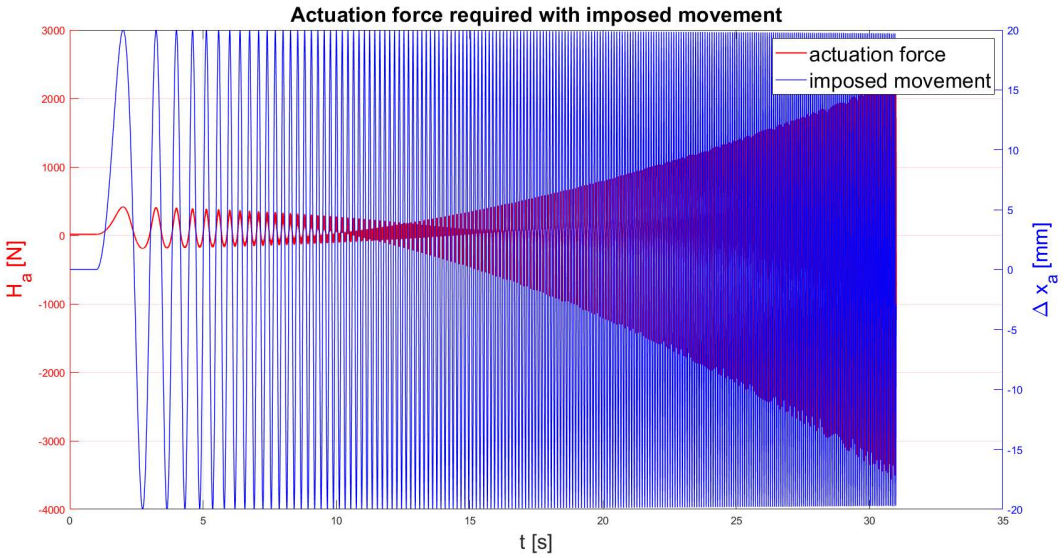

Figure 56. Force with imposed actuator position, lever V12, d=0.5, mood5_20240910_1008.dat

Even when actuating the motor by imposing a certain position, in accordance with the sweeped signal, we can appreciate the same behaviour described before, regarding the phase inversion. In Figure 57 we can see that the imposed position is in phase with the required force.

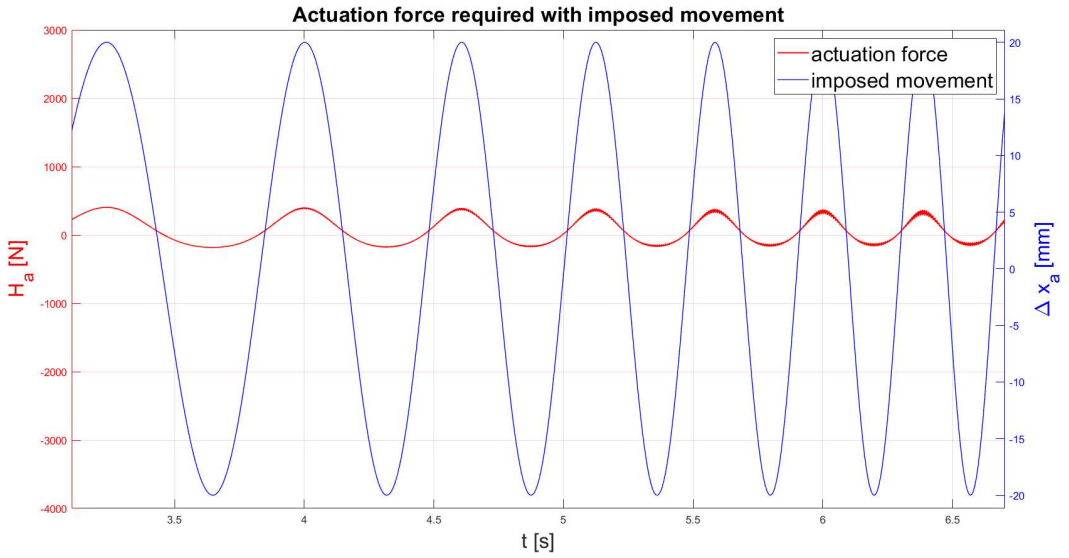

Figure 57. Force required when a position is imposed with a frequency less than the natural frequency.

In Figure 58 we can appreciate that the imposed position is now out of phase in respect with the required force.

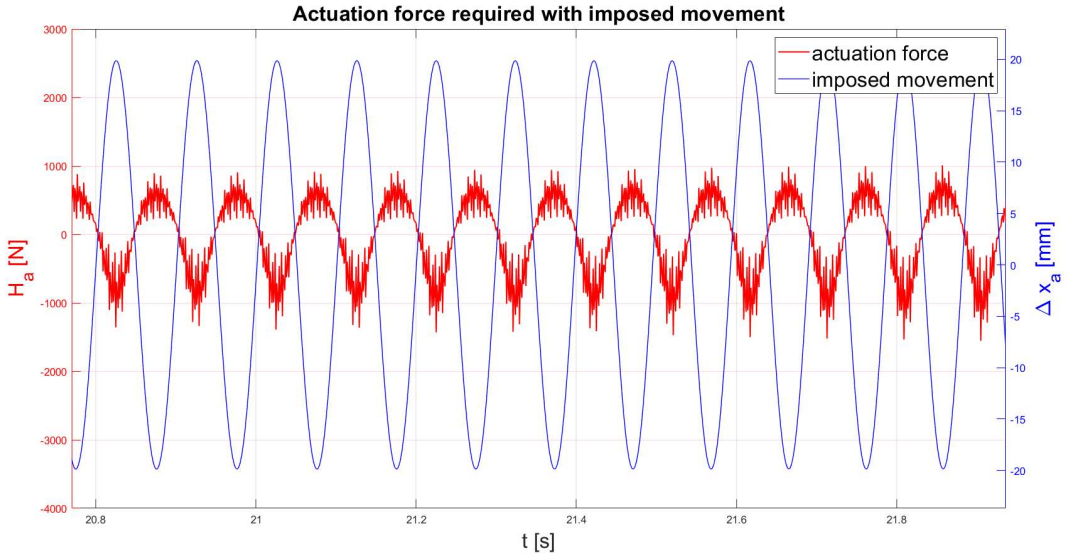

Figure 58. Force required when a position is imposed with a frequency greater than the natural frequency.

We can conclude that the Simscape model can represents the more detailed dynamic aspect of the system, as they emerged in the Abaqus simulation.

Chapter 7 Frequency response study

With the model dutifully developed and validated we can now perform several experiments that, as stated before, would require a functioning prototype. One of the most interesting is the study of the time-based frequency response analysis. According to the model of the load, we expect a resonance frequency of 8.24Hz. In this scenario there are no other bodies with mass, apart from the one modelling the morphing aileron.

We actuate the system with a force behaving as a sinewave signal. We start with a low frequency and increase it every few seconds, after the system has settle in the new excitation frequency.

7.1 Dynamic system massless

First, we perform this test without considering the mass of the moving parts introduced by the mechanism. We achieve this by setting the density of the mechanism's components to a very low value. In Figure 59 and Figure 60 we can see how the amplitude of the monument spikes at the natural frequency.

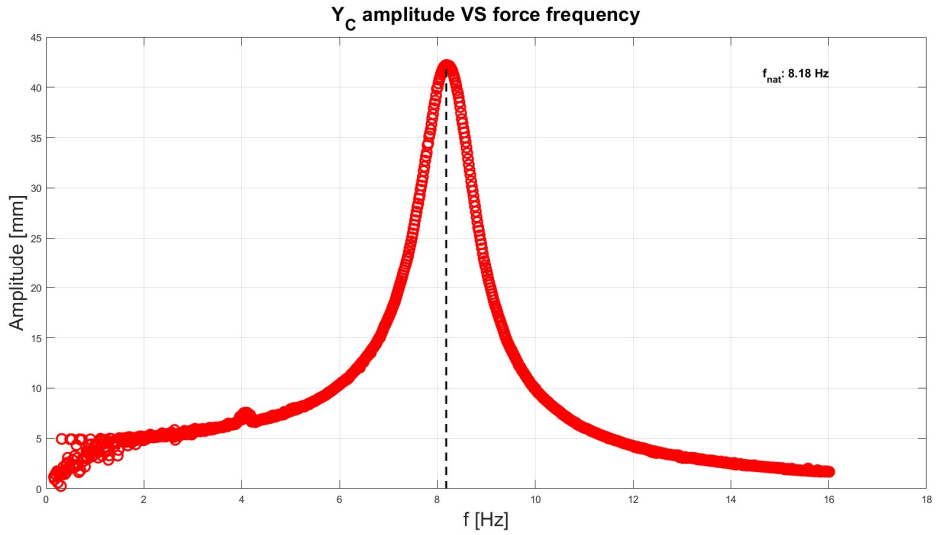

Figure 59. Dynamic massless simulation. amplitude vs frequency

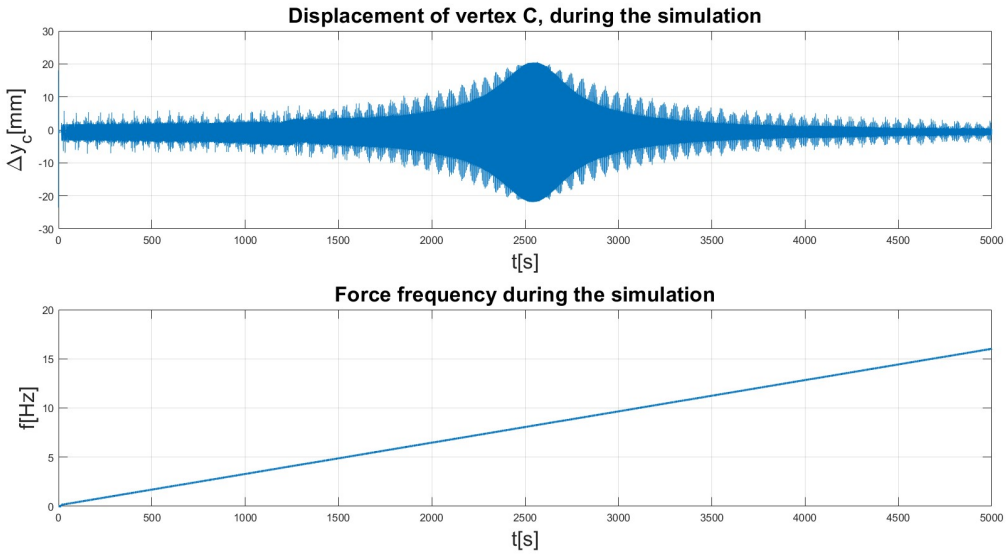

Figure 60. Dynamic simulation, with increasing force frequency. lever_V12, A=50N, $\omega_{start} = 1\,rad/s$, d=62, $\rho = 1\,Kg/m^3$, $\rho_{CF} = 1\,Kg/m^3$, mood0_20240906_1127.dat, mood0lite_20240906_1127

The results are well aligned with the expected natural frequency, from the model of the load.

7.2 Dynamic simulation, steel components

We can now introduce the mass of the stem and of the linkages. We consider at first all the components as manufactured in steel. From the 3D model developed in Fusion 360, we can easily obtain the mass of the different component, as shown in Figure 61.

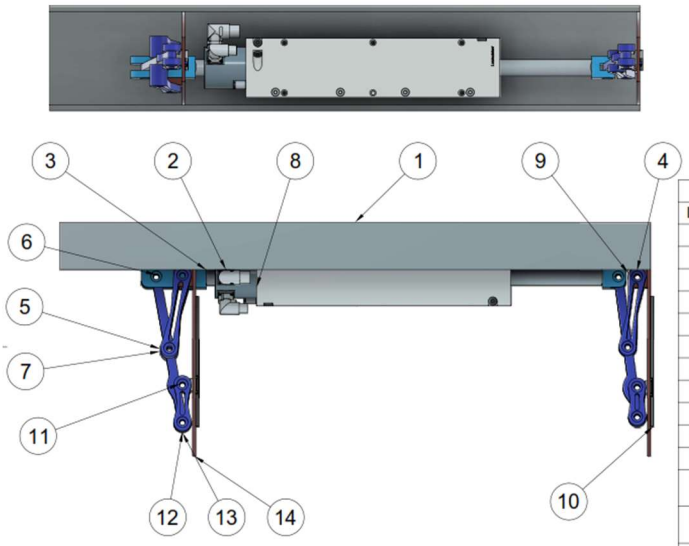

Parts List

Item	Qty	Part Number	Material	Mass
1	1	Spar	Steel	24881.975 g
2	1	Stator	Steel	12841.347 g
3	1	Shaft	Steel	4357.31 g
4	1	Right_kinematism	Steel	1012.832 g
5	1	Linker_up_left	Steel	310.779 g
6	1	Lever_left	Steel	345.749 g
7	1	Linker_low_left	Steel	310.779 g
8	1	Flange	Steel	18587.089 g
9	1	Rib	Steel	1876.135 g
10	1	Slider	一般	79.511 g
11	1	Slider_left	一般	66.145 g
12	1	Linker_slider_up_left	Steel	133.651 g
13	1	Linker_slider_down left	Steel	133.651 g
14	1	Rib_left	Steel	1987.906 g

Figure 61. List of the mechanism's components, with their mass.

In Table 7 and Figure 62 we can see what components contribute more to the overall mass. Notable is the shaft's mass. For the nature of the motor, since it will be moved by electromagnetic fields, this cannot be manufacture in lightweight materials and cannot even be hollow.

Table 7 Mass contribution of steel components

Components mass. Steel components.				
item	**quantity**	**name**	**mass [kg]**	**CF possible**
3	1	shaft	4.36	n
4	1	right_kinematism	1.01	y
5	1	Linker_up_left	0.31	y
6	1	Lever_left	0.35	y
7	1	Linker_low_left	0.31	y
10	1	Slider	0.08	n
11	1	Slider_left	0.07	n
12	1	linker_slider_up_left	0.13	y
13	1	Linkjer_slider_down_left	0.13	y
na	20	bearing	0.14	n
		total	**6.89**	

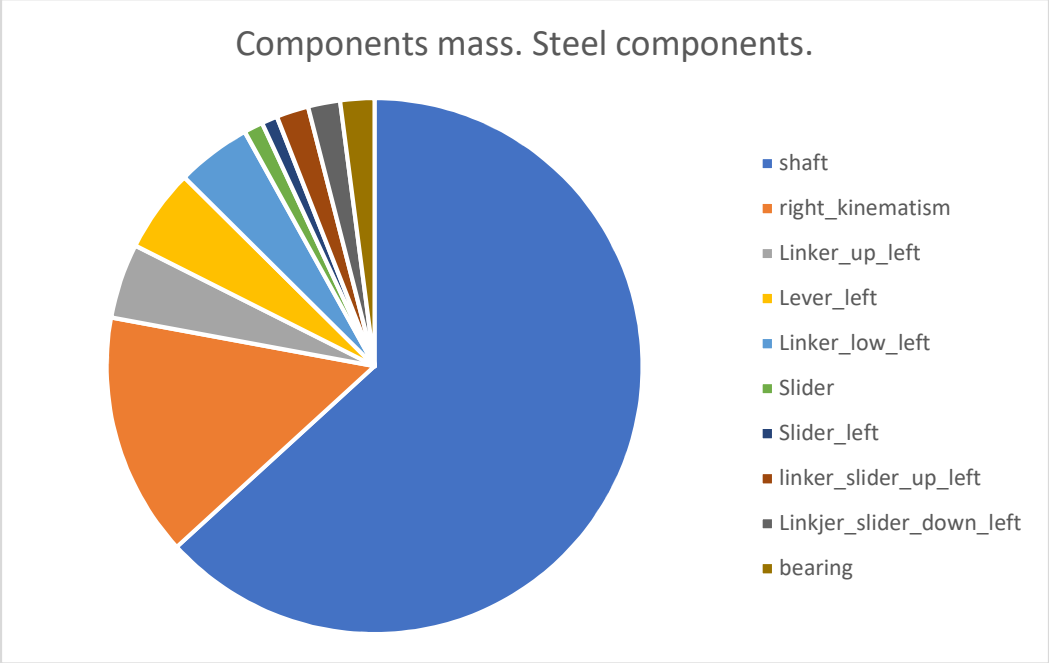

Figure 62. Mass distribution of steel components

Since we have introduced the mass of the mechanism we expect a reduction of this frequency. If we run the very same simulation that the one run in the previous chapter, the natural frequency decreases significantly, as shown in Figure 63 and Figure 64.

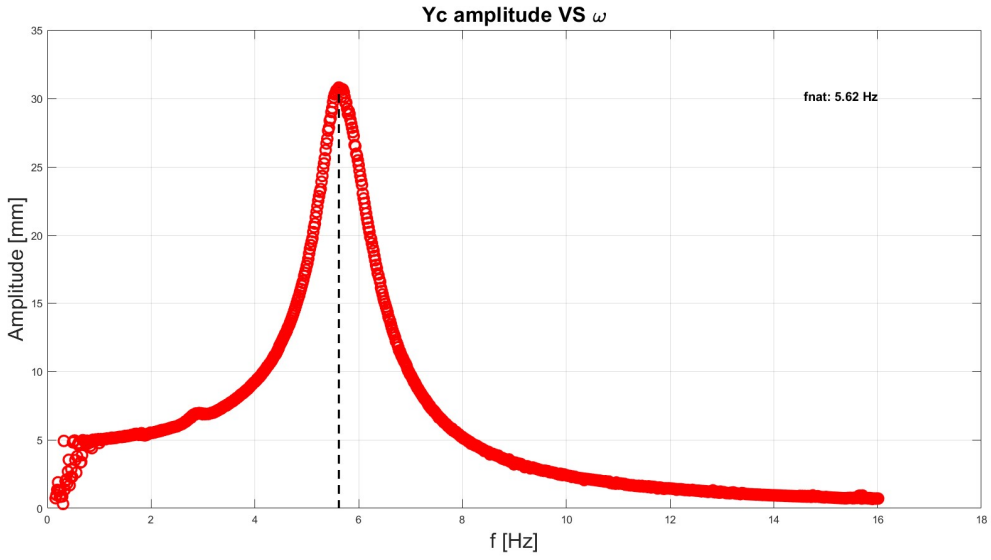

Figure 63. Dynamic massless simulation with steel components

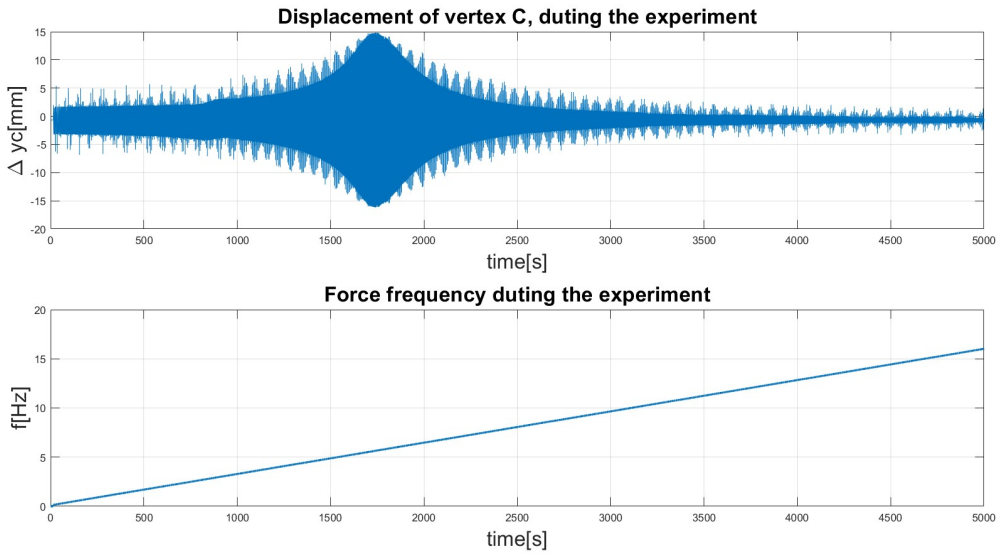

Figure 64. Dynamic simulation, with increasing force frequency. lever_V12, A=50N, $\omega_{start} = 1\, rad/s$, d=62, $\rho = 7800\, Kg/m^3$, $\rho_{CF} = 7800\, Kg/m^3$, mood0_20240905_1305.dat, mood0lite_20240905_1305.dat

7.3 Dynamic simulation, CF components where possible

To increase the natural frequency, we could try to reduce the weight of the mechanism. Not all components are manufacturable in carbon fibre, but many are. At the cost of a significant increase in cost and manufacturing complexity, we can reduce the weight by approximately 25%, bringing down, as shown in Table 8 and Figure 65, the overall mass from 6.89kg to 5.14kg.

Table 8 Mass contribution of components (steel and carbon fibre)

Components mass. CF components where possible.				
item	**quantity**	**name**	**mass [kg]**	**CF possible**
3	1	shaft	4.36	n
4	1	right_kinematism	0.23	y
5	1	Linker_up_left	0.07	y
6	1	Lever_left	0.08	y
7	1	Linker_low_left	0.07	y
10	1	Slider	0.08	n
11	1	Slider_left	0.07	n
12	1	linker_slider_up_left	0.03	y
13	1	Linkjer_slider_down_left	0.03	y
na	20	bearing	0.14	n
		total	**5.14**	

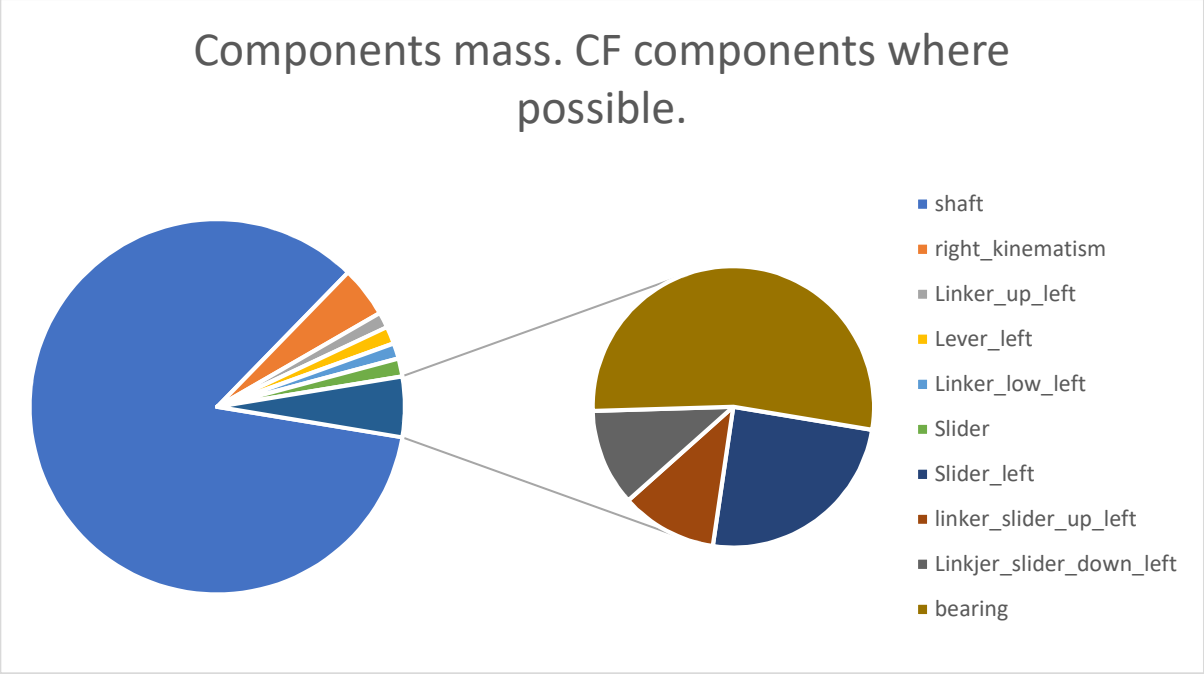

Figure 65. Mass distribution using CF when possible

We run again the same simulation with updated values of density.

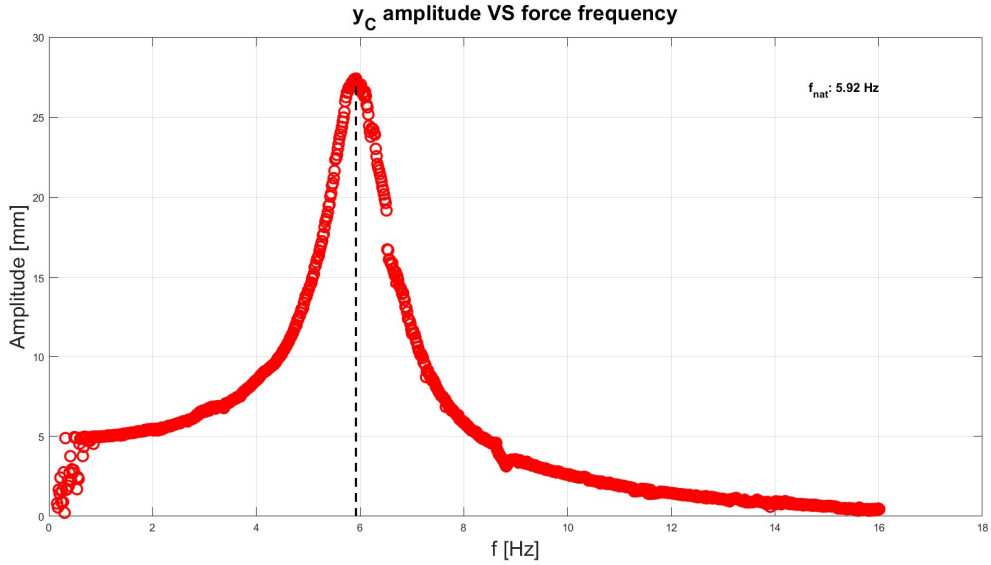

Figure 66. Dynamic massless simulation with CF components, where possible.

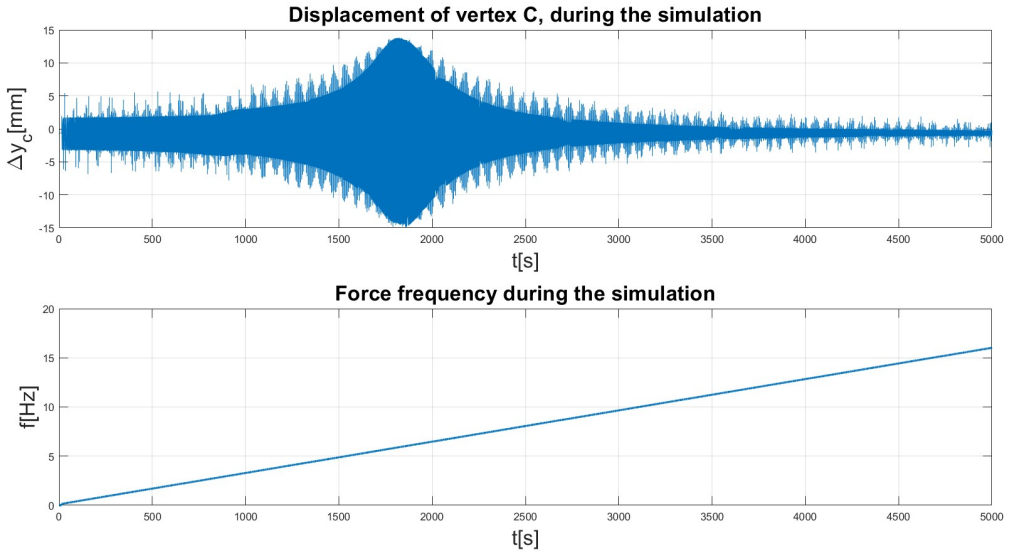

Figure 67. Dynamic simulation, with increasing force frequency. lever_V12, A=50N, $\omega_{start} = 1\,rad/s$, d=62, $\rho = 7800\,Kg/m^3$, $\rho_{CF} = 1733\,Kg/m^3$, mood0_20240906_1342.dat, mood0lite_20240906_1342.dat

7.4 Dynamic simulation, spring assist

Another strategy for increasing the resonance frequency would be to increase the stiffness of the system. This could be obtained by adding a spring in parallel to the current solution, as shown in Figure 68. Adding such a spring would also tackle the problem of the asymmetry of the load.

As described in previous chapters the mechanism provides a leverage which changes according to the configuration. This allows for a more convenient leverage when the mechanism is in the highest position, and a far less convenient leverage when the mechanism is in the lower position. This behaviour could be alleviated by introducing a spring which would help the motor when the mechanism is in the most disadvantageous position.

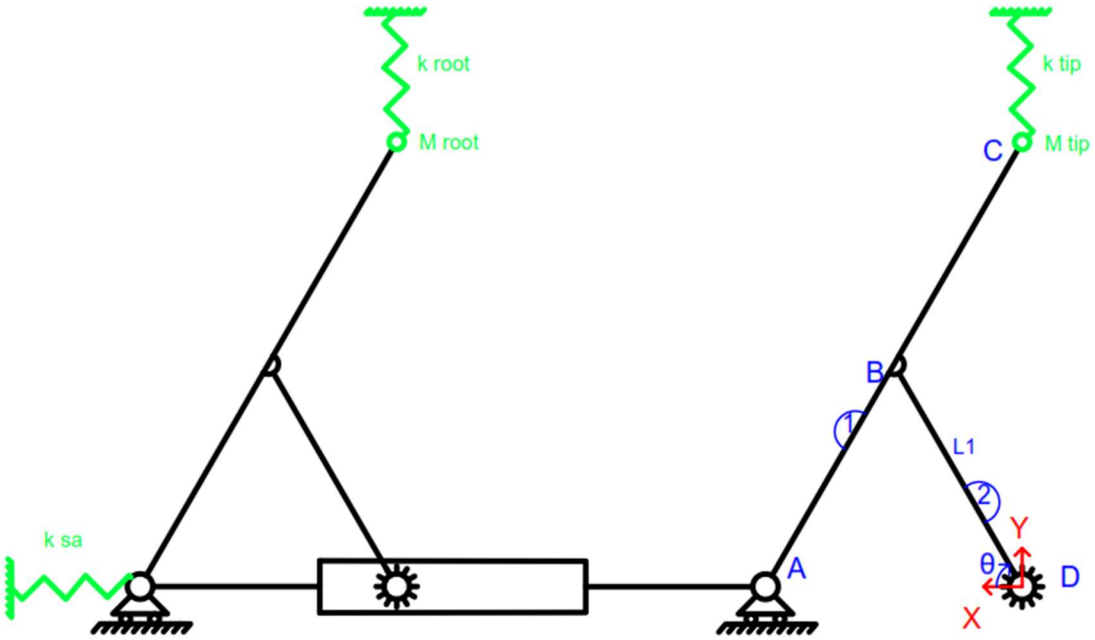

Figure 68. Double Scott Russell mechanism with spring assist

In a static configuration the effect of the spring will be of reducing the maximum force needed, but increasing the minimum force needed, as shown in Figure 69. We must be wary of the limit on the motor. There's in fact a significant difference between the force that the motor can provide continuously (920N) and what in can achieve for a brief period (2700N). The limit between continuous and non-continuous is not clearly defined since it depends upon the performance of the motor's liquid cooling system. Ailerons are needed to perform a roll manoeuvre; it is worth noting that a typical roll lasts an order of magnitude of unit of seconds. At any rate, we limite the actuation of the spring at the continuous force limit.

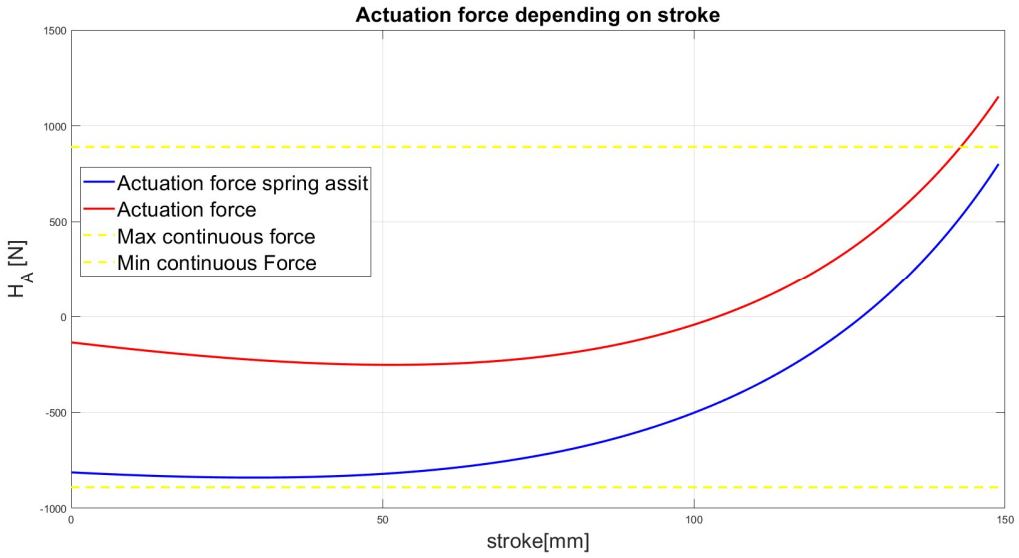

Figure 69. Stroke position vs actuation force with and without spring assist

This is a trade-off which would be acceptable because of the intrinsic asymmetry of the mechanism. Unfortunately, the effect of the spring is not just to "shift" the force required, but it increase also the power needed since the spring act now as an element which requires internal work.

The main effect of the spring would be to increase the resonance frequency, back towards the massless case, toward which we are aiming to go back to. As we can see in Figure 70 and Figure 71, after running the same simulation as before, we are able to increase significantly the natural frequency.

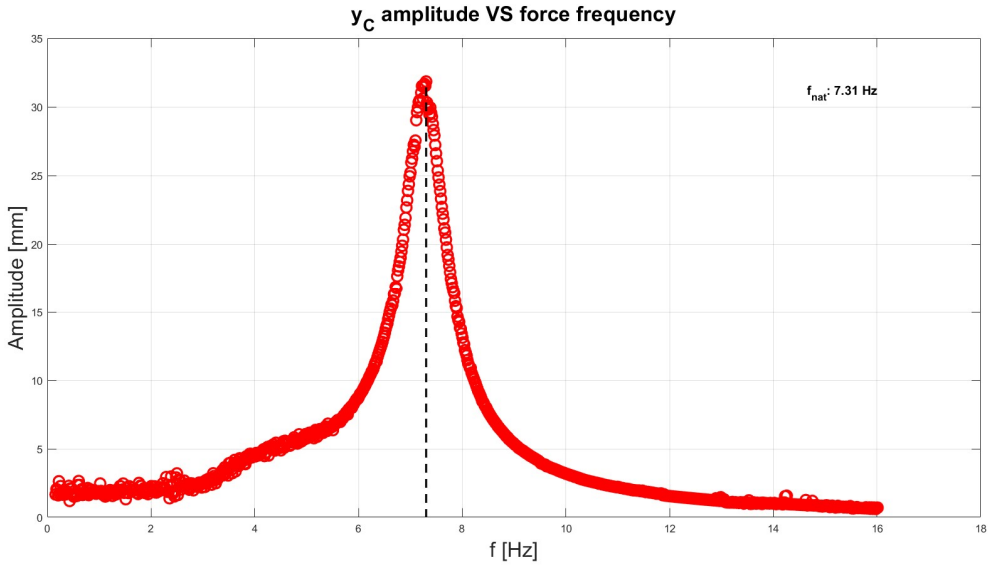

Figure 70. Dynamic massless simulation with SA

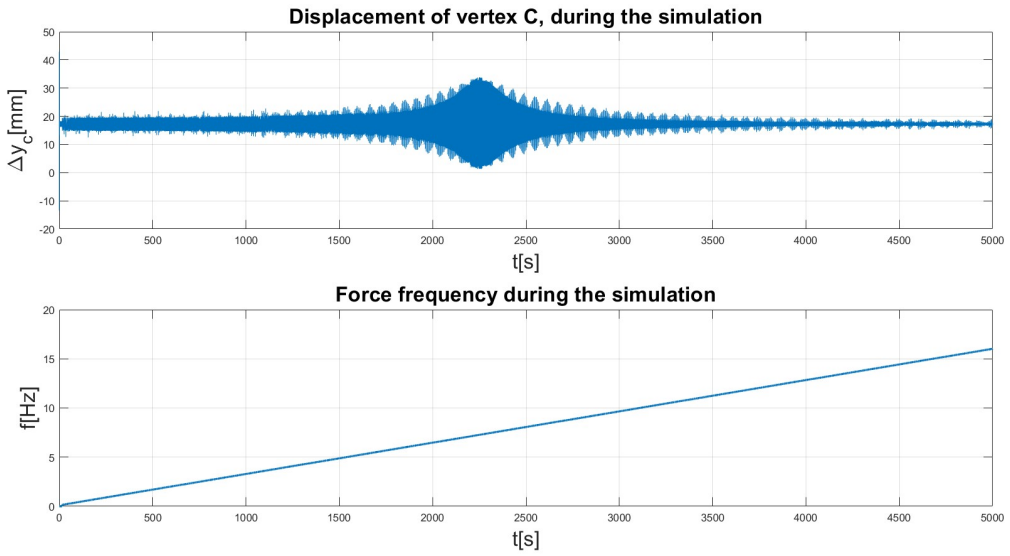

Figure 71. Dynamic simulation, with increasing force frequency. lever_V12, A=50N, $\omega_{start} = 1\,rad/s$, d=62, $\rho = 7800\,Kg/m^3$, $\rho_{CF} = 7800\,Kg/m^3$, $x_{A0} = x_{aNeutral} + 21.7$, mood0_20240906_1620.dat, mood0lite_20240906_1620.dat

7.5 Dynamic simulation, spring assist and CF where possible

If we combine the previous solutions, employing carbon fibre components where possible, and using a spring for assisting the motor, we manage to increase even further the resonance frequency, as shown in Figure 72 and Figure 73.

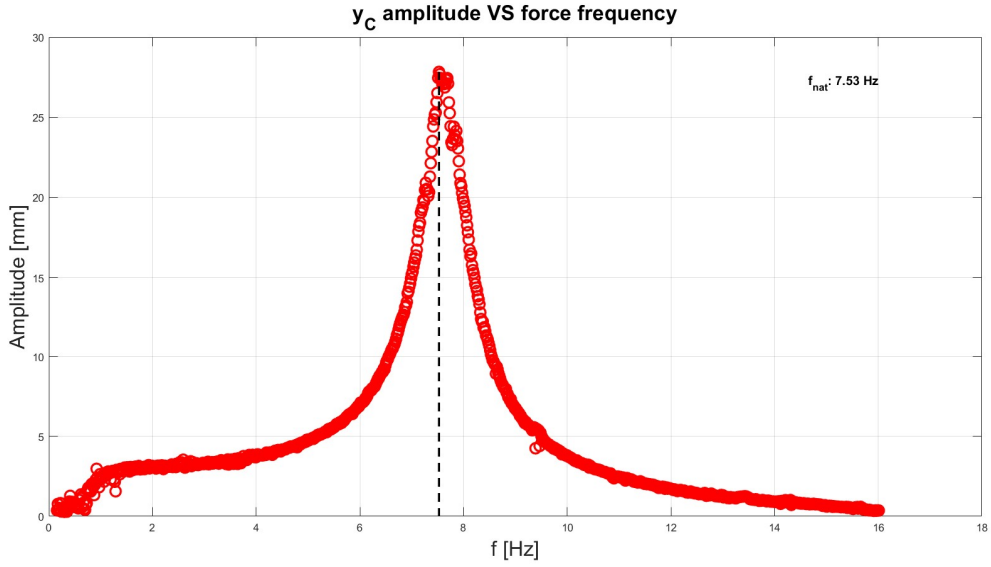

Figure 72. Amplitude vs ω, SA and CF where possible

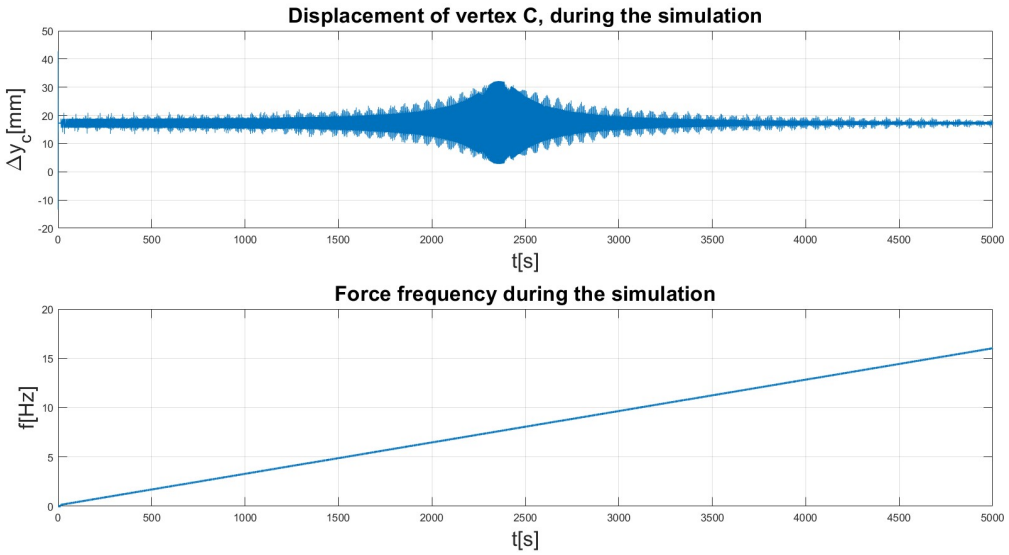

z

Figure 73. Dynamic simulation, with increasing force frequency. lever_V12, A=50N, $\omega_{start} = 1\,rad/s$, d=62, $\rho = 7800\,Kg/m^3$, $\rho_{CF} = 1733\,Kg/m^3$, $x_{A0} = x_{aNeutral} + 21.7$, mood0_20240906_1952.dat, mood0lite_20240906_1952.dat

7.6 Solution comparison

In Figure 74 and Table 9 we can finally compare all the configurations we have tested.

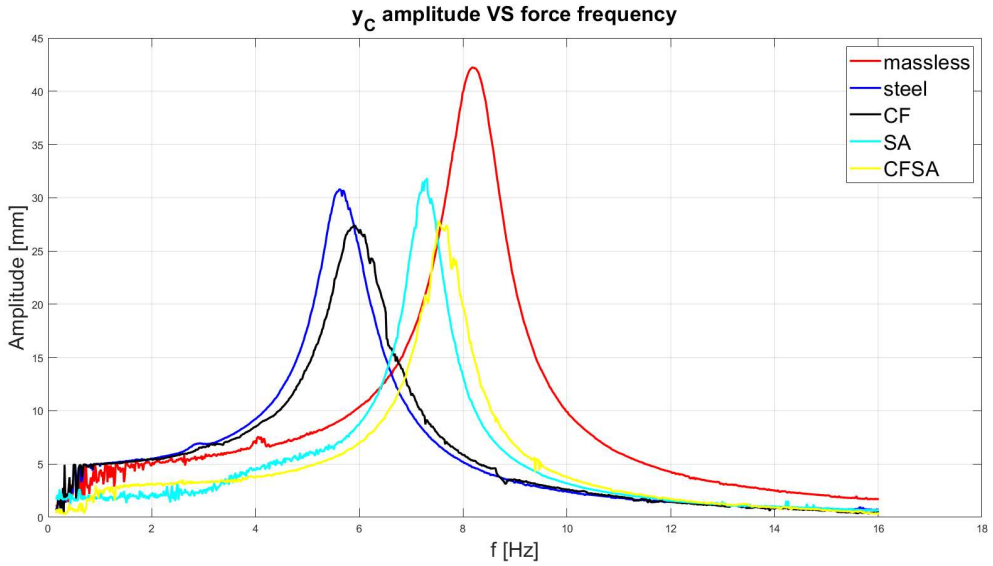

Figure 74. Frequency response with different scenarios. massless, steel, CF, SA, CF and SA

The response diagram of the previous Figure 74, have been obtained from the time response of the system, to the sinusoidal force, displayed in Figure 75.

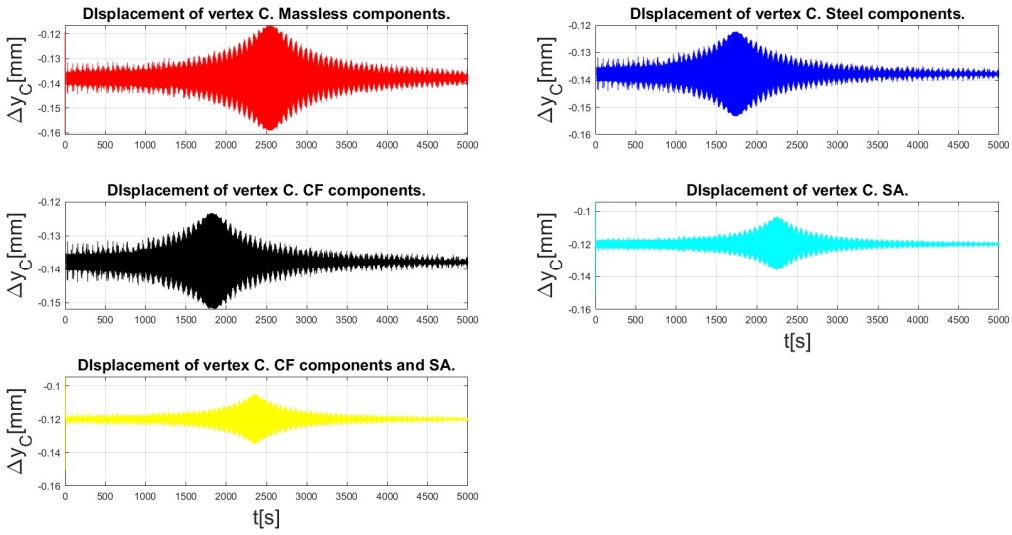

Figure 75. Comparison of different configurations for the dynamic simulation.

Table 9 Comparison of different tactics for increasing resonance frequency

Solution	f_{res}*[Hz]*	*% massless solution*
massless	8.18	100
Steel components	5.62	68.7
CF where possible	5.92	72.4
SA	7.31	89.4
CF where possible + SA	7.53	92.1

Deploying different strategies, using light components and a spring assist, it is possible to go back close to the massless case, which would be the case without the intrusion of the mechanism.

Chapter 8 Control problem

Another aspect that can be tackled once we have developed a model, is the control dynamics. We can try different approaches for solving the problem and gauge the result in a time-based environment. A controller must be implemented because the pilot does not impose a force on the actuator, but rather a desired aileron deflection. This is done for many reasons, for instance for more easily integrate the actuation in the autopilot or for integrating trimming logic. In this peculiar case, furthermore, the relationship between force applied and stroke position presents a plateau, as shown in Figure 42 therefore it is difficult to find the desired position in an open loop logic.

At the most basic level, the goal of the control system is to actuate the linear motor to reach a set-point in an appropriate manner. This can be easily parametrized to allow the user to pick between a more aggressive dynamic and a slower one which allows for a more compliant change of geometry and provides the aerodynamics to conform to the new shape in the more seamless way possible. A bare bone logic can be implemented according to Figure 76.

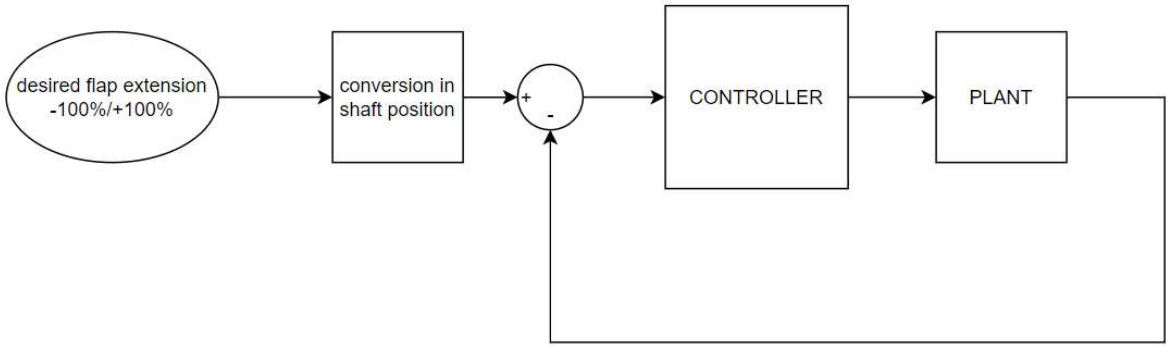

Figure 76. Plant controller scheme

The plant, as always, has 1 DOF, provided by the encoder of the motor which can provide quite high levels of precision, according to Table 10.

Table 10. From motor datasheet LINEAR MOTORS P10-70X400U, encoder spec

Resolution [mm]	0.001
Repeatability [mm]	±0.01
Linearity [mm]	±0.01

The information about the position of the shaft allows us the determine the position of the vertex of the mechanism.

Since we have now access to the model, we can try different kinds of controllers, we can model uncertainties and disturbances, into the plant, and see how the system responds, control wise. We can change the geometry of some critical components, and gauge how much such a change would affect the control performance, and we can do all this while in a digital realm.

8.1 PID controller, single setpoint

Considering the maximum continuous force that the motor can provide, we can try to deploy a PID controller. This is one of the simplest controllers we can implement, and it is quite well supported by Simulink. We can start by setting its gains according to the setup shown in Figure 77.

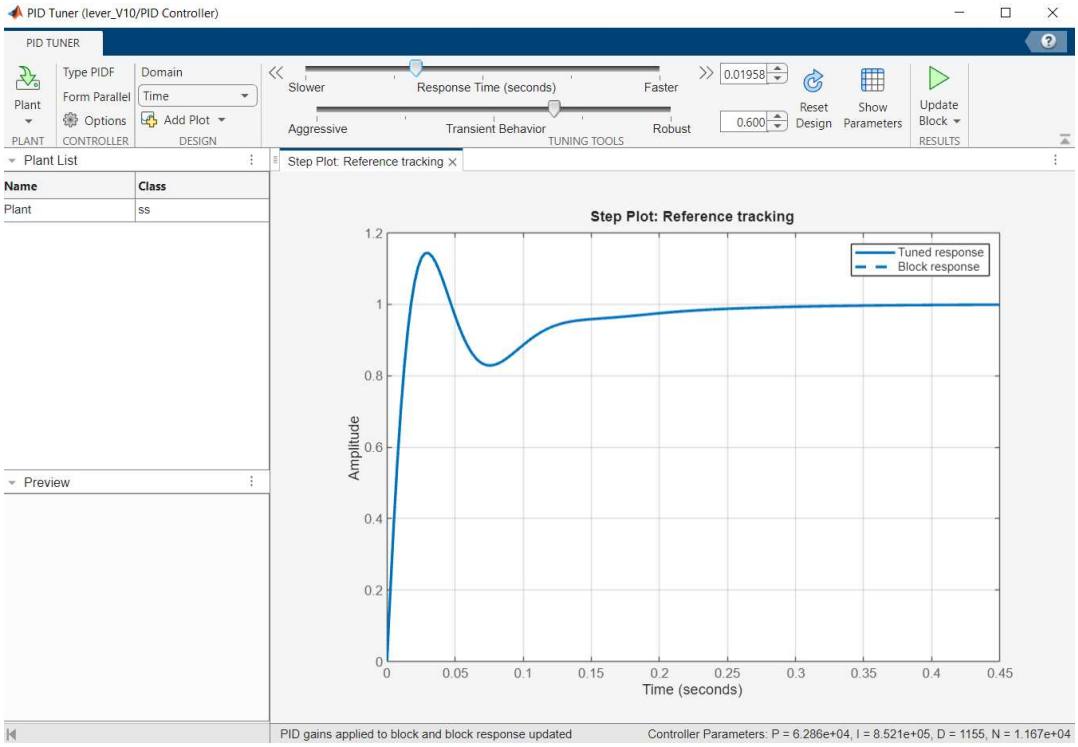

Figure 77. PID controller settings P=6285.0, I=852137.0, D=1155.1, N=11673.2

With these settings we can see how fast the system reaches a desired setpoint, given in a range of ±100% deflection of the aileron. To evaluate this, we can see in what time the position is reached, under a certain tolerance as shown in Figure 78. It takes the controller 0.2455s to reach the desired position with the indicated tolerance.

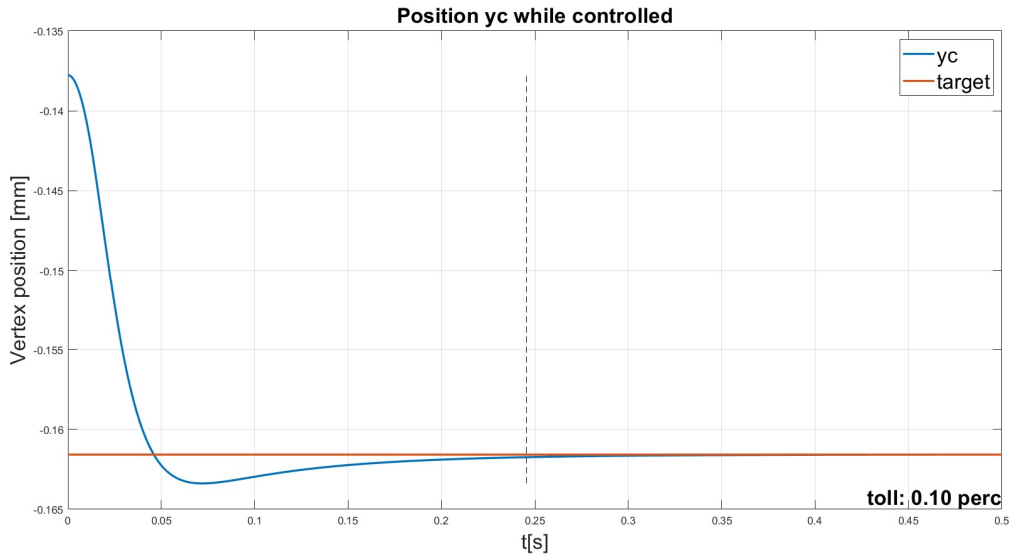

Figure 78. Single set point; target = 60%

To reach and maintain this desired position, the actuator must exert a force, described in Figure 79.

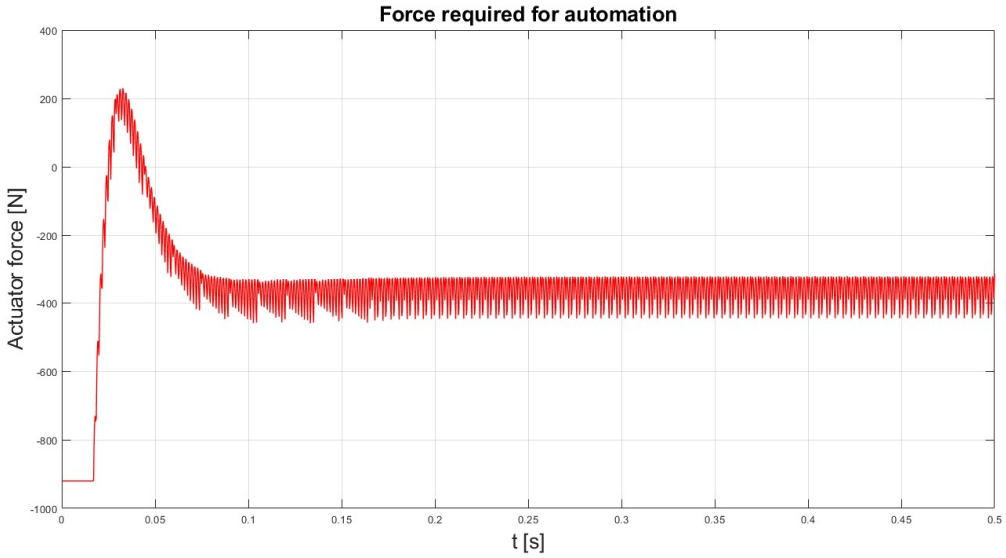

Figure 79. Actuation force for setpoint

8.2 PID controller, serie of setpoints

Since we want to evaluate the performance of a PID controller, we could test the system with a series of setpoints, which it must reach. These setpoints are a sort of a stress test, since they don't represent a realistic manoeuvre. They can give an insight in the overall performance of the system. We can see the behaviour of the mechanism in Figure 80.

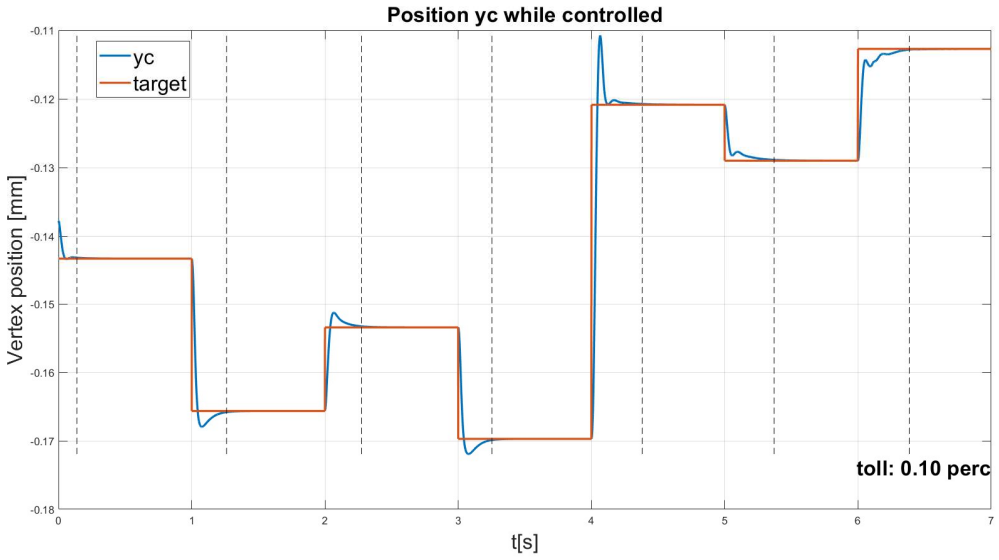

Figure 80. Setpoints 15%, 70%, 40%, 80%, -40%, -20%, -60%

The force needed to reach and maintain the desired setpoints, is shown in Figure 81.

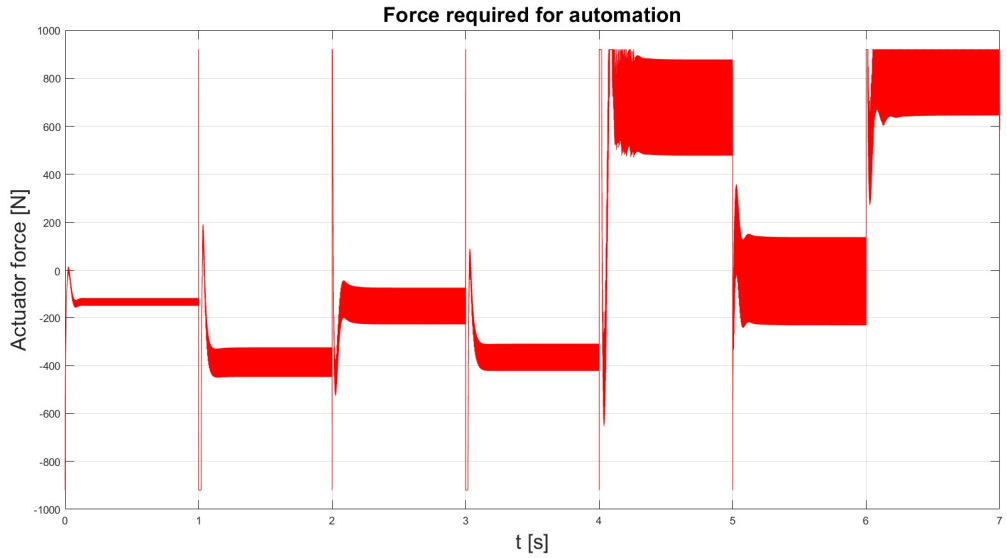

Figure 81. Actuation force for series of setpoint

We can valuate, in Table 11, the time needed to reach the desired setpoint, given a tolerance of 0.1% on the position.

Table 11. Time for reaching each setpoint

setpoint [-100% 100%]	**t[s]**
15	0.0746
70	0.2298
40	0.2239
80	0.2147
-40	0.3806
-20	0.2109
-60	0.2235

8.3 PID controller, manovre

The previous settings for the controller are intended to demonstrate the capability of the system, especially when employing advanced techniques that take advantage of the very high frequency response offered by this solution. In a more common scenario, for instance during a roll manoeuvre, we aim to provide 2 counter impulses to achieve the desired turn.

In this case we shall use a much more comfortable PID settings, with the settings of Table 12.

Table 12. PID settings for roll manoeuvre

P	62855.0
I	852137.1
D	1155.1
N	11673.2

With the specified settings, if we aim for a roll manoeuvre composed of two impulses of +45% and -45%, the system performs as shown in Figure 82.

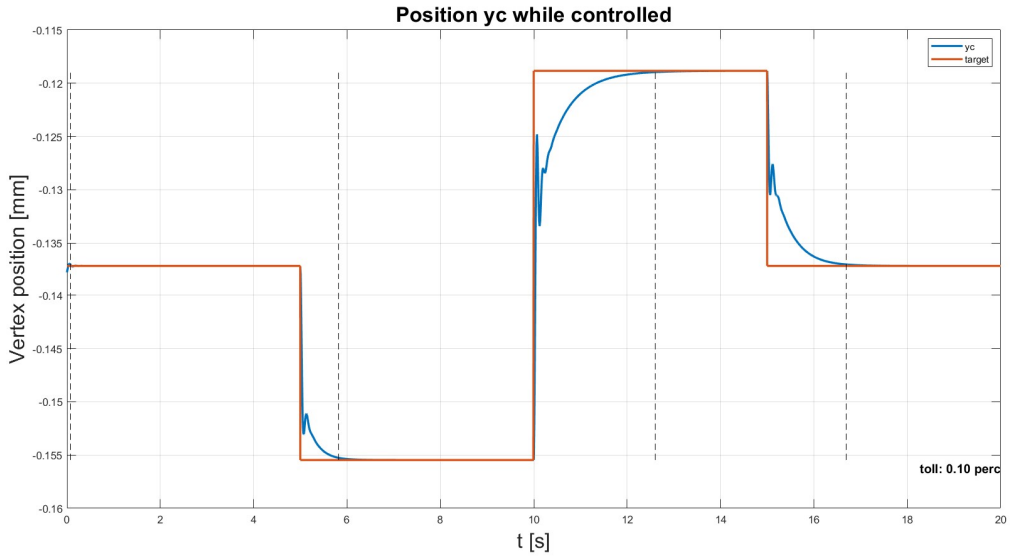

Figure 82. Roll manoeuvre

The time required for reaching each setpoint is gather in Table 13.

Table 13. Time for reaching setpoint during manoeuvre

setpoint [-100% 100%]	**t[s]**
0	0.0733
45	0.8153
-45	2.6016
0	1.6955

8.4 PID, response to gust

It is also possible to study the controller's response to a gust. The vertical gust will change the effective incidence of the aerodynamic surfaces, causing changes in the lift forces that will impact the dynamic response of the aircraft. We can model such effect as a deterministic phenomenon, as described in Figure 83. It is important for the whole design of the aircraft, to calculate the response in terms of both rigid body and flexible modes. The conditions that need to be taken into consideration are defined by the Airworthiness Authorities.

Although gust is a complicated atmospherically phenomena, it can be modelled with a discrete function, where the gust velocity changes in a deterministic manner.

We will consider the peculiar effect that the gust causes in the context of the actuation of the ailerons with linear induction actuators. As stated before, this kind of motors, unlike the classic lead/screw design, are reversible. This means that if we want to maintain a certain position of the shaft, we need to constantly provide a certain amount of force. If the load increases, the motor must deploy an even bigger force, to contrast the increased load, and maintaining the desired position. During manoeuvres, this issue falls under the supervision of the controller, which must try to maintain the pilot input, no matter the behaviour of the load. Usually the study of the dynamic response of the aircraft is carried on with the airplane in a steady state configuration but we are interested to study the effects that a gust will bring, on this kind of novel actuators.

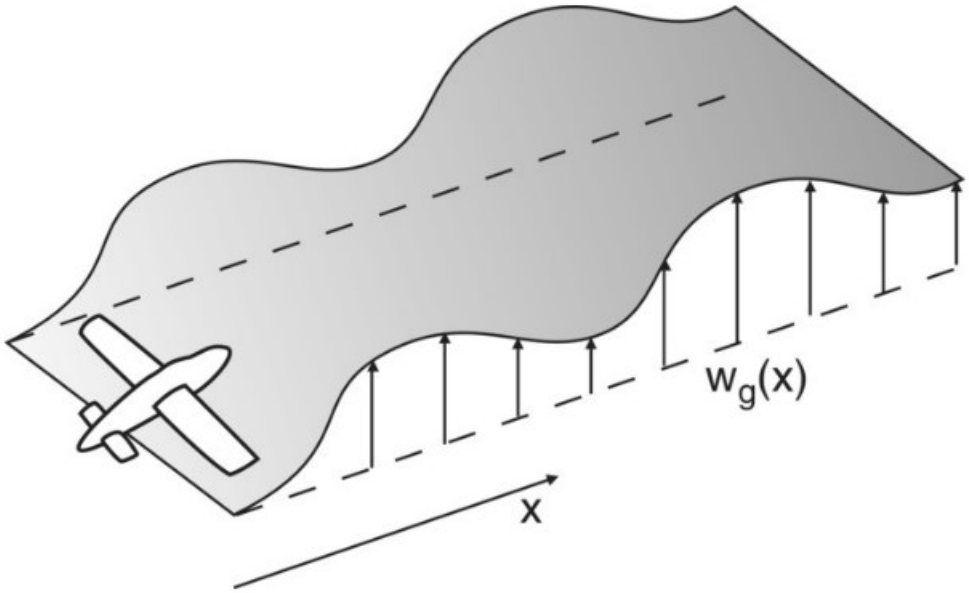

Figure 83. Representation of a deterministic gust [4]

According to EASA [2], the gust is described in chapter "CS 25.341 Gust and turbulence loads" as an increase in vertical speed described by the function depicted in Figure 84.

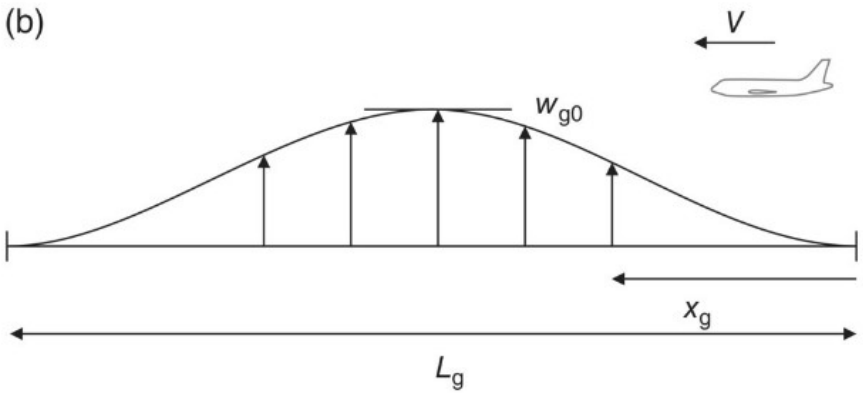

Figure 84. Model of a deterministic gust [4]

$$L_g = 2H$$

$$w_g(x_g) = \frac{w_{g0}}{2}\left[1 - \cos\left(\frac{\pi x_g}{H}\right)\right], for\ 0 \le s \le 2H \text{ [5]}$$
$$w_G = 0\,, for\ x_g > 2H$$

Where xg is the distance the aircraft has penetrated into the gust.

The maximum speed the gust can reach, wg0, is obtained after extensive empirical data gathering at different heights.

We need to calculate the response in the time domain, therefore we must change the equation into a temporal function. Considering the airplane moving with constant velocity V:

$$w_g(x_g) = \frac{w_{g0}}{2}\left[1 - \cos\left(\frac{\pi V t}{H}\right)\right], for\ 0 \le t \le \frac{2H}{V}$$

$$w_G = 0\,, for\ t > \frac{2H}{V}$$

EASA CS-25 provides similar guidelines that the FAA FAR-25.

The norms instruct us to study a gust gradient parameter H from 9m to 107m and to study for each the response of the system.

The effect of the gust translates into a periodic increase of the lift. With different values for parameter H, which specify the length of the gust, we can see how the controlled system reacts.

With the fastest gust admissible the system responds as shown in Figure 85.

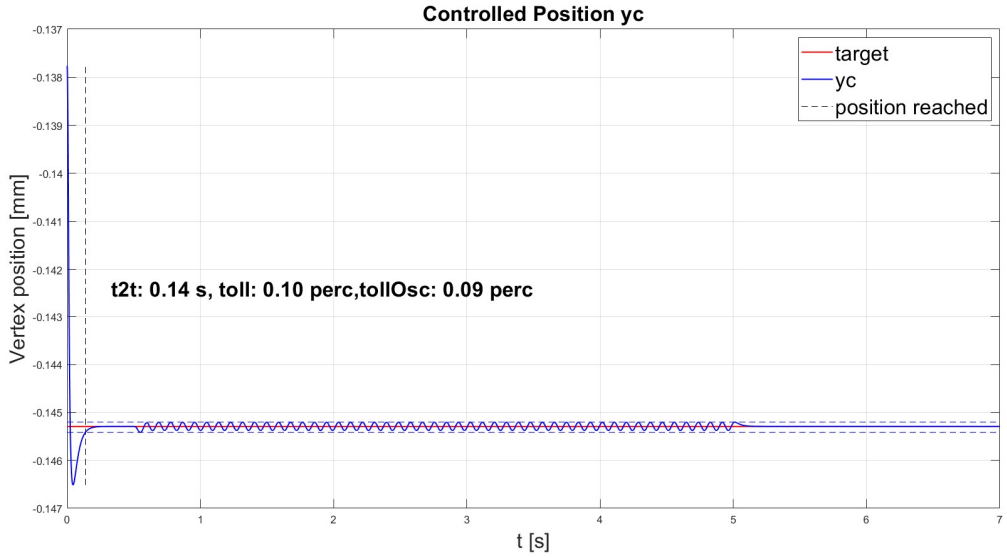

Figure 85. Target position 20%, lever_V12, d=0.5, H=9m, $V_{gust} = 200\,m/s$

We can see in Figure 86 that the actuator must match the extra aerodynamic lift provided by the gust.

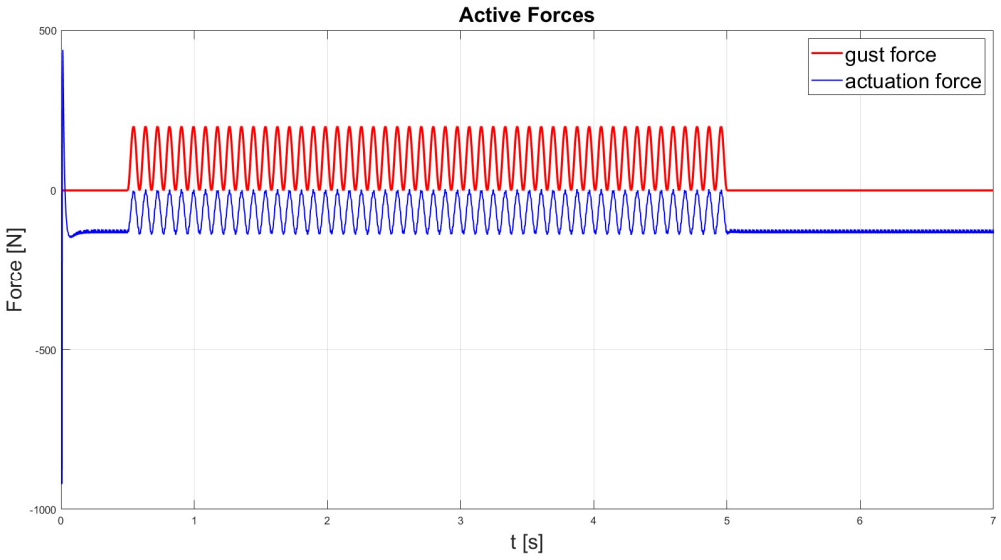

Figure 86. Forces during gust manoeuvre, H=9m

If we slow down the gust to a midrange value, we obtain the response shown in Figure 87.

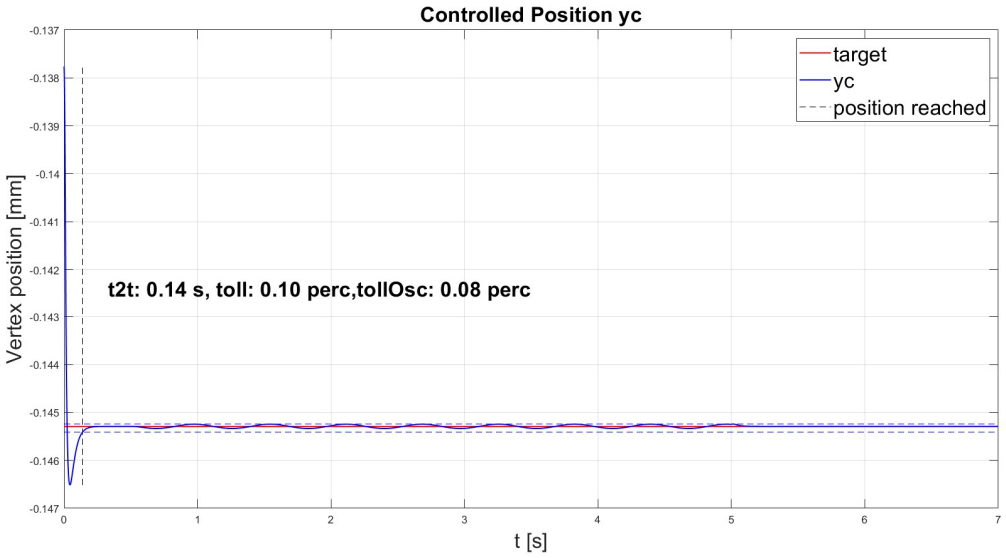

Figure 87. Lever_V11, H=57m, $V_{gust} = 200\,m/s$

As was true in the previous case, we can see in Figure 88 that the actuator must match the extra load.

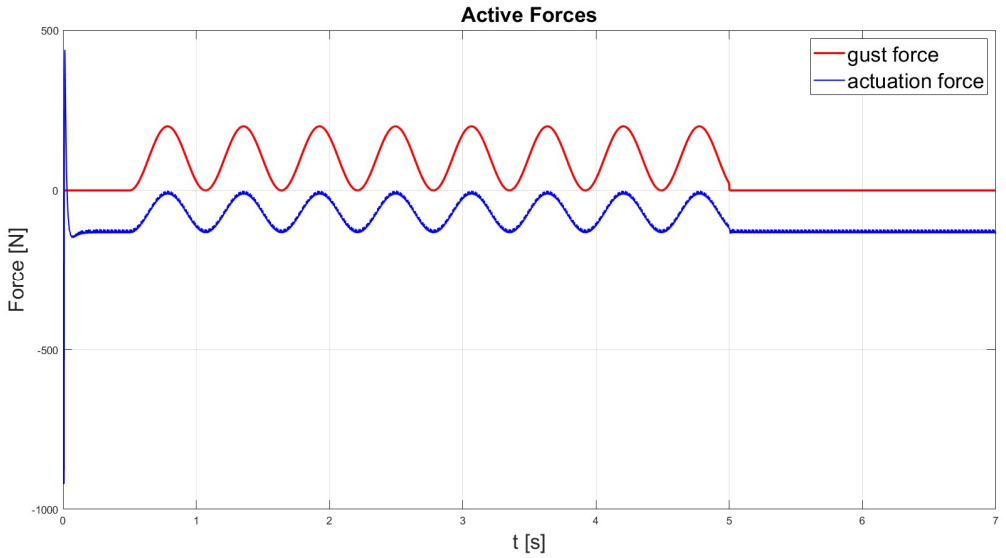

Figure 88. Forces during gust manoeuvre, H=57m

Finally, we can try to test the system with the slowest gust admissible, in figure Figure 89.

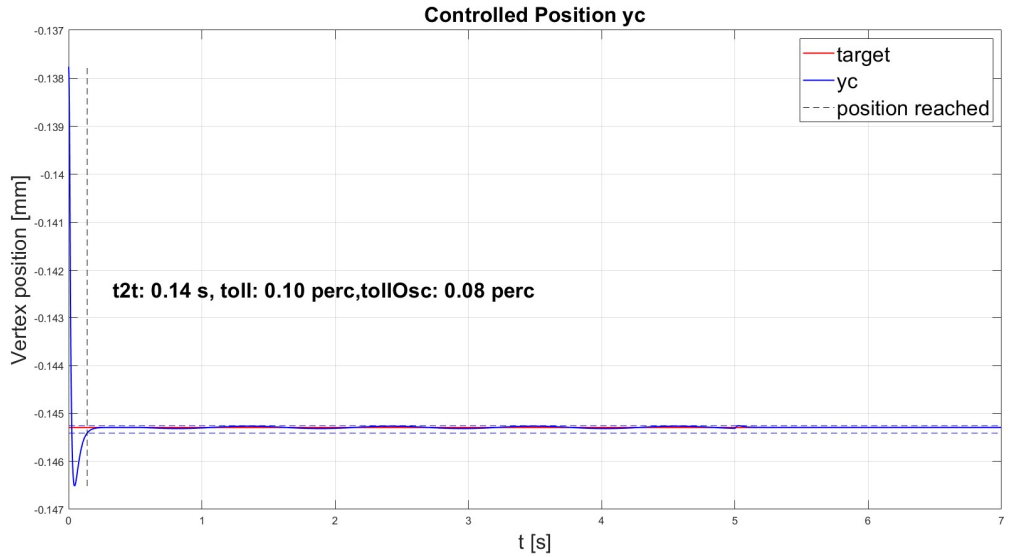

Figure 89. Lever_V11, H=107m, $V_{gust} = 200\,m/s$

This slowest gust requires an extra force developed by the actuator, shown in Figure 90.

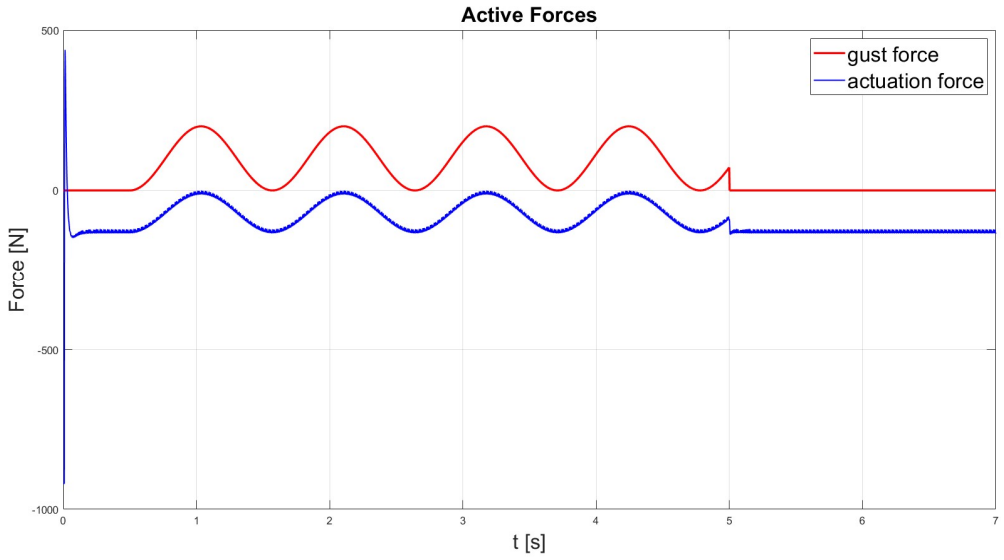

Figure 90. Forces during gust manoeuvre, H=107m

The controller manages to keep the position close to the desired target with a reasonable accuracy. We can gauge the performance of the controller, in keeping the desired position when subjected to a gust, in Table 14.

Table 14. Position error during gust

H [m]	Position error [perc]
9	0.09
58	0.08
107	0.08

Facing this scenario, we have set the PID with a somewhat more aggressive response. This is another advantage of a fully digital system: we can change on the fly the settings of the controller, thereby changing, within a few milliseconds the behaviour of the controller that can become more suitable to face the situation at hand. When facing a gust, we can set the response of the controller with the parameters of Table 15.

Table 15. PID setting for gust response

P	320757.3
I	3758606.7
D	3514.2
N	505.9

8.5 PID, static validation

As described in the chapter 6.1 regarding the validation of the static model, without a controller we were not able to perform a test in configurations where the relationship between force applied and position obtained was not monotone, as shown in Figure 91. To reach those positions, we need indeed a controller. We can, with a controller, check the required force needed to reach a desired configuration.

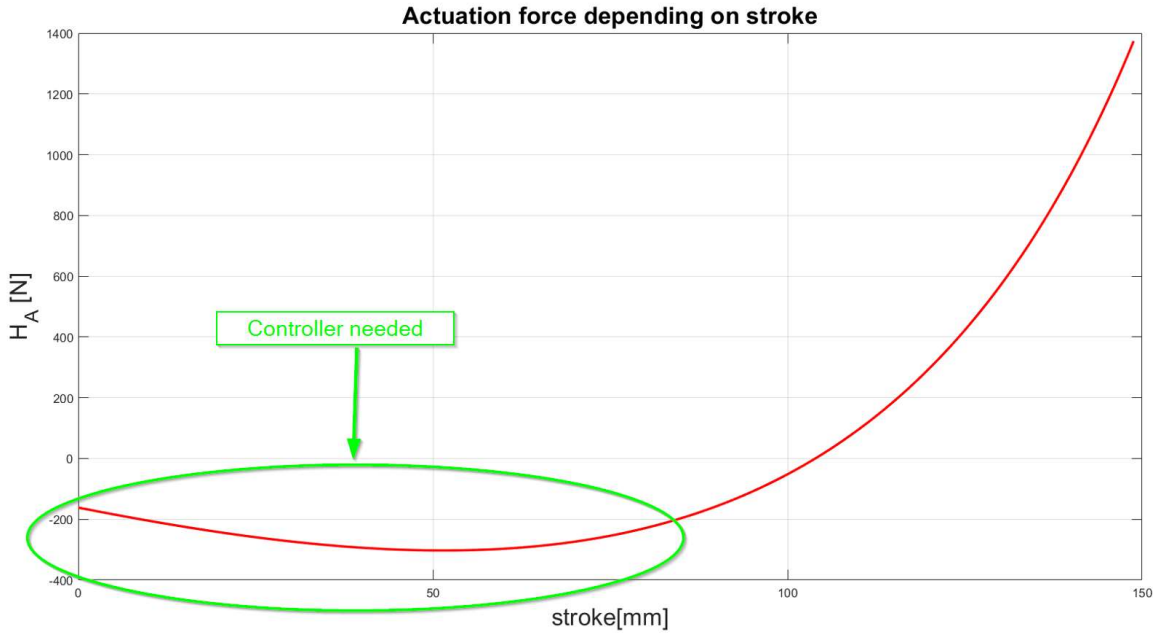

Figure 91. Stroke position vs actuation force

We are going to explore a few of these positions in which the controller is mandatory. We start by imposing a required aileron deflection of 60%, which translates to a target stroke position of 60.22mm. We can see in Figure 92 the actuation force and the theoretical required force.

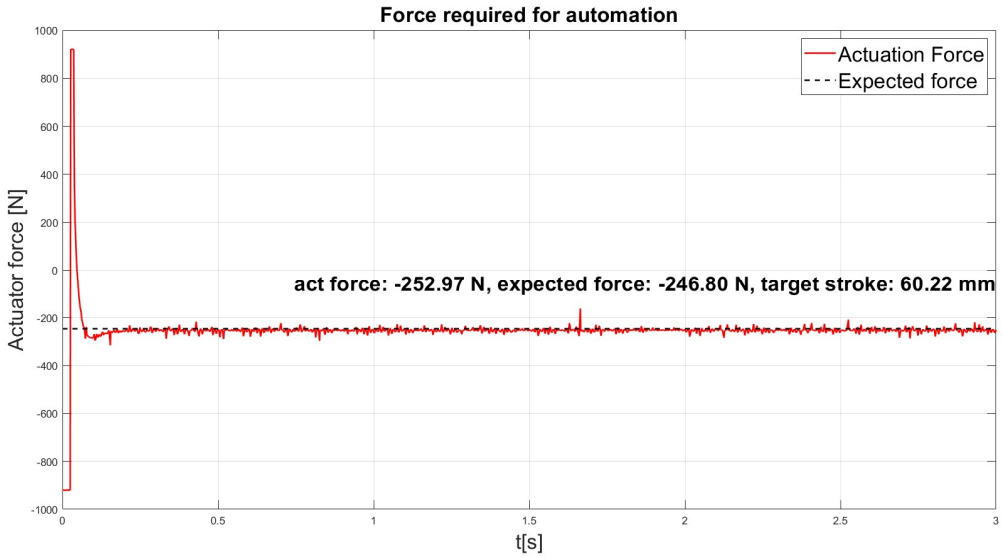

Figure 92. Lever V12, d=5, position 60%

We find that the actual force is well aligned with the theoretical value. In Figure 93, Figure 94, Figure 95 we can see the response of the system respectively when we set the target deflection to 70%, 80%, 90%.

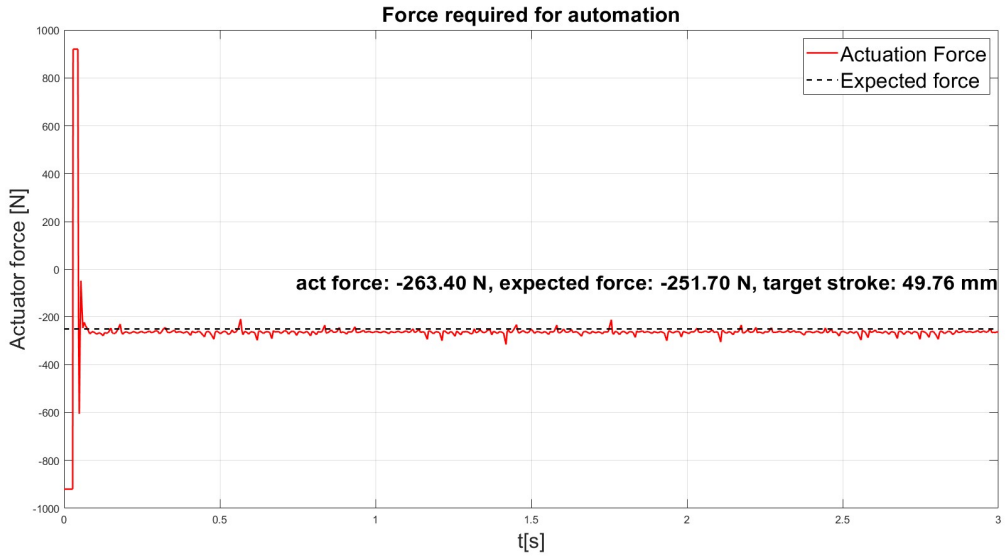

Figure 93. Lever V12, d=5, position 70%

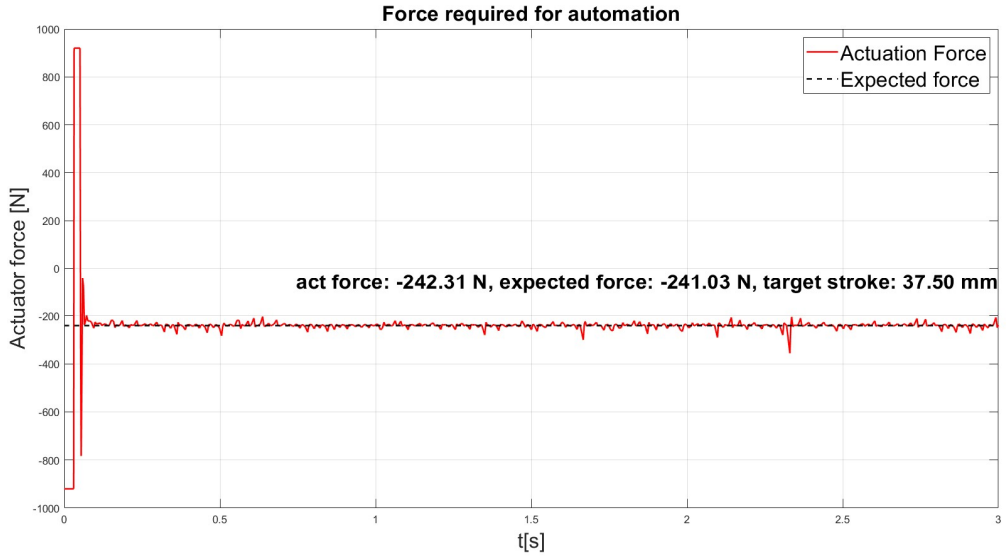

Figure 94. Lever V12, d=5, position 80%

Figure 95. Lever V12, d=5, position 90%

We can see in Table 16 that the expected value is close to the one we expect from the analytical solution.

Table 16. Position validation with controller

Stroke [mm]	Act force [N]	Expected force [N]	Error [perc]
60.22	-252.97	-246.8	-2.5
49.76	-263.4	-251.7	-4.65
37.50	-242.31	-241.03	-0.53
22.26	-211.13	-208.37	-1.32

The model represents well the expected force needed to maintain a desired position, when compared with the expected value from the analytical solution.

Finally, we can use the PID controller for double checking the results obtained in chapter 6.1 itself. In said chapter we simply applied a non-controlled actuation force and compared the obtained position with the analytical solution. We can use the PID controller to further check those results, by imposing a target stroke position and measure the force that was required for reaching said position. We use the final positions reached in Figure 43, Figure 44, Figure 45, Figure 46 as target for our PID controller. We can see the result of the controlled simulation respectively in Figure 96, Figure 97, Figure 98 and Figure 99.

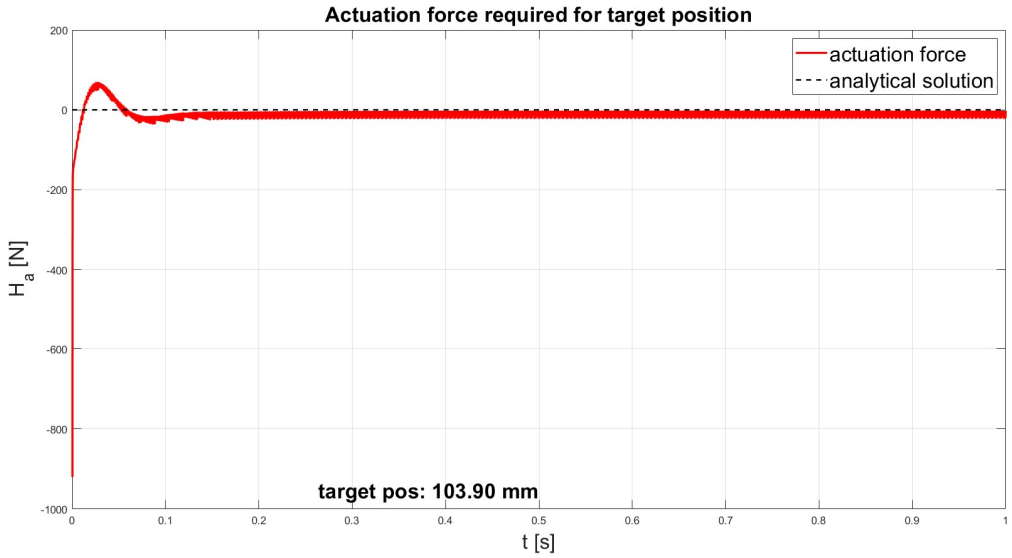

Figure 96. Controlled force required for reaching target position that would have required analytical force of 0N

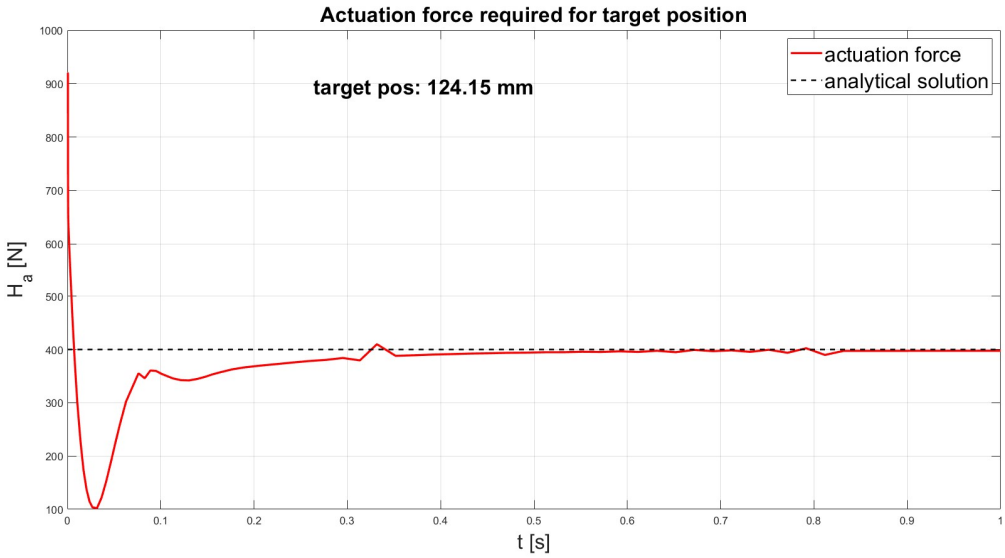

Figure 97. Controlled force required for reaching target position that would have required analytical force of 400N

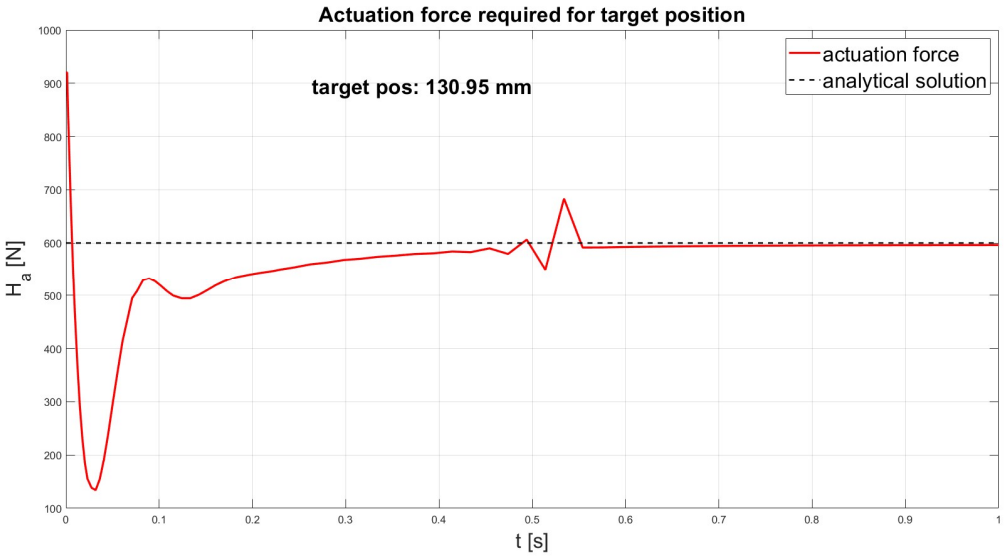

Figure 98. Controlled force required for reaching target position that would have required analytical force of 600N

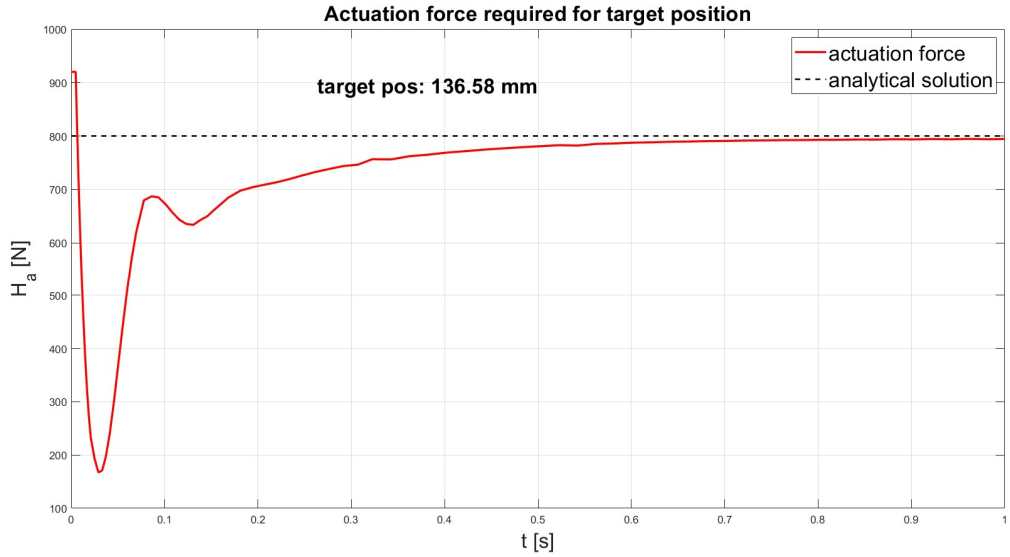

Figure 99. Controlled force required for reaching target position that would have required analytical force of 800N

We can appreciate that the force with which the controller drove the motor, converges to the values used in chapter 6.1.

Chapter 9 Discussion and Evaluation

Employing the Abaqus simulation, we were able to verify the capacity of the digital twin to manifest the first natural frequency of the system. More detailed behaviours of the mechanism are also captured, such as the phase inversion that occurs if we actuate the system with a force greater than its natural frequency, and the decreasing force with increasing frequency, if we impose a sinusoidal position.

The static validation was performed in two stages. In the second half of the machine's range of motion we were able to verify its fidelity by simply applying a force and to note, after a transient, the position. In the first half of the mechanism's range of motion we were not able to deploy such a simple technique because of the non-monotony characteristic of the relationship between force and position; we had to deploy a PID and validate the force required to reach certain key positions, against the analytical value.

Both stages of validation brought excellent result. The underlying Scott Russell mechanism is simple, with only 1 DOF and having an easy to use analytical solution has been key to gain trust in the digital twin. We are now confident we can use this model as an accurate representation of the dynamics of the actuator and this will allow us to carry on the development of the system with great freedom.

The building of the digital twin is, in many ways, only the beginning of this novel approach. Now we ought to carry on developing design aspect that would have classically needed a first prototype or else a rigid mathematical model, not well suited for exploring a developing space which is in many ways not explored. The dynamics of a legacy system, complex as it might be, have been empirically pinned down during the decades. An electric actuator for managing control surfaces is something for sure to be explored further.

The fact that the aileron itself is a morphing structure adds to this complexity. We had to introduce a new model for describing the load, to be plugged in the digital twin. Even the load of the model is somewhat a novelty and can be improved upon more detailed studies. Here another strength of this approach makes itself evident, a more complex load model can be easily plugged in, and the difference in the response of the system can be clearly evaluated.

One of the first aspect that can be improved is importing the exact geometry in Simscape, from Fusion 360. Once all tolerances and the finer dimensions have been there finalized, it is possible to import the mashed geometry into Simscape. As of now the components are built using native tools. Importing the exact geometry will approximate reality even better but it will bring only small variations to the results here find, since at a dynamic level, only the mass distribution matter.

The validation phase is fundamental and must be performed with most varied methods. Once we have a digital twin a lot of system design will be carried out on such a model, and only when the prototype will be available, possible months or years down the project's pipeline, we will be able to evaluate our results. At that point an issue with the model could possibly mean costly refittings and code revisions that are to be avoided. As of now we can trust the model to be used in the design process.

Chapter 10 Conclusion and Recommendations

We developed an actuation system able to reach the stringent performance required in terms of bandwidths, force and small enough to be fitted in the high aspect ratio wing, thanks to the introduction of a Scott Russell mechanism. We were able to actuate the aileron with an induction electric motor able to provide the static force necessary to deflect the morphing structure. Finally, with the development of the digital twin we were able to perform several simulations and test that would have required a functioning prototype thereby streamlining the design process of this system and of the many subsystem this actuation implementation requires. We were able to implement a PID controller, as a first approach to the control problem, which would allow for quick profile selection thank to the digital nature of the motor driver itself.

Naturally were then able to validate the model with data coming from trustworthy sources and thanks to these results we are confident in the future development of such a model.

The model based approach that led to the development of the digital twin provides, in fact, the designer several key advantages:

- Modularity: the model can be designed independently by a specific purpose. In the same way one may build a prototype and on it attach ad hoc instruments and actuators, to obtain a desired effect, the digital twin can be augmented with the required instruments and actuators. Once the core model has been developed, it can be shared between fields of study, where multiple people can employ it according to their necessity and requirement. The effort spent developing the core model can be taken advantage of in future studies. The multi domain nature of a digital twin opens further possibilities: a model for the thermal management of the actuator can be developed, since the temperature of the induction actuator must be strictly monitored and must remain in certain parameters. A model of the electromechanics components of inductor motor can be further developed, providing an even more deep insight in workings of such an actuator.
- Continuous improvement. Different aspects of the model can be further development in a progressive manner. Once the final shape of the components has been defined, it can be imported in the model, thereby improving the approximation of the distribution of mass of the moving components. Further model can be studied for improving critical aspects, such as the damping of the joints. A more sophisticated model can be developed for describing the load. All these aspects, and many other, can be developed in time and easily integrated in the model, to improve the accuracy.
- Parallelization: due to the nature of the increase complexity in designing such a novel system, the time to prototype has also significantly increased. The cost and the complexity in searching for a supplier that can provide the appropriate certifications, further increase the time spent before creating the first physical prototype. A digital twin can be created starting by a relatively small number of parameters and can be improved when new information becomes available. This allows the designer the ability to start to study certain critical aspects of the system, well before the construction of the prototype, allowing for a greater number of design iterations that would otherwise have to wait the physical model. We can therefore postpone the purchase of the components needed to build the actual prototype as much as possible.

In the light of these aspects, developing a model based digital twin can provide fundamental advantages that can streamline and decrease the development process especially of complex and novel system such as the object of this study. Since the literature is not as abundant as with legacy solutions, fostering a cross team development with each team adding and improving on the base model is key for exploring the space of the many the design choices available. The model can begin with significant approximations and progressively grow more and more granular after complex aspects have been individually tackled and modelled.

This approach lend itself particularly well in the current project managing environment, both for time and cost savings and for postponing critical decision points, since it provides tools that allow to make a much more informed guess, before buying components and building the first prototype.

The hope is for this model to become an instrument for developing further certain topics that at this stage were minimally tackled, and to perform further tests and experiments, from improve control theory, to fatigue analysis, that would lead to a more in depth understanding of this novel system.

The push to move away from conventional design, in the contest of control surface logic, comes from the desire to have more and more efficient and environmentally friendly air travel. This aim fosters the development of solution that would have been hard to imagine a few decades ago. The introduction of an electrically driven, morphing structure is a prime example of this. The novel approach although forces us the re imagine a system with almost a century of R&D, moves us towards a much deeper understanding of aerodynamics and of control theory that can be explored with the tools described in this study that hopefully will lead to the development of much more safe, efficient and clean solutions.

Summary

Due to the continuous push for electrification in air travel, a series of projects are being developed, with the intent of lowering environmental emissions both in form of noise and pollution. HERWINGT project is developing technologies that would render possible a local transport civil aircraft with significantly lower emissions. It aims to reach this goal, implementing a series of new technologies; among those, it aims to lower aerodynamic drag by 15% implementing a high aspect ratio wing and an integrated aileron. Such aileron will be actuated by an electric motor, to avoid the complications and environmental concerns of a hydraulic system.

In this study we will develop such an actuation method, in accordance with performance requirement and dimensional constraints. We will then develop a digital twin that would allow us to perform several important simulations. This work will contribute to a global effort in developing a digital twin of the entire aircraft, with all its subsystem. Having a digital twin will be relevant for the implementation of many HUMS strategies that would make possible to increase safety while lowering maintenance costs.

Once such a model has been developed, a range of simulation will be run. A frequency response study will allow us to understand how different configurations impact the dynamic response; a gust response study will show us how the (reversible) mechanism will handle sudden load increase; the implementation of a PID controller will allow us to evaluate the performance of a control logic.

Naturally such a model will need to be validated. The validation will take advantage of results coming from an Abaqus model. Since the mechanism chosen, a Scott Russel mechanism is simple, an analytical solution is known, thereby rendering possible the comparison with the exact data.

Since model-based design allows especially for collaboration between different fields, the model developed for purposes specific for this work, can be in a straightforward manner be improved upon and employ in the design of different subsystems rendering the model here developed only a first step, into a much more sophisticated and all-encompassing digital twin.

Bibliography

1. Aero-structural design of an high-aspect ratio wing. Pietro Catalano, Gianluca Diodati, Davide Lucariello, Pier Luigi Vitagliano. CIRA Italian Aerospace Research Center, Capua (CE), 81043, Italy
2. CS-25, Amendment 8
3. Northwest orient airlines Boeing 727-51/251 Maintenance training manual
4. Introduction to Aircraft Aeroelasticity and Loads. Wright, Jan R.;Cooper, Jonathan;Belobaba, Peter;Seabridge, Allan; & Jonathan E. Cooper
5. Gust Loads on Aircraft. Hoblit, Frederic M
6. Fundamentals of Aerodynamics. J. Anderson
7. MULTI–OBJECTIVE DESIGN OPTIMIZATION OF A MORPHING AILERON FOR A HYBRID ELECTRIC REGIONAL AIRCRAFT. Alessandro De Gaspari, Vittorio Cavalieri, Matteo Corti, Sergio Ricci
8. European Commission and Directorate-General for Research and Innovation. Fly the Green Deal - Europe's vision for sustainable aviation. Publications Office of the European Union. 2022.
9. De Gaspari A and Ricci S. A two–level approach for the optimal design of morphing wings based on compliant structures. Journal of Intelligent Material Systems and Structures. Vol. 22, No. 10, pp. 1091–1111. 2011.
10. Weisshaar T. Morphing aircraft systems: historical perspectives and future challenges. Journal of aircraft. Vol. 50, No. 2, pp. 337–353. 2013